Aus dem Physiologischen Institut – Lehrstuhl für Physiologische Genomik
der Ludwig-Maximilians-Universität München
Vorstand: Prof. Dr. Magdalena Götz

Identifying the progeny of single neural stem cells in the adult murine forebrain

Dissertation
zum Erwerb des Doktorgrades der Medizin
an der Medizinischen Fakultät der
Ludwig-Maximilians-Universität München

vorgelegt von
Julia Michel
aus
Spremberg
2016

Mit Genehmigung der Medizinischen Fakultät
der Universität München

Berichterstatterin:	Prof. Dr. Magdalena Götz
Mitberichterstatter:	Prof. Dr. Michael Kiebler Prof. Dr. Rainer Glaß Priv. Doz. Dr. Ulrich Schüller
Mitbetreuung durch den promovierten Mitarbeiter:	Dr. Jovica Ninkovic
Dekan:	Prof. Dr. med. dent. Reinhard Hickel
Tag der mündlichen Prüfung:	28.01.2016

Eidesstattliche Versicherung

Ich erkläre hiermit an Eides statt, dass ich die vorliegende Dissertation mit dem Thema selbständig verfasst, mich außer der angegebenen keiner weiteren Hilfsmittel bedient und alle Erkenntnisse, die aus dem Schrifttum ganz oder annähernd übernommen sind, als solche kenntlich gemacht und nach ihrer Herkunft unter Bezeichnung der Fundstelle einzeln nachgewiesen habe.

Ich erkläre des Weiteren, dass die hier vorgelegte Dissertation nicht in gleicher oder in ähnlicher Form bei einer anderen Stelle zur Erlangung eines akademischen Grades eingereicht wurde.

München, den _____

(Unterschrift)

Für meine Familie

For my family

LIST OF FIGURES

LIST OF TABLES AND FORMULAS

Abstract

The process of the production of new neurons is called adult neurogenesis. It occurs in specific regions in the adult mammalian brain. The new neurons are being produced by so called adult neural stem cells (aNSCs). Two niches that harbour these cells are the subgranular zone (SGZ) of the dentate gyrus of the hippocampus and the subependymal zone (SEZ) of the lateral ventricle. aNSCs in the SEZ produce transit-amplifying progenitors (TAPs) which give rise to neuroblasts (NBs) that migrate via the rostral migratory stream (RMS) to the olfactory bulb (OB) where they mature to different interneuron subtypes. The properties of the aNSCs in these regions have been extensively investigated either by *in vitro* or *in vivo* population studies. However, little is known about the behaviour of an individual aNSC in the SEZ.

In order to overcome this missing knowledge, an analysis method was established in this thesis by using double heterozygous mice for GLAST^{CreERT2} and R26R-Confetti. This method allows the lineage tracing of aNSCs in the murine brain. By titration of the dose of Tamoxifen that was injected intraperitoneally into these mice, sparse labelling of individual GLAST+ aNSCs was achieved. This method was then used to analyse the behaviour of single aNSCs of the SEZ, as well as their progeny (TAPs, NBs and neurons) over the course of time.

These aNSCs are able to produce a large progeny already within 3 and 7 days after induction and show a drive towards neuronal maturation in between 3 and 8 weeks. The amplification step occurs at the level of the progeny. This analysis at the single cell level showed insights into the temporal and spatial profile of aNSCs. Compared to other analyses performed at the population level, the progeny of aNSCs in the SEZ reduces with time. It seems that the continuous neurogenesis is maintained at the population level and therefore reflects a population property. Furthermore, it was found that a single aNSC is capable of producing multiple interneuron subtypes, however the majority of cells produced are the deep granule interneuron subtype.

Zusammenfassung

Die Produktion von neuen Neuronen wird als adulte Neurogenese bezeichnet und läuft in spezifischen Regionen des Säugetiergehirns ab. Diese neuen Neurone werden durch sogenannte adulte neurale Stammzellen (aNSZ) produziert. Zwei Nischen, die neurale Stammzellen beherbergen, sind die subgranuläre Zone (SGZ) des Gyrus dentatus des Hippocampus und die subependymale Zone (SEZ) der lateralen Ventrikel. Die aNSZ der SEZ produzieren sogenannte „Transit-amplifying progenitor" Zellen (TAPs). Diese teilen sich und generieren Neuroblasten (NBs), die den rostralen migratorischen Strom (RMS) entlang migrieren und im Bulbus olfactorius (OB) zu unterschiedlichen Subtypen von Neuronen reifen. The Eigenschaften dieser adulten neuralen Stammzellen (aNSZ) sind entweder durch *in vitro* oder *in vivo* Studien auf Populationsebene umfangreich untersucht. Jedoch ist das Wissen über die Eigenschaften einer einzelnen aNSZ in der SEZ bisher begrenzt.

Um diesem Forschungsbedarf nachzugehen, wurde in dieser Dissertation eine neue Analysemethode entwickelt, die die Verfolgung der Nachkommen einer aNSZ ermöglicht. Mit Hilfe der Titration von geringen Dosen Tamoxifen, die intraperitoneal in heterozygote Mäuse für GLAST^{CreERT2} und R26R-Confetti injiziert wurden, war es möglich eine spärliche Kennzeichnung von einzelnen GLAST+ aNSZ zu erreichen. Diese erlaubte die Untersuchung der Eigenschaften einer individuellen aNSZ und deren Nachkommen *in vivo* über einen definierten Zeitraum.

Diese Zellen sind in der Lage, bereits im Zeitraum von 3 und 7 Tagen nach der Induktion mit Tamoxifen, eine große Anzahl an Nachkommen zu generieren. Ebenfalls zeigen sie eine starke Dynamik der Produktion von reifen Neuronen. Der Schritt der Amplifikation scheint auf der Ebene der Nachkommen stattzufinden.

Diese Analyse auf Einzelzellebene bietet Erkenntnisse über das zeitliche und räumliche Profil einer aNSZ. Verglichen mit Analysen auf Populationsebene, zeigt sich, dass sich die Anzahl der Nachfahren im Verlauf der Zeit reduziert. Aus diesem Grund scheint die kontinuierliche Neurogenese eine Eigenschaft zu sein, die auf Populationsebene entsteht. Ebenfalls zeigten erste Versuche, dass eine einzelne aNSZ in der Lage ist, verschiedene Typen von Neuronen (Neurone der inneren und äußeren Körnerzellschicht und Periglomeruläre Zellen) zu bilden. Der Häufigste Interneuron-Subtyp, der produziert wurde, waren die Neurone der inneren Körnerzellschicht.

ABBREVIATIONS

%	Per cent
°C	Degree Celsius
bp	Base Pairs
BrdU	5'-Bromo-2'-Deoxyuridine
CalB	Calbindin
CalR	Calretinin
CFP	Cyan fluorescent protein
cm	Centimetres(s)
CNS	Central nervous system
Cre	Cre recombinase
CSF	Cerebrospinal fluid
DAPI	4,6-diamidine-2-pheylidoledihydrochloride
Dcx	Doublecortin
dGC	Deep granule cells
DNA	Deoxyribonucleic acid
dNTP	Desoxyribonukleosidtriphosphate
dpi	Days post induction
dpo	Days post operation
E	Embryonic day
EDTA	Ethylene-diamine-tetra-acetic-acid
EGF	Epidermal growth factor
Emx1	Empty piracles Homeobox 1
ERT2	Estrogen ligand-binding domain
EtBr	Ethidium bromide
EtOH	Ethanol
FACS	Fluorescent activated cell sorting
FGF	Fibroblast growth factor
Fig.	Figure
g	Gram(s)
G	Gauge
GABA	γ-Amino Butyric Acid
GC	Granule cells
GCL	Granule cell layer
GE	Ganglionic eminence
GFAP	Glial fibrillary acidic protein
GFP	Green fluorescent protein
GL	Glomerular layer
GLAST	Astrocyte-specific glutamate transporter
h	Hour(s)
HCl	Hydrochloric acid
hGFAP	Human glial fibrillary acidic protein
hpi	Hours post induction
INM	Interkinetic nuclear migration
IP	Intraperitoneal
IPL	Internal plexiform layer
JGC	Juxtaglomerular cells

kg	Kilogram(s)
L	Ladder
loxP	locus of X-over P1
LV	Lateral ventricle
M	Molar (mol/litre)
mA	Milliampere
Mash1	Mammalian Achaete Scute Homolog1
MCL	Mitral cell layer
mg	Milligram(s)
MGE	Medial ganglionic eminences
min	Minute(s)
mk-	Marker negative
mL	Millilitre(s)
mM	Millimolar
mm	Millimeter(s)
mpi	Month(s) post induction
mRNA	Messenger ribonucleic acid
n	number of samples
NaCl	Sodium Chloride
NeuN	Neuronal Nuclei
ng	Nanogram(s)
nm	Nanometer(s)
nM	Nanomolar
NSC	Neural stem cell
OB	Olfactory Bulb
ONL	Olfactory nerve layer
PBS	Phosphate buffered saline
PCNA	Proliferating cell nuclear antigen
PCR	Poly chain reaction
PFA	Paraformaldehyde
PGN	Periglomerular cell
PSA-NCAM	Polysialic acid neural cell adhesion molecule
RFP	Red fluorescent protein
RMS	Rostral migratory stream
RNA	Ribonucleic acid
RT	Room temperature
SD	Standard deviation
sec	Second(s)
SEM	Standard error of the mean
SEZ	Subependymal zone
sGC	Superficial granule cells
SGZ	Subgranular zone
Sox2	Sex determining region-Y box2
SVZ	SubVentricular zone
TAM	Tamoxifen
TAP	Transit-amplifying progenitor
Taq	Taq DNA polymerase

TBE	Tris/Borate/EDTA
TBS	Tris-buffered saline
TE	Tris/EDTA
TX	TritonX
UV	Unltraviolet
VZ	Ventricular zone
WT	Wild-type
x g	Times gravity (acceleration)
YFP	Yellow fluorescent protein
β-Gal	β-galactosidase
µg	Microgram(s)
µl	Microliter(s)

1 Introduction

Neurodegenerative diseases like Parkinson's, Alzheimer's and Huntington's disease, epilepsy or traumatic brain and spinal cord injuries, are important elements of present-day medical practice and have a high influence on public health issues. Not only they are the cause of 12% of deaths worldwide, they are also responsible for disabilities and made up for 6.3% of the global burden of disease in 2005, their percentages increasing (World Health Organization, 2006). To find appropriate treatments for these disorders and to inhibit the neurodegenerative processes underlying them, have become a pressing issue in the field of neuroscience.

One common feature of these diseases is their altered adult neurogenesis, which can be observed in animal models (Winner and Winkler, 2015) as well as in humans (Ernst et al., 2014). This process is the most important finding of the last twenty-five years in the field of neuroscience and describes the production of new neurons in the adult mammalian brain (Ming and Song, 2011). The underlying neural stem cells, their niches and the technical methods used investigate their properties and behaviour will be reviewed in this chapter before the new analysis method established in this thesis will be discussed in more detail.

1.1 Adult neurogenesis

1.1.1 The history of adult neurogenesis in a nutshell

The central nervous system (CNS), which enables us to receive sensory information from our environment, to integrate the input and to react to it at an equally complex level (Trepel, 2008) is the most complex system of the mammalian body.

It consists of two major cell types: the neurons and the glial cells. The adult human brain for instance consists of approximately 86 billion neurons and of almost the same amount of glia cells (Herculano-Houzel, 2009). For a long time it was believed that once this complex architecture of cells was formed during embryogenesis, it stays inert and no generation and integration of new neurons into the already existing neuronal network of the adult mammalian would occur (Ming and Song, 2011). In his book "degeneration and regeneration of the nervous system" Nobel Prize winner and neuroscientist Ramón y Cajal wrote that "[…] in the adult centres, the nerve paths are something fixed, ended, and immutable. Everything may die, nothing may be regenerated." (Cajal, 1928).

Altman *et al.* published the first observations that proved this hypothesis to be incorrect in the 1960s. By using [^{3}H]-thymidine autoradiography, which labels the progeny of cells that had just divided and hence allows the spatial and temporal birth dating of these cells, he could show that new neurons were indeed being generated in the brain of the adult rat (Altman, 1962, 1969; Altman and Das, 1965). However, it happened only more recently that Altman's initial findings were widely accepted in the field (Gould, 2007; Gross, 2000). The discovery of adult neurogenesis in the avian brain (Alvarez-Buylla and Nottebohm, 1988; Goldman and Nottebohm, 1983) and technical advances like the application of BrdU

(5-Bromo-3'-deoyuridine) in combination with cell specific immunohistochemical markers such as NeuN for neurons made this possible.

With those advances Altman's observations from 30 years before were proven to be correct. Regions where adult neurogenesis occurs are the subgranular zone (SGZ) of the dentate gyrus of the hippocampus (Cameron et al., 1993; Gould et al., 1992; Kuhn et al., 1996; Okano et al., 1993), as well as the subependymal zone (SEZ) of the lateral wall of the lateral ventricle (Lois and Alvarez-Buylla, 1993; Luskin, 1993; Rousselot et al., 1995) of most mammals (Fig. 1-1). Neuroblasts (NBs) that were generated migrate via the rostral migratory stream (RMS) to the olfactory bulb (OB) where they mature to neurons. More recently also the hypothalamus was shown to harbour newly born neurons (Kokoeva et al., 2005; Lin and Iacovitti, 2015).

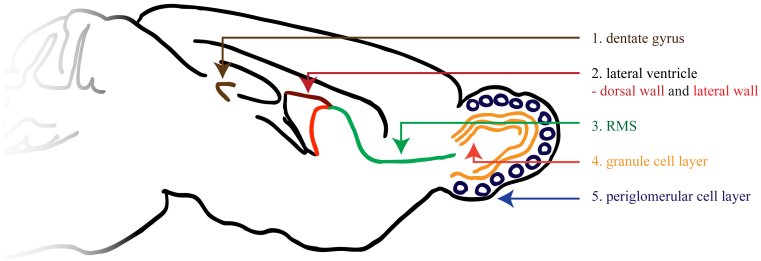

Figure 1-1. Areas of neurogenesis.
(1.) depicts the dentate gyrus (DG) of the hippocampus with its SGZ and the SEZ of the lateral ventricle (2.). Cells migrate via the rostral migratory stream (RMS) to the olfactory bulb (OB).

Compared to the current understanding of the adult neurogenesis in animal models, the knowledge about human neurogenesis is still little. The major finding that neurogenesis can also be observed in the adult human brain was provided by Eriksson *et al.* He used autoptic brain material of cancer patients who had been given BrdU to measure the tumour cell proliferation and could show that new neurons were generated in the SEZ and dentate gyrus of the adult human brain (Eriksson et al., 1998). Since then, these findings have been supported by *in vitro* data, which show that cells which were isolated from human SEZ and the hippocampus, were able to be proliferate in cell culture (Johansson et al., 1999; Kukekov et al., 1999; Leonard et al., 2009; Sanai et al., 2004). Furthermore, more recently Frisen and his colleagues discovered that in the human hippocampus (Spalding et al., 2013), as well as the lateral ventricle wall, new neurons are being generated by using the concepts of the radiocarbon-dating technique (Ernst et al., 2014; Ernst and Frisen, 2015; Kheirbek and Hen, 2013). The newly generated cells of the SEZ however seem not to migrate to the olfactory bulb (OB) as it can be observed in the murine brain, but integrate into the striatum instead (Bergmann et al., 2012; Ernst et al., 2014).

As mentioned, adult neurogenesis is a process that is shared by many mammalian species and is due to the proliferation and differentiation of a cell population called adult neural stem cells (aNSCs) (Braun and Jessberger, 2014b). These cells, their properties and methods to analyse them will be discussed in the following chapters.

1.2 Adult neural stem cells

1.2.1 General principles and analysis methods

Different methods have been used to investigate adult neurogenesis and the properties of the responsible cells. The term "**stem cell**" is a very frequently discussed nomenclature in science and is defined by two major features:

1. Capacity of **self-renewal** and
2. **Multipotency** (Riquelme et al., 2008).

Translated to adult neurogenesis, these aNSC should show self-renewal as well as the property to differentiate into both glia cells (astrocytes, oligodendrocytes) and neurons.

Early on, cells isolated from tissue taken from neurogenic regions of the adult brain were shown to possess these properties. These cells could divide *in vitro* (Reynolds and Weiss, 1992; Richards et al., 1992), showed self-renewal (Gritti et al., 1996; Morshead et al., 1994) and multipotent properties because they could generate astrocytes, oligodendrocytes and neurons. However these observations were made in cell culture and under the influence of growth factors like epidermal growth factors (EGF) and fibroblast growth factor 2 (FGF2). Costa *et al.* showed by live imaging of single cells that without the exposure of those factors, aNSCs of the SEZ only produced neuronal progeny. The exposure to growth factors leads to the resume of proliferation and production of astroglial progeny (gliogenesis) (Costa et al., 2011). By using the same technique mentioned above, it was shown that the same aNSC of the SEZ never produces both oligodendroglia and neurons (Ortega et al., 2013). These examples show that even though *in vitro* analyses have laid the base of our current understanding of adult neurogenesis and neural stem cells, this method cannot reflect the properties of an endogenous aNSC in its niche. Therefore, two terms concerning these properties have to be distinguished. The first one is the term *potential*. It describes the properties of an aNSCs that can be observed when these cells are exposed to different environments *in vitro,* hence it refers to what the cell is capable of (Beckervordersandforth et al., 2010; Gotz et al., 2015; Ming and Song, 2011). The *lineage* of an aNSC refers to what this cell can do *in vivo*. These differences are depicted for aNSCs in the SEZ in Fig. 1-2. The *potential* of these cells observed *in vivo* is their property of multipotency whereas *in vivo* data could so far only prove the generation of neuronal progeny (*lineage*) (Gotz et al., 2015).

The *in vivo* analyses profited from the introduction of BrdU as already mentioned above. This thymidine analogue can integrate into the DNA of dividing cells during S-Phase and be visualised by immunohistochemistry. It therefore labels cells, which are actively dividing (Ming and Song, 2005) and can be used to trace them (Dhaliwal and Lagace, 2011; Lin and Iacovitti, 2015). In combination with other cell-specific markers it is possible to also analyse the fate of these newly produced cells as well as their progeny, making it a good tool for analysis (Dhaliwal and Lagace, 2011; Kuhn et al., 1996).

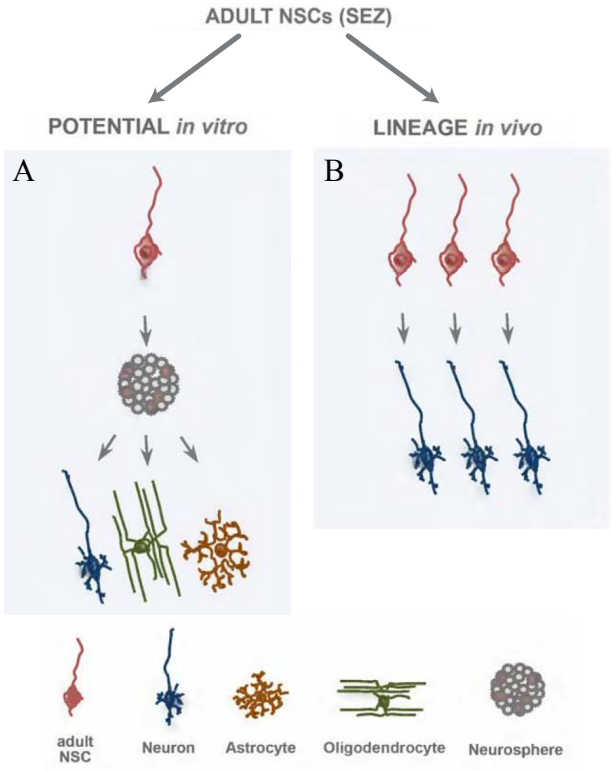

Figure 1-2. Potential and lineage of an aNSC.
The figure depicts the difference of the two terms "potential" and "lineage" when analysing the properties of an aNSC. (A) Potential refers to what the aNSC is capable of when being exposed to different environments *in vitro* (being multipotent) whereas (B) lineage refers to the properties observed by *in vivo* analysis (only producing cells of the neuronal lineage). *Modified from Götz et al. 2015* (Gotz et al., 2015).

Another analysis method used is the labelling of aNSCs with retroviruses that express fluorescent proteins. They can only integrate into the DNA of cells in mitosis and hence have been frequently used to label dividing cells (Ming and Song, 2005). They enable the intensive study of the generation of new cells in the SEZ and their migration and maturation in the OB (Doetsch et al., 1999b) as well as their integration into the neuronal network (Carleton et al., 2003). Petreanu *et al.* used such a retrovirus to analyse the temporal differentiation of newly produced progeny in the SEZ as well as their change in morphology (Petreanu and Alvarez-Buylla, 2002). Both, BrdU and retroviruses, among other things, allow the birth dating of cells and their progeny since they integrate into the DNA. However, while BrdU labels all dividing cell populations, the retrovirus can be injected into the region of interest. Therefore it can label a limited cell population. Furthermore retroviruses show the complete cell morphology whereas BrdU only visualises the nucleus of the labelled cell (Ming and Song, 2005). BrdU and retroviruses cannot label non-dividing cells and therefore quiescent cells. Since a large proportion of aNSC are thought to be quiescent (Doetsch et al., 1999a), (Morshead et al., 1994; Seri et al., 2001) this subpopulation cannot be analysed by them but need new analysis methods.

With the introduction of transgenic mice, the methods analysing neurogenesis were transformed to a new level. Different transgenic mouse lines have been used. There are constitutive reporter mice, for example hGFAP-GFP mice (Zhuo et al., 1997) that continuously express a reporter, for example green fluorescent

protein (GFP) under a cell-specific promoter (hGFAP). Furthermore, there are conditional transgenic mice, like Emx1^{Cre} (Iwasato et al., 2000). In the genome of these mice, a cell-specific promoter is combined with a Cre-recombinase. This recombinase is a site-specific enzyme of the bacteriophage P1 and recognises loxP sites. Pieces of DNA that are flanked by them are stochastically excised. It therefore enables the deletion or turning-on of specific genes (Sauer, 1998). When this mouse line is crossed with a fluorescent reporter mice, like EGFP (Mao et al., 2001), which consists of a floxed stop codon (lined by loxP sites) upstream of the EGFP cassette, all cells expressing Emx1 as well as their progeny will express EGFP.

The most advanced transgenic mouse line, which enables labelling of specific cell types at different time points and therefore fate-mapping (Ninkovic and Gotz, 2013), is the Tamoxifen (TAM) inducible CreERT2 mouse line. With the introduction of fusion proteins of the Cre recombinase and a mutant human oestrogen receptor binding domain, it became possible to conditionally activate the recombinase (Feil et al., 2009). Due to the mutations, the receptor does not recognise the internally produced oestrogen but can only be activated by the application of the oestrogen receptor antagonist TAM. Differently mutated binding domains have been used. The most common one used is CreER^{T2} with a triple mutation (G400V/M543A/L544A) (Feil et al., 2009). Compared to the CreER^{T} recombinase it is 10x more sensitive in basal keratinocytes (Indra et al., 1999) reducing the amount of TAM and therefore its toxicity. With this tool it is now possible to create site-specific mutations at any time point of development as well as in the adult mouse by combining Cre-expressing mouse lines with mice with floxed genes (Feil et al., 2009). Recently new reporter lines have been introduced to the field (R26R-Confetti (Snippert et al., 2010) and mosaic analysis with double markers (MADM) (Zong et al., 2005)) which also use the loxP system to introduce the possibility of different recombination events, leading to different colour distributions. Fig. 1-3 shows the principle of recombination with the example of the glutamate aspartate transporter GLAST^{CreERT2}//R26R-Confetti (from now on referred to as GLAST^{CreERT2}//Confetti), which were used in this thesis. In cells that are expressing GLAST, the Cre recombinase is not active but expressed. Only by treating these mice with TAM, the enzyme can enter the nucleus (Fig. 1-3.2) and catalyse recombination in between the loxP sites of the Confetti cassette resulting in theoretically four exclusively different results (Fig. 1-3.3).

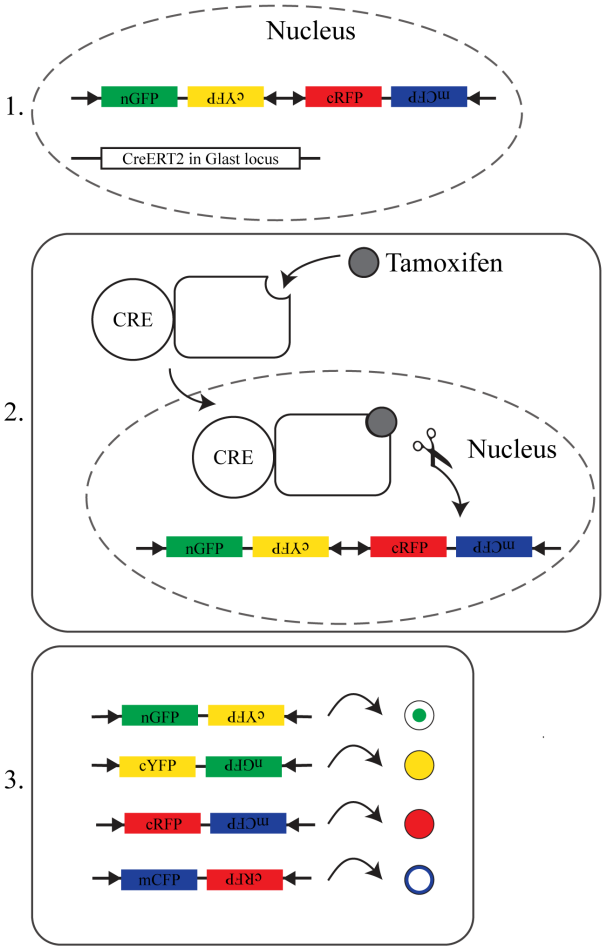

Figure 1-3. Inducible GLAST^{CreERT2}//Confetti mice as an example of inducible transgenic mice.
Double heterogeneous mice for Confetti and GLAST^{CreERT2} (1) possess four different fluorescent proteins (FP) (nuclear green FP (nGFP), cytoplasmic yellow FP (cYFP), cytoplasmic red FP (cRFP) and membrane cyan FP (mCFP) enclosed by loxP sites (arrows) in the Rosa 26 locus as well as a sequence encoding for the Cre recombinase in the GLAST locus. In cells where GLAST is active, the Cre recombinase is also being transcribed and translated. The administration of TAM enables the Cre recombinase to enter the nucleus (2). Only there it can catalyse recombination events between the loxP sites. Inversion and excision create four stochastically different outcomes for the expression of fluorescent proteins: nGFP, cYFP, cRFP or mCFP. *Modified from Feil et al., 2009* (Feil et al., 2009) and *Snippert et al., 2010* (Snippert et al., 2010).

1.1 Neural stem cells niches

The two neurogenic regions, which will be discussed further in this thesis, are the SGZ of the dentate gyrus and the SEZ of the lateral ventricle. They are also referred to as “niches”, because they seem to generate a certain microenvironment that enables aNSCs to survive and proliferate (Morrison and Spradling, 2008). Much research has been performed on deciphering the signals within the niches and the vasculature seems to play a significant role in both neurogenic regions (Palmer et al., 2000; Shen et al., 2008). Especially in the SEZ the basal process of the stem cell is in close contact with blood vessels (Mirzadeh et al., 2008). Other components of the niche are diffusible factors like EGF and FGF, cell-cell and cell-extracellular interactions, axonal neurotransmitter release and interactions between cells and the basal lamina (Ming and Song, 2011; Riquelme et al., 2008). These local extrinsic cues seem to be very important for determining the fate of the progeny generated. When aNSCs from neurogenic regions, as the SEZ, are transplanted into non-neurogenic areas, they differentiate into glial cells (Faigle and Song, 2013; Seidenfaden et al., 2006). However, when cultured hippocampal progenitors are grafted into the

“rostral migratory pathway”, they are capable of migrating and differentiating into interneurons of the OB whereas when they are transplanted into the non-neurogenic cerebellum of the adult, no neurons were generated (Suhonen et al., 1996).
With the help of the different analysis methods mentioned above, especially the immunohistochemistry and transgenic mouse lines, the aNSCs could be investigated in more detail. Much information was given on the general principles of the aNSC and the analytical methods used to describe them, however the identity of these cells has not yet been discussed.

First of all, these cells have been found to be derived from radial glia cells, which act as neural stem cells during development (Merkle et al., 2004; Taverna et al., 2014). Not only these radial glia cells express glial characteristics, also the aNSC show the expression of astrocytic markers (Kriegstein and Alvarez-Buylla, 2009), like Nestin (Gilyarov, 2008), Sex determining region-Y box2 (Sox2) (Episkopou, 2005), glial fibrillary acidic protein (GFAP) (Doetsch et al., 1999a; Garcia et al., 2004) and GLAST (Chojnacki et al., 2009; Mori et al., 2006; Ninkovic et al., 2007; Platel et al., 2009). Even though the markers labelling the astrocytes and aNSC overlap, the morphology of the aNSC is thought to be different. In the neurogenic regions of the adult mammalian brain, the aNSCs giving rise to neurons are thought to have a radial glia-like morphology (Beckervordersandforth et al., 2010; Ming and Song, 2011; Mirzadeh et al., 2008).
The basic principles of adult neurogenesis are the following four processes: cell proliferation, migration, cell survival and neuronal differentiation” (Gage and Temple, 2013). aNSCs divide and give rise to a fast proliferating progeny, which in turn produces NBs, which then differentiate into neurons. Different nomenclature is being used to describe these different cell populations. Tab. 1-1 shows an overview of these terms as well as the different markers expressed by the by the different cell populations. The terms highlighted by the bold writing will from now on be used in this thesis.

Table 1.1. Overview of the different terminology used in adult neurogenesis as well as markers expressed by the different cell populations.
Terminology marked in bold will be used in this thesis.
Modified from (Bonaguidi et al., 2012; Ming and Song, 2011).

		adult neural stem cell (aNSC) →	**Progenitor cells** →	**Neuroblasts (NBs)** →	**Immature Neurons** →	**Mature Neurons**
SGZ	Different terminology	• Radial glia-like cell • Type 1 cell • **aNSC**	• **Intermediate progenitor cell (IPC)** • Type 2 cell	• **NB** • Type 3 cell	• Immature Neuron	• **Neuron**
	Markers	Nestin	Mash1	Prox 1		
		GFAP	Tbr2			NeuN
		Sox2		Dcx		
SEZ	Different terminology	• Radial glia-like cell • Type B cell • **aNSC**	• **Transient amplifying progenitor (TAP)** • C cell	• **NB** • Type A cell	• Immature Neuron	**Neuron** • **Deep granule neuron (dGC)** • **Superficial granule neuron (sGC)** • **Periglomerular cell (PGN)**
	Markers	Nestin		Dcx		NeuN
		GFAP	Mash 1			
		GLAST	Dlx			

1.1.1 Neurogenesis in the dentate gyrus of the hippocampus

The dentate gyrus of the hippocampus plays an important role in learning, memory and mood regulation (Whitman and Greer, 2009). Within 3 days, aNSCs (Beckervordersandforth et al., 2014; Bonaguidi et al., 2012; Suh et al., 2007) divide in the SGZ to give rise to intermediate progenitor cells (IPCs), which in turn generate NBs that migrate into the granule cell layer. They mature by extending their axons and dendrites and integrate into the already existing neuronal network within 4 to 8 weeks (Braun and Jessberger, 2014a; Whitman and Greer, 2009; Zhao et al., 2006). Fig. 1-4 shows an illustration of this process. These newly generated neurons seem to play a role in enhancing the discrimination of input signals (Gage and Temple, 2013).

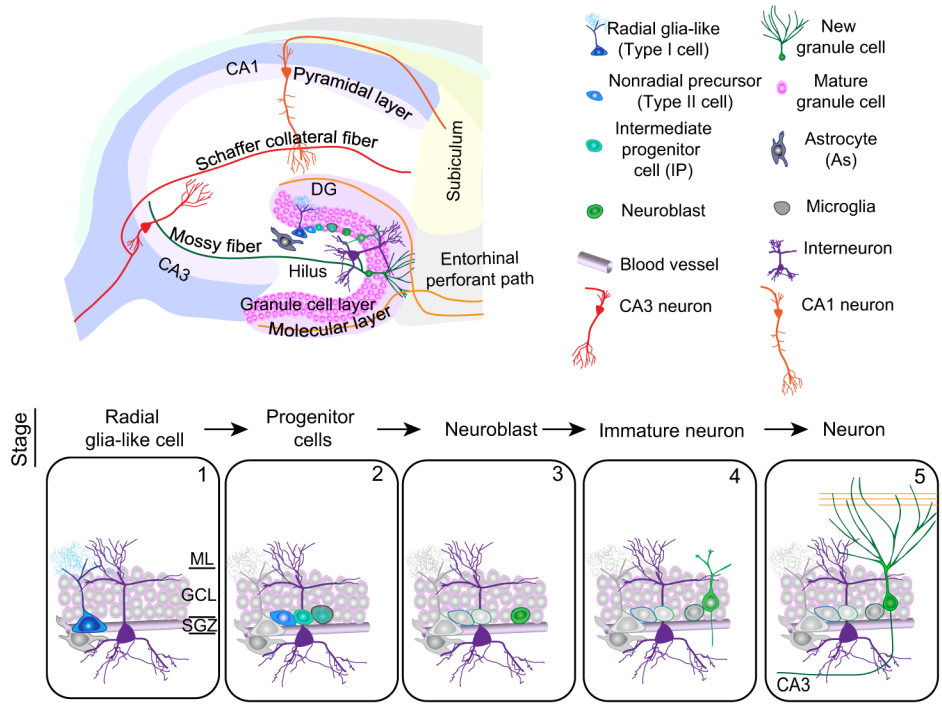

Figure 1-4. Neurogenic niche of the dentate gyrus of the hippocampus.
(1) shows a radial glia cell (aNSC) in the subgranular layer, which divides and gives rise to IPCs (2) that in turn proliferate and produce NBs (3). These NBs mature (4) and integrate into the molecular layer (5).
DG: dentate gyrus; GCL: granular cell layer; ML: molecular layer. SGZ: subgranular zone. *Modified from Ming and Song, 2011 (Ming and Song, 2011).*

In the dentate gyrus of the hippocampus GFAP, GLAST and Nestin (Ming and Song, 2011) expressing cells are thought to represent the aNSCs (Tab. 1-1). However, it has recently been shown that there seems to be a functional heterogeneity between said stem cell populations resulting in a different contribution to adult neurogenesis in the dentate gyrus (DeCarolis et al., 2013). The Nestin+ aNSCs seem to only be capable of a limited number of divisions before they are exhausted (Encinas et al., 2011). Furthermore analysis of single Nestin+ aNSCs revealed a production of only a small number cells before many of the aNSC were depleted (Bonaguidi et al., 2011).

1.1.2 Neurogenesis in the olfactory system

1.1.2.1 SEZ as the stem cell niche

The structure of the adult SEZ (also referred to as subventricular zone (SVZ) in literature) and the maturation of cells generated by neural precursors harboured by it, differs massively from the dentate gyrus (Fig. 1-4). However, also in this region, the radial glia-like cells are regarded as being the aNSC (Doetsch et al., 1999a; Doetsch et al., 1997; Mirzadeh et al., 2008). They are thought to express markers such as GFAP (Doetsch et al., 1999a; Garcia et al., 2004) and GLAST (Mori et al., 2006; Ninkovic et al., 2007; Platel et al., 2009) (Tab. 1-1). The aNSCs lie in the centre of a pinwheel-like structure formed by multi-ciliated ependymal cells, which line the walls of the ventricles (Fig. 1-5B). It has one Prominin+ immobile cilium (Beckervordersandforth et al., 2010) that is in contact with the cerebrospinal fluid (CSF) in the lateral ventricle (Beckervordersandforth et al., 2010; Doetsch et al., 1999b; Mirzadeh et al., 2008) and its basal process touches blood vessels (Mirzadeh et al., 2008). These cells are capable of repopulating the niche after depletion of all dividing cells (Doetsch et al., 1999b). The other subgroup of the GFAP+ astrocytic cells (B2 cells in Fig. 1-5) is located close to the striatal parenchyma (Ihrie and Alvarez-Buylla, 2011; Shen et al., 2008). Figure 1-5B depicts this special architecture.

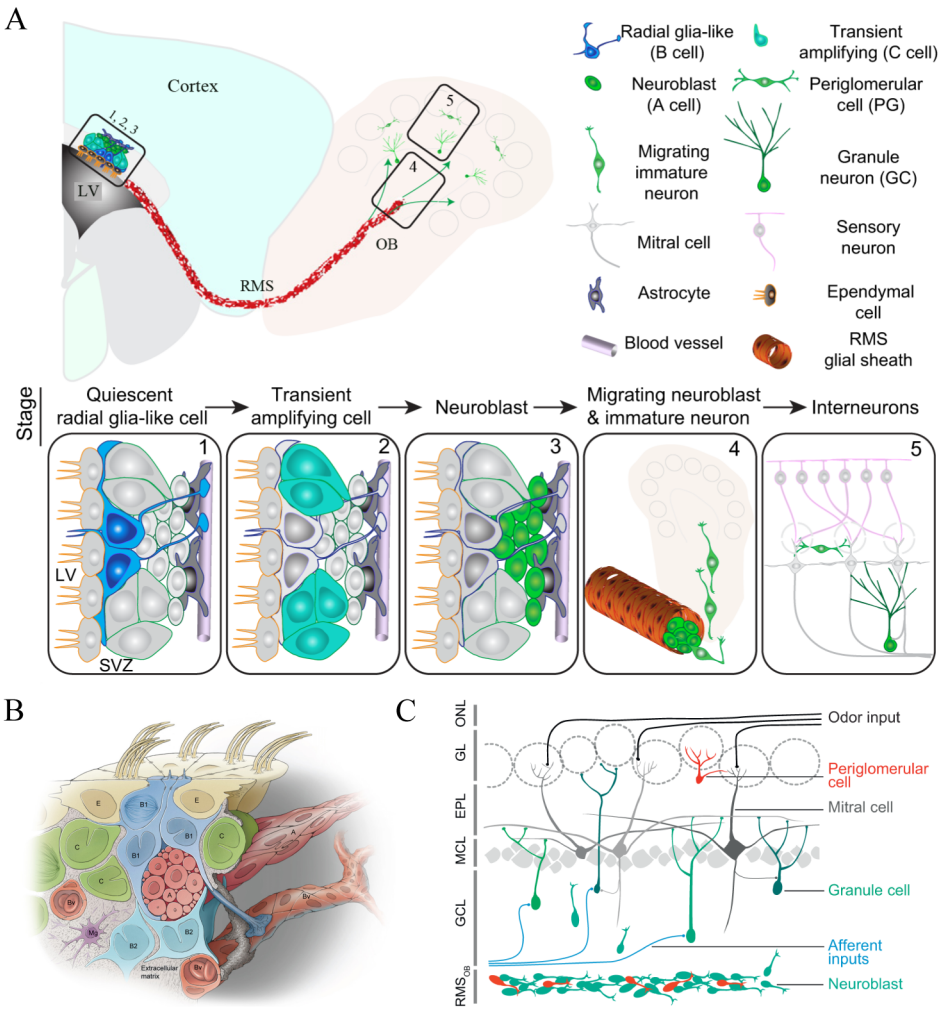

Figure 1-5. Neurogenesis in the olfactory system.
Neurogenesis occurs at the lateral wall of the lateral ventricle. Located underneath the ependymal layer, the SEZ (A) harbours aNSCs (A1) that divide and give rise to transit-amplifying precursors, TAPs (A2). These TAPs proliferate and in turn generate NBs (A3) which migrate ensheated in a glial tube in the (RMS) (A4) towards the OB where they integrate into the already existing neuronal network (5).
(B) shows a schematic drawing of the SEZ, with radial astrocytes (depicted in blue, B1) in the centre of a pinwheel-like structure formed by ependymal cells (depicted in beige). The long process of the radial cells is in contact with blood vessels (depicted in red, Bv). (C) illustrates the structure of the OB. The olfactory nerve layer (ONL) harbours the axons of the primary sensory neurons, which are in contact with mitral cells (depicted in dark grey) in the glomerular layer (GL). The cell bodies of these neurons are located in the mitral cell layer (MCL). Periglomerular cells (PGNs), located in the GL and granule cells in the granule cell layer (GCL), are being newly generated in the adult brain. The granule cells can be subdivided into superficial and deep granule cells (dGCs), the last ones are located in the deeper part of the GCL and their dendrites only reach into the deeper part of the epiplexiform layer (EPL). The RMS is located in the centre of the OB and contains newly generated and migrating NBs. Tufted cells are not depicted here.
(A) LV: lateral ventricle; OB: olfactory bulb; RMS: rostral migratory stream; SVZ: subventricular zone; (B) A: NBs; B1: aNSC; B2: multipolar astrocytes; C: TAPs; E: ependymal cells; Bv: blood vessel. (C) ONL: olfactory nerve layer; EPI: epiplexiform layer; GCL: granule cell layer; GL: glomerular layer; MCL: mitral cell layer.
(A) *modified from Ming and Song, 2011* (Ming and Song, 2011). (B) *modified from Ihrie et al., 2011* (Ihrie and Alvarez-Buylla, 2011) (C) *modified from Breton-Provencher, 2012* (Breton-Provencher and Saghatelyan, 2012).

Areas of the ventricle, where adult neurogenesis occurs, are the lateral, anterior and medial wall (Mirzadeh et al., 2008) and the dorsal wall (Brill et al., 2009; Ventura and Goldman, 2007) of the lateral ventricle. To some extent cells capable of producing neurons are also present in the RMS (Alonso et al., 2008; Hack et al., 2005; Merkle et al., 2007).

The SEZ differs from the dentate gyrus because of its complex structure, but also the maturation process of its progeny is very distinct: The aNSC slowly divides and gives rise to transit-amplifying progenitors (TAPs) (Doetsch et al., 1999a). These cells amplify very rapidly and express markers like Mash1 (Ascl1) and Dlx (Doetsch et al., 2002; Parras et al., 2004) and then give rise to NBs which express markers like Doublecortin (Dcx) and polysialylated neuronal cell adhesion molecule (PSA-NCAM) (Ihrie and Alvarez-Buylla, 2011; Whitman and Greer, 2009). However these markers are not 100% cell specific, it rather seems that there is a smooth transition of the expression of different markers. NBs for example can be labelled with antibodies recognising Dlx and Mash1 (Parras et al., 2004) as well. In cell culture another intermediate step in the lineage progression has been described. Here the slow dividing aNSC have shown to symmetrically divide to fast proliferating astroglia cells which in turn divide asymmetrically by giving rise to another astroglia and a TAP or divide symmetrically producing two TAPs (Costa et al., 2011).

These NBs migrate tangentially in chains, ensheated in an astrocytic tube (Doetsch et al., 1997; Jankovski and Sotelo, 1996; Lois et al., 1996; Peretto et al., 1997) in the RMS. For travelling the distance of 3-5 mm (Lois and Alvarez-Buylla, 1994) to the OB in mice, it takes them between 2-7 days (Petreanu and Alvarez-Buylla, 2002) or 10-12 days in the rat (Belluzzi et al., 2003).

1.1.2.2 The olfactory bulb and its cell types

The OB itself is a very complex structure (Fig. 1-5C). It is the place where the sensory information of different odours is processed and transferred. It consists of 6 layers, which harbour different cells and their processes. In the olfactory nerve layer (ONL) the axons of the primary sensory neurons are located (Whitman and Greer, 2009). They contact dendrites of mitral or tufted cells in the glomerular layer (GL).

Olfactory nerves with the same odour receptor project only into one or two glomeruli (Feinstein and Mombaerts, 2004; Mombaerts et al., 1996). The projection neurons of the OB, mitral cells, as well as tufted cells get information from one glomerulus (Treloar et al., 2002). Thus the specific odour information is kept and projected by these secondary sensory neurons mostly into the piriform cortex (Whitman and Greer, 2009). The other cell types present in the OB are Periglomerular neurons (PGNs) and granule cells (GCs). These interneurons modulate mitral and tufted cells and many of these are continuously produced in the adult mammalian brain (Ming and Song, 2011).

PGNs modulate the information within, as well as in between, glomeruli. They can be subdivided into three major groups: tyroxine hydroxylase positive (TH+), Calbindin+ (CalB) and calretinin+ (CalR) cells. All of the TH+ and CalB+ and 65% of the CalR+ cells were also GABAergic (Kosaka and Kosaka, 2007). Recently, a small subset of neurons, glutamatergic juxtaglomerular cells, has been found to also be adult generated (Brill et al., 2009).

The anaxonic (Price and Powell, 1970), mostly GABAergic (Breton-Provencher and Saghatelyan, 2012) GCs can be found in the granular cell layer (GCL) and make up the biggest neuronal population of the OB (Whitman and Greer, 2009). They are thought to enhance contrast of odour perception (Shepherd et al., 2007). According to their location within this layer they can be classified as superficial and deep GCs (sGCS and dGCs). Whereas sGCs form dendrodendritic synapses with tufted cells in the more superficial part of the EPL, dGCs interact with mitral cells in the deeper part of the EPL (Breton-Provencher and Saghatelyan, 2012; Whitman and Greer, 2009).

1.1.2.3 Migration and maturation of NBs in the OB

Approximately 30.000 NBs migrate via the RMS into the OB each day (Alvarez-Buylla et al., 2001). When the NBs have reached the OB, they migrate radially into the GCL or GL and mature (Whitman and Greer, 2009). Only 5% of new born neurons differentiate into PGNs, the rest becomes GCs (Lledo and Saghatelyan, 2005). For these GCs the whole process takes about 15-30 days (Petreanu and Alvarez-Buylla, 2002) in the mouse, whereas for PGNs this process take up to 4 weeks (Carleton et al., 2003). The GCs and PGNs have been shown to functionally integrate into the neuronal circuit (Belluzzi et al., 2003; Carleton et al., 2003). However, not all neurons integrate. A large proportion of newly born cells undergo apoptosis in between 15-45 days after their birth (Lemasson et al., 2005; Petreanu and Alvarez-Buylla, 2002). Some new interneuronal subtypes also have been observed, however their potential function in the circuit is still under discussion (Merkle et al., 2014).

The function of these other newly generated neurons have been implicated in several functional contexts. On the one hand, these cells are more sensitive to odour input, which could make them more adaptable to changes in the environment compared to early born interneurons (Breton-Provencher and Saghatelyan, 2012; Sakamoto et al., 2014). On the other hand, this turnover is important for the maintenance and reorganisation of the olfactory network (Imayoshi et al., 2008). New neurons are continuously added to the GL, the proportion of neurons added to the GCL reaches a plateau over time and also contributes only to a small proportion of OB network (Ninkovic et al., 2007). This plateau-reaching addition mode is also

observed in the SGZ of the dentate gyrus in mice (Ninkovic et al., 2007). Here about 10% of GCs are being exchanged, compared to the majority of GCs in the human hippocampus (Spalding et al., 2013) and the majority of GCs in the OB (Imayoshi et al., 2008).

1.2 Heterogeneity of aNSC and new methods for analyses

Most of what has been discussed so far has been derived from analysis based on the population level. This means that when the properties of aNSCs were analysed with viruses or by using transgenic mouse lines, a whole population of aNSCs was labelled at the same time. This however does not allow the detection of heterogeneity of aNSCs.

An example of heterogeneity concerning aNSC is that there seem to be location-specific subsets of aNSCs along the wall of the lateral ventricle that produce only a certain subset of interneurons. Merkle et al. used an adenovirus, which infects cells only in a restricted area, to trace the progeny of aNSCs in different regions of the SEZ and showed that, for example aNSC located in the dorsal wall of the lateral ventricle, produce sGCs, as well as TH+ PGNs, whereas aNSCs in the ventral part of the SVZ produce dGCs and a CalB+ subset of PGNs (Merkle et al., 2007). Furthermore it was shown that also the RMS seems to harbour aNSCs which largely produce PGNs (Hack et al., 2005; Merkle et al., 2007) and cells in the dorsal wall of the lateral ventricle produce a small number of glutamatergic interneurons (Brill et al., 2009). Also after heterotopic transplantation of these cells, they continued to produce their original interneuron type, which suggests that this information is intrinsically set. Fig. 1-6 shows a summary of this regionalisation.

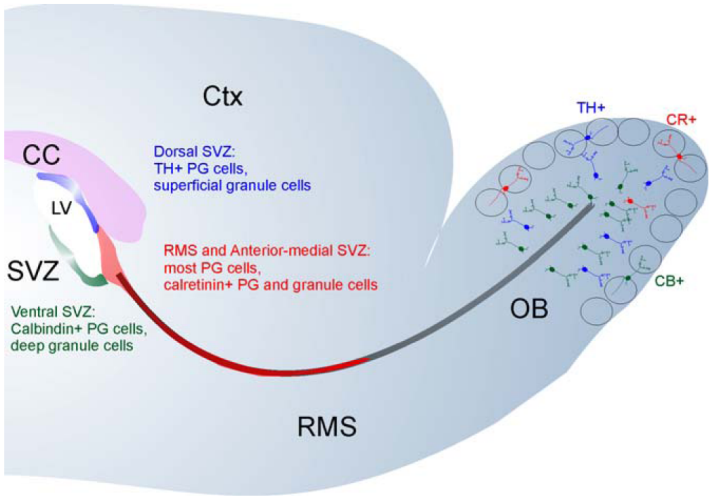

Figure 1-6. Regionalisation of aNSCs.
aNSCs in different regions of the walls of the lateral ventricle give rise to different interneuronal subtypes. Cells in the dorsal SEZ generate sGCs, but also to TH+ PGNs. Most of the PGNs and GCs arise from the RMS and the anterior-medial SEZ, whereas cells in the ventral SVZ generate CalB+ as well as dGCs. CC: corpus callosum; Ctx: cortex; LV: lateral ventricle; OB: olfactory bulb; RMS: rostral migratory stream; SVZ: subventricular zone; CR: calretinin; CB: calbindin; TH: tyroxine hydroxylase. *Modified from Whitman et al., 2009* (Whitman and Greer, 2009).

In the dentate gyrus the neurons produced are homogeneous (Lledo et al., 2008). However recent data showed that there also seems to be heterogeneity in the aNSC population. Lineage tracings of aNSCs in

the dentate gyrus performed by Encinas et al. showed that the aNSC are being used up (Encinas et al., 2011) whereas by clonal analyses of these cells properties such as self-renewal could be observed (Bonaguidi et al., 2011). The term "clonal analysis" refers to a method that allows the analysis at the single cell level. Bonaguidi *et al*., 2011 established this fate mapping technique by using Nestin-CreER^{T2}//Z/EG mice and a low dose of TAM for sparse labelling of aNSCs in the dentate gyrus. Their work was focused on the behaviour of the aNSC and they found that the cells labelled with their technique were able to produce cells of the neurogenic and astrocytic lineage hence being able of multilineage differentiation, but could also self-renew. Additionally, they also observed a big decrease of aNSCs within a clone over time but at the same time still observed clones with an aNSC that survived long-term (over 12 months). A study done with a similar mouse strain, however induced with a higher dose of TAM labelling many aNSCs at the same time, found that they decrease over time after rapid divisions and finally convert to astrocytes (Encinas et al., 2011).

Different theories have been generated to explain these differences, the first one being the different induction doses (Bonaguidi et al., 2012; Taylor, 2011), which could result in a selection of a certain subtype of neural progenitors (quiescent vs. active aNSCs). This example however makes clear, that the different approaches used to research neurogenesis in the mammalian brain in the past decades have a great influence on the way aNSC properties have been interpreted (Bonaguidi et al., 2012; DeCarolis et al., 2013). aNSCs expressing different markers (e.g. Nestin and GLAST) might actually reflect different heterogeneous subpopulations of aNSCs in the SGZ (DeCarolis et al., 2013), for example, a slow dividing aNSC and a fast proliferating astroglia progeny as it has been observed by Costa *et al.* (Costa et al., 2011). Whether such heterogeneity, beside the spatial regionalisation, exists also for aNSCs in the SEZ has to be elucidated by analysis of the progeny of a single aNSC in the SEZ.

That is why a clonal analysis technique was established in this thesis in order to sparsely label aNSCs in the adult SEZ of the murine forebrain.

1.3 Aims of this study

The present understanding of adult neurogenesis and their underlying aNSCs was either deduced from *in vitro* data or from population analysis *in vivo* (with viruses or other fate mapping techniques using transgenic mice). This generates a pitfall, since the data and properties obtained from analyses of a pool of aNSCs cannot be converted to explain the behaviour of a single aNSC. For example, Fig. 1-7 shows a schematic drawing of a certain number of progenitors being produced. By analysing NSCs at the population level, it cannot be known whether this number of progenitors was produced by few NSC generating many cells or by many NSCs capable of producing only a small cell number.

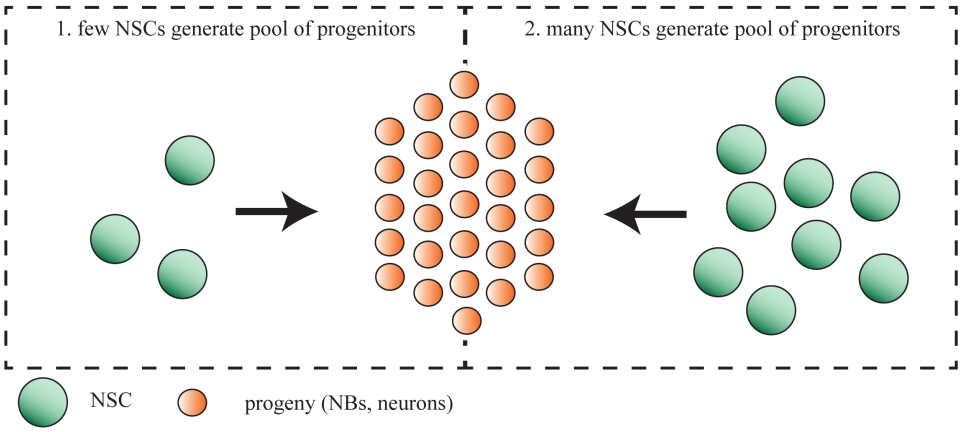

Figure 1-7. The problem of population analyses.
To generate a certain progenitor pool there are two possibilities: (1.) Few aNSC produce a large progeny, adding up to a certain cell pool or (2.) many aNSC produce a small progeny each, leading to the same amount of progeny.

The same applies for the generation of the diverse interneuronal subtypes. Since it has ben observed that the aNSCs are regionally specified, one possibility would be that there are certain subsets of NSCs that are only capable of producing a single neuron subtype (Fig. 1-8.1). However, it is also possible that a single NSC generates a heterogeneous population of interneurons, because their neuronal fate is set at a later stage (e.g. TAP- or NB-level) (Fig. 1.8-2 and 3).

The aim of this thesis was to gain insights into the progeny of a single aNSC in the SEZ of the lateral ventricle. Key questions that need to be answered are the following:

1. What is the progeny of a single aNSC?
    a. How big is the size of progeny produced?
    b. What is the temporal profile of the aNSC and their progeny?
    c. Are there multiple waves of neuron production?
    d. Do aNSC self renew?
    e. Is there an exhaustion of the aNSC?
2. Does a single aNSC generate a homogeneous neuron population? (Fig. 1-7. 1)

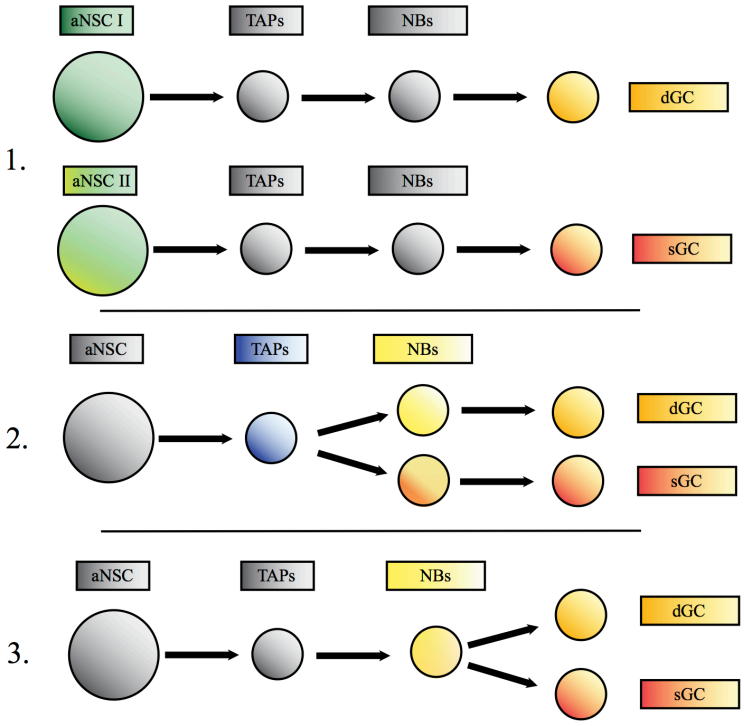

Figure 1-8. Neuronal diversity.
A single aNSC is only capable of producing one interneuronal subtype (1.). Different neurons are being generated by a single aNSC and the fate is being set at the TAP-level (2.) or the NB-level (3.). aNSC: neural stem cell; dGC: deep granule neuron; sGC: superficial granule neuron.

All these questions taken together, ask for a new method of analysis, which is why a new lineage tracing technique in the SEZ was established. It enables the users to analyse the progeny of single aNSCs in the adult murine brain. In order to achieve this, the TAM-inducible GLAST^{CreERT2} mouse (Mori et al., 2006) was crossed with the multicolour Confetti reporter mouse line (Snippert et al., 2010). Since the CreERT2 fusion protein is so sensitive to TAM (Indra et al., 1999), it can also be used for lineage analysis at the clonal level. By titrating the dose of TAM, which was intraperitoneally (IP) injected, aNSCs in the dentate gyrus of the hippocampus and the SEZ of the lateral ventricle could be sparsely labelled. This method was then used to analyse the behaviour of single aNSCs of the SEZ, as well as their progeny over the course of time.

2 Material

2.1 Equipment

Equipment	Company (name)
Centrifuge	Eppendorf Centrifuge (5415D)
Heater	Eppendorf (Thermomixer compact)
Incubator	Shel Lab (1012 Hybridization oven)
Microwave	Severin
Minitube shaker	VWR (Galaxy mini)
Perfusion pump	Gilson (Minipuls 3)
Refrigerators and Freezers	Liebherr and Siemens
Running chambers	Harnischmacher and Biorad
Scales	Kern (470)
Scales	Kern (ABS)
Shaker	Heidolph (Unimax 1010)
Thermocycler	Biorad (My Cycler)
Ultrasoundbath	VWR (Ultrasound)
Vibratome	Microtome (HM 650 V)
Vortex	Neolab (7-2020)
Waterbath	GFL

2.2 Consumables

Consumables	Company
24-well plates	Falcon multiwell
Consumables	Company
Cover slips	Menzel Deckgläser
Eppendorf tubes	Eppendorf
Glass slides	Elka
Gloves	Nitrile (meditrade and KimTech)
Parafilm	Bemis (PM99)
PCR tubes	Thermo Scientific (AB-0266)
Syringes	Braun Omnifix-Tuberkulin
Tubes	Sarstedt

2.3 Kits

Kits	Company	Catalogue number
Taq PCR Core Kit	Qiagen	201223

2.4 Chemicals

Chemical	Company	Ordering number
0,9% NaCl solution	Braun	
2 - Propanol	Merck	1.09634
Acetic acid	Merck	1.00063
Agarose	Biozym	870055
Aqua Poly/Mount	Polyscience Inc.	18606
BrdU (5-bromo-2'-deoxyuridine)	Sigma	B5002-5

Corn oil	Sigma-Aldrich	08267
DAPI (4',6-diamidino-2-phenylindol)	Sigma	D9564
DNA Ladder (Generuler 1kb)	Thermo Scientific	SM0311
EDTA	Merck	1084180250
Ethanol	Merck	1.00983
Ethidium bromide	Roth	2218
Glycerol	Roth	3783
Hydrochloric acid	Merck	1.00319
Normal goat serum (NGS)	Biozol	S-1000
Orange G	Sigma	O-3756
Paraformaldehyde (PFA)	Roth	0335.3
PCR dNTP Mix (25µmol each)	Thermo Scientific	R1121
Potassium chloride	Merck	4936
Potassium dihydrogen phosphate	Merck	104873
Proteinase K	Roth	7528.2
SDS (Natriumlaurylsulfate)	Roth	2326.2
Sodium chloride	Merck	1.06404
Sodium hydrogen phosphate	Merck	T876
Sodium hydroxide	Roth	6771.1
Sodium tetraborate	Merck	1.06306
Tamoxifen (>99%)	Sigma-Aldrich	T5648-SG
Tris Base	Merck	1.08382
Triton-X100	Roth	3051

2.5 Anaesthesia

Pharmaceuticals	**Company**
Ketavet 100 mg/ml Ketaminhydrochlorid	Pfizer
Rompun 2% Xylazin	Bayer Health Care

2.6 Buffers and solutions

2.6.1 General

2.6.1.1 10x PBS

10x PBS (Phosphate buffered saline) 0,1 M, pH 6.8	
1379.3 mM	NaCl
27.0 mM	KCl
80.8 mM	$Na_2HPO_4 \cdot 7H_20$
14.7 mM	KH_2PO_4
in miliQ water, adjust pH with HCl	

A 5 l stock solution of 10x PBS was prepared by dissolving 400 g NaCl, 10 g KCl, 72 g $Na_2HPO_4 \cdot H_20$ and 10 g KH_2PO_4 in milliQ water. pH was adjusted with HCl. By diluting 1:10 a 1x PBS solution with a pH of 7.4 was achieved.

2.6.2 DNA preparation and genotyping PCR

2.6.2.1 Lysis buffer and Proteinase K

Lysis Buffer	
0.1 M	Tris HCl (pH 8.5)
5 mM	EDTA
0.2 %	SDS
200 mM	NaCl
	in milliQH_20
100 µg/ml	Proteinase K

For 1 l of Lysis Buffer mix, 100 ml Tris HCl (pH 8.5), 10 ml 0.5 M EDTA, 20 ml 10% SDS, 200 ml 1 M NaCl were dissolved in 660 ml milliQ water. For every 500 µl of Lysis Buffer 5µl of 10 mg/ml of Proteinase K were added.

2.6.2.2 TAE buffer

10x TAE, pH 6.0	
242 g	Tris Base
57 ml	Acetic acid
100 ml	0,5 M EDTA

The ingredients were dissolved in milliQ water and the pH is adjusted with acetic acid.

2.6.3 Tissue preparation

2.6.3.1 Tamoxifen

Tamoxifen (20 mg/ml)	
100 mg	Tamoxifen
5 ml	Corn oil (37°C)

The TAM should be protected from light at all times. 5 ml of hot (~37°C) corn oil are added to the 100 mg of Tamoxifen and an ultrasound bath was used to dissolve it with intermittent vortexing. Storing at 4°C.

Tamoxifen (1 mg/ml)	
0.5 ml	Tamoxifen (20 mg/ml, corn oil)
9.5 ml	Corn oil (37°C)

2.6.3.2 BrdU for short pulse

5-Bromo-2′-deoxyuridine (BrdU)	5 mg/ml (dissolved in PBS)

2.6.3.3 Anaesthesic solution

Anaesthetic solution	
5 mg/ml	Ketavet
0.1%	Rompun

0.5 ml of 100 mg/ml Ketavet and 0.5 ml of 2% Rompun were diluted in 0.9% NaCl solution.

2.6.3.4 4% PFA

4% Paraformaldehyde (PFA), pH 7.4 at RT	
50 ml	10x PBS
400 ml	miliQ H_2O
20 g	PFA
1-2 tablets	NaOH
50 ml	miliQ H_2O

For 500 ml of 4% PFA, 20 g PFA are dissolved at low temperature in miliQ H_2O. The pH was carefully adjusted in between values of 7.2 and 7.4 with HCl and 10xPBS was quickly added after having reached the pH. Additional miliQ H_2O was added to fill up the volume to 500 ml. At the end the solution was filtered.

2.6.4 Immunohistochemistry

2.6.4.1 Blocking/dilution buffer

Blocking solution	
0.5%	TritonX
10.0%	NGS

2.6.4.2 DAPI

4′,6-Diamidin-2-phenylindol (DAPI)	
200 µg/ml	4′,6-Diamidin-2-phenylindol (DAPI)

DAPI was used at a dilution of 1:1000 (0.2 µg/ml).

2.6.4.3 Borate buffer

Borate Buffer (0.1M), pH 8.5	
2.01 g	$Na_2B_4O_7$
100 ml	milliQ H_2O

2.7 PCR Primers

2.7.1 Confetti Primers

Forward primer confetti	Rosa26 confetti fwd	5'-GAA TTA ATT CCG GTA TAA CTT CG-3'
Reverse primer confetti	Rosa26 confetti rev	5'-AGA GTA TAA AAC TCG GGT GAG C-3'

Forward primer WT	Rosa26 WT fwd1	5'-CTC CTG GCT TCT GAG GAC C-3'
Reverse primer WT	Rosa26 WT rev2	5'-CCA GAT GAC TAC CTA TCC TC-3'

Fwd… forward
WT… Wild type

2.7.2 Emx1^{Cre} Primers

Forward primer	Emx1_forward22	5'-GTG AGT GCA TGT GCC AGG CTT G-3'
Reverse primer	Emx1_reverse22	5'-TGG GGT GAG GAT AGT TGA GCG C-3'
Cre	TestCre1	5'-GCG GCA TAA CCA GTG AAA CAG C-3'

2.7.3 GLAST^{CreERT2} Primers

Forward primer	GLAST F8	5'-GAG GCA CTT GGC TAG GCT CTG AGG A-3'
Reverse primer	GLAST R3	5'-GAG GAG ATC CTG ACC GAT CAG TTG G-3'
Cre-ERT2 specific primer	CER 1	5'-GGT GTA CGG TCA GTA AAT TGG ACA T-3'

2.8 Hard- and Software

Hardware	
Confocal microscopes	Olympus FV1000 Leica TCS SP5
Epifluorescent microscope	Axioplan 2 Imaging

Software
Olympus FV1.7 viewer software Version 4.0b
FiJi
Microsoft Excel
Photoshop CS5
Illustrator CS5

3 Methods

3.1 Animals

All animals used were kept in the animal facility of the Helmholtz Zentrum Munich at a 12h dark-light circle. In order to perform the experiments the following mouse strains were used.

3.1.1 Mouse strains

R26R-Confetti reporter mice:

A reporter line, which includes the Brainbow 2.1 (Livet et al., 2007) cassette driven by a CAGG promotor. LoxP sites flanking four different fluophores: Yellow fluorescent protein (YFP), cyan fluorescent protein (CFP), GFP and red fluorescent protein (RFP) (Fig. 4-2) (Snippert et al., 2010).

$Emx1^{Cre}$ mice:

The Cre recombinase gene was inserted into the Emx1 locus, a homebox gene expressed in the dorsal telencephalon from embryonic day 10 (E10) till adulthood (Gulisano et al., 1996; Iwasato et al., 2000).

$GLAST^{CreERT2}$ mice:

A TAM inducible Cre recombinase was inserted into the GLAST locus (Mori et al., 2006).

3.1.2 Genotyping

3.1.2.1 DNA extraction

Because different mouse strains and crossings of these were used in the experiments, genotyping of tail clips was necessary. In order to extract the DNA for PCR, small pieces of tails were collected from ear-marked, 4-5 week old animals in 1.5 ml eppendorf tubes. After adding 500 µl of Lysis buffer and 5 µl of 10 mg/ml of Proteinase K the tail clips were kept at 55°C in an incubator over night. After the digestion, the tubes were vortexed and then centrifuged at 16,100 x g for 20 min and the supernatant was poured into new tubes with 500 µl of Isopropanol. After mixing well, the tubes with the precipitated DNA were again centrifuged for 5 min at 16,100 x g . The excess fluid was discarded and the tubes with the DNA pellet were left to dry. After addition of 250-300 µl of milliQ water to the pellets, the tubes were placed again into a 55°C hot incubator over night in order to dissolve the DNA.

3.1.3 Polymerase Chain Reaction (PCR)

For the PCRs of the R26Confetti, Emx1^{Cre} and GLAST^{CreERT2} mice the following mixtures and Thermocycler conditions were used.

	Confetti	**Emx1^{Cre}**	**GLAST^{CreERT2}**
10x buffer	2.5 µl	2.5 µl	2.5 µl
Q solution		5.0 µl	5.0 µl
dNTPs	0.5 µl	0.5 µl	0.5 µl
Primer confetti fwd/WT fwd	0.5 µl		
Primer confetti rev/WT rev	0.5 µl		
Primer Emx1 fwd		0.5 µl	
Primer Emx1 rev		0.5 µl	
Primer TestCre1		1.0 µl	
Primer GLAST F8			1.0 µl
Primer GLAST R3			1.0 µl
Primer CER 1			1.0 µl
MiliQ water	18.8 µl	12.8 µl	11.8 µl
Taq	0.2 µl	0.2 µl	0.2 µl
DNA	2.0 µl	2.0 µl	2.0 µl

	Confetti		**Emx1^{Cre}**		**GLAST^{CreERT2}**	
	Temp.	**Time**	**Temp.**	**Time**	**Temp.**	**Time**
Initialising step	96°C	5 min	94°C	4 min	94°C	5 min
Denaturation step	96°C	30 s	94°C	30 s	94°C	45 s
Annealing step	58°C	45 s	64°C	1 min	55°C	45 s
Elongation step	72°C	1 min	72°C	30 s	72°C	45 s
Cycles	35		36		35	
Final elongation	72°C	5 min	72°C	2 min	72°C	2 min
Final hold	20°C	∞	20°C	∞	20°C	∞
Fragment size WT band: Recomb. Band:	 270 bp 400 bp		 200 bp 500 bp		 700 bp 400 bp	

3.1.3.1 Agarose electrophoresis of DNA

The amplified DNA fragments were separated by gel electrophoresis. Agarose was dispersed in 1x TAE buffer by heating in a microwave to receive a 1% gel. 5 µl Ethidium Bromide (EtBr) of a concentration of 10 µg/ml were carefully added to 100 ml of cooled down agarose to receive a final concentration of 0.05% before the gel was poured into a cast and left to harden. The gel was placed into a horizontal gel chamber filled with 1x TAE buffer. 1x Orange G was added to the PCR products before 20 µl of it were loaded into the wells of the gel. A 1 kb DNA ladder was used for comparison. The electrophoresis was run at approximately 120V for about 20-25 minutes until the PCR products were well separated. The DNA bands were then visualised by UV-light and photographed (Fig. 3-1).

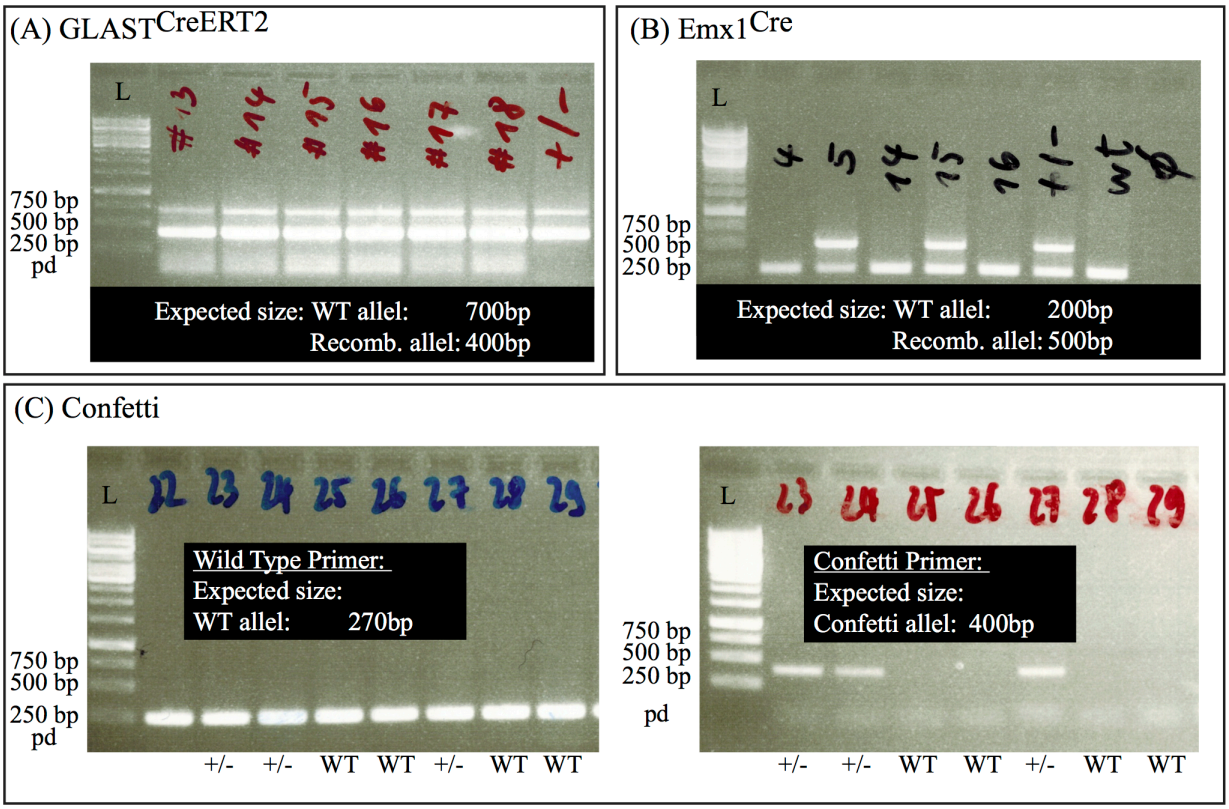

Figure 3-1. Gel electrophoresis of GLAST^{CreERT2}, Emx1^{Cre} and Confetti genotyping.
(A) represents the DNA bands received after performing the PCR with the GLAST^{CreERT2} primers, (B) Emx1^{Cre} and (C) with the two separate master mixes of the Confetti genotyping. bp, base pairs; L, DNA ladder; pd, primer dimmer; wt, wild type, +/-, heterozygote.

3.2 Animal experiments

3.2.1 Tamoxifen treatment

8-10 weeks-old, double heterozygous animals for GLAST^{CreERT2} and Confetti were intraperitoneally (IP) injected with TAM of different concentrations ranging from a single injection with 5 µg/g body weight up to 5 injections twice a day with 40 µg/g body weight. Further description of the titration method can be found in the "method establishment" part of the results chapter.

3.2.2 BrdU treatment

BrdU being an analogue of thymidine, is incorporated into newly synthesised DNA. By treating mice with BrdU 1 h prior to their sacrifice, presumably only fast cycling cells are being labelled by the analogue. For such a short pulse, the animals were IP injected with 50 µg/g body weight BrdU.

3.2.3 Anaesthesia

Prior to the perfusion, the animals were anaesthetised by IP injection of a solution of 5 mg/ml Ketamine and 0.1% Rompun (100 µg/g body weight Ketamine and 20 µg/g body weight Rompun).

3.2.4 Perfusion

Anaesthetised animals were perfused according to the temporal experimental scheme. A thoracotomy was performed on mice that were fixed on a polystyrene block. A needle, attached to a minipump system was inserted into the left ventricle and the right atrium was opened. First, PBS was pumped through the vascular system before the solution was changed to 4% PFA in PBS. Approximately 100-150 ml of PFA were used for the perfusion before the brains were dissected and post-fixed in 4% PFA for 1-4 h at 4°C.

3.3 Tissue preparation

3.3.1 Sectioning

For further processing, the hemispheres were embedded in a 3% agarose gel before they were sequentially cut in a sagittal orientation by using a vibratome (Fig. 3-2A). In some cases, the OB was cut in a coronal plane (from now on indicated by an asterisk) whereas the remaining hemisphere was cut sagittally (Fig. 3-2A). The 80 µm thick, free-floating sections were kept in their original order in a 24-well plate prior to immunohistochemistry.

3.3.2 Immunohistochemistry

3.3.2.1 General method

Immunohistochemistry was used for detecting and visualising antigens. In this method primary antibodies bind to target antigens. Since the antibody was raised in a specific animal, a secondary antibody can be used to recognise that species-specific part of the antibody. In this case these secondary antibodies are labelled with a fluorophore, which enables the visualisation with fluorescence microscopes. Another method was to use a secondary antibody, which was coupled with several biotin molecules. These could then be recognised by streptavidin-fluorophore-conjugate, also enabling signal detection.

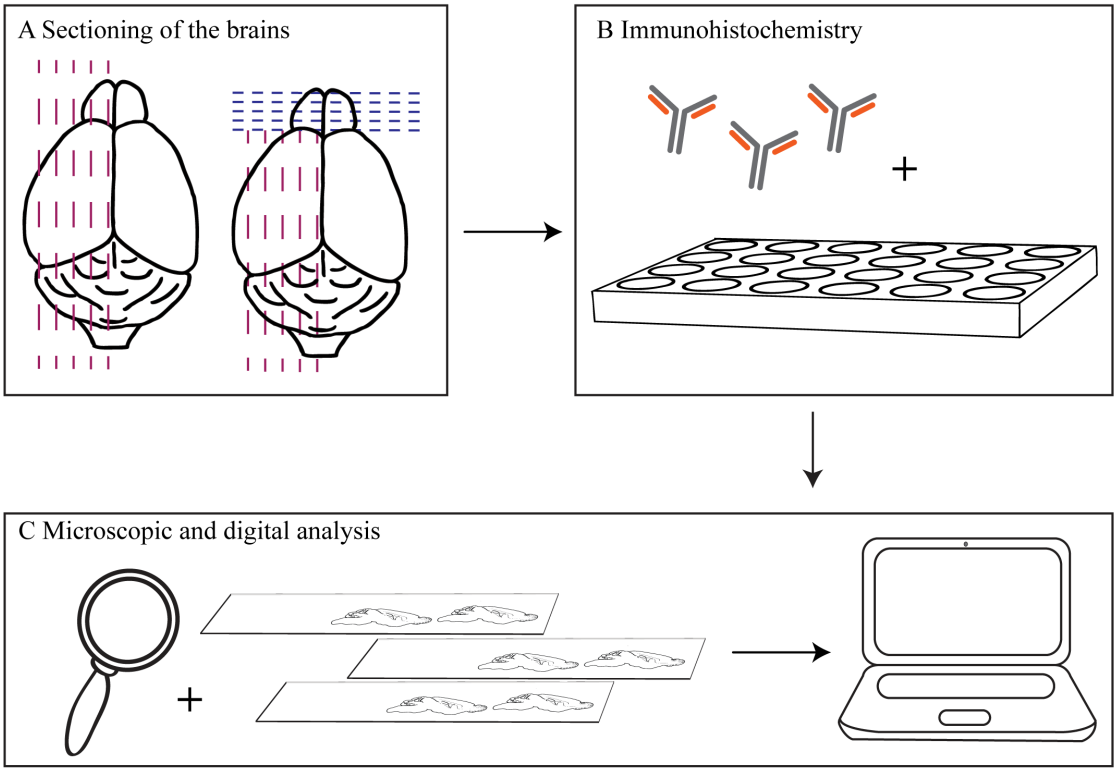

Figure 3-2. Algorithm of tissue preparation.
An overview of the usual tissue preparation is depicted. Brains were sequentially cut in 80 µm thick sections with a vibratome. If not stated otherwise the whole hemisphere was cut in a sagittal orientation (A). Sometimes the OB was first cut coronally and the rest of the hemisphere was sectioned sagittally. The resulting floating sections were kept in order by placing them into a 24-well plate (B) before being used for immunohistochemistry. The sections were mounted on glass slides and analysed using a confocal microscope (C). The pictures obtained from the scanning were processed with FiJi (Schindelin et al., 2012).

Free floating sections of PFA fixed hemispheres were used for this procedure. Antibodies were diluted in a solution of 0.5% TritonX-100 in 1x PBS. Because of the vast majority of secondary antibodies used in this thesis were raised in goat, blocking of the sections was done with 10% of normal goat serum to prevent non-specific binding. The sections were incubated with the primary antibody for one night at 4°C. After careful washing with 1x PBS, the secondary antibody was added for 2 h at room temperature. This protocol was used for trial stainings and the 32h-analysis (high dose), which will be referred to later on.
Because it was observed that the first protocol lead to uneven staining results, which could in theory lead to problems with visualising the clones, the procedure was slightly altered in order to receive a better penetration of the antibodies. Therefore the primary antibodies were left with the sections for the course of two nights and the secondary antibodies for one night at 4°C. The biotin-conjugated and streptavidin-coupled antibodies, as well as the counterstaining with DAPI were treated the same way as the secondary antibodies and were kept with the sections for 1 night at 4°C. In between the different incubation times, washing steps consisting of 3-4 times washing with 1x PBS for 45-60 minutes were performed. Tab. 3-1 and 3-2 show an overview of all antibodies and dilutions used in this thesis.
For the clonal analysis the sequential sections were always treated with a combination of chick anti-GFP, rabbit anti-RFP, guinea pig anti-Dcx and mouse anti-GFAP for primary antibodies and anti-chick-A488, anti-rabbit-A546, anti-mouse A647, biotinylated anti-guinea pig and streptavidin-A405 and DAPI (Dcx and DAPI being in the same channel) for secondary antibodies.

After finishing the immunohistochemical staining, the sections were mounted with a paintbrush on glass slides. A mounting medium, which enhances and retains fluorescent signal, was added on top of the sections before slides were covered with the coverslip.

3.3.2.2 BrdU staining

In order for the BrdU antibody to bind the DNA incorporated BrdU, nuclear DNA had to become accessible. This is why the sections had to be treated with 2 N HCl for 30 minutes at room temperature (RT) to denature the DNA and to receive single strands where the antibody can bind to its destination. The sections were then buffered by using 0.1 M Borate buffer for two to three times for 15 min. Afterwards the sections were washed with 1x PBS and incubated with the BrdU antibody dilution.

3.4 Analyses

3.4.1 Microscopic and digital analyses

The murine brain sections were analysed by using the Axioplan 2 fluorescence microscope and the laser scanning confocal microscopes (Olympus FV1000 or Leica TCS SP5). The software used to analyse the pictures taken was Fiji (ImageJ 1.47c) (Schindelin et al., 2012).

3.4.2 Statistical Analyses

The arithmetic mean:

$$\bar{x} = \frac{1}{n} \cdot \sum_{i=1}^{n} x_i$$

The median:

$$\text{n is odd:} \quad x_{med} = x_{\frac{n+1}{2}}; \qquad \text{n is even:} \quad x_{med} = \frac{1}{2} \cdot \left(x_{\frac{n}{2}} + x_{\frac{n}{2}+1} \right)$$

And the standard deviation of the mean:

$$s = \sqrt{\frac{1}{n-1} \cdot \sum_{i=1}^{n} (x_i - \bar{x})^2}$$

And the standard error of the mean:

$$SE_{\bar{x}} = \frac{s}{\sqrt{n}}$$

were calculated using Microsoft Excel. One hemisphere analysed represents the value of one n.

Table 3.1. Overview of primary antibodies

Primary Antibodies

Recognised Antigen	Host-animal (Ig subtype)	Company	Dilution and pre-treatment conditions*
BrdU	rat (IgG2a)	Abcam (ab6326)	1:100, 30 min 2N HCL, 2x 15 min Borate Buffer pH 8.5, 3x10 min PBS
Dcx	guinea pig	Millipore (#AB2253)	1:2000
GFP	chicken	Aves Lab (#GFP-1020)	1:1000
	rabbit	eBioscience (14-6774-81)	1:1000
GFAP	mouse (IgG1)	Sigma-Aldrich (G3893)	1:500
RFP	chicken	Milipore (AB3528)	1:1500
	rabbit	Rockland (600-401-379)	1:1500

*if different from general instructions

Table 3.2. Overview of secondary antibodies

Secondary antibodies

Antibody	Host species	Label	Company	Dilution
anti-chicken IgG	goat	Alexa488	Invitrogen (A11039)	1:500
		Alexa546	Invitrogen (A11040)	1:500
anti-rabbit IgG	goat	Alexa488	Invitrogen (A11008)	1:500
		Alexa546	Invitrogen (A11010)	1:500
anti-mouse IgG	donkey	Alexa647	Invitrogen (A31571)	1:500
anti-guinea pig IgG	goat	Alexa647	Invitrogen (A21450)	1:500
	goat	biotinylated	Vector laboratories (BA-7000)	1:200
anti-rat IgG	goat	Alexa647	Invitrogen (A21247)	1:500
	rabbit	biotinylated	Vector laboratories (BA-4001)	1:200
streptavidin		Alexa405	Invitrogen (S32351)	1:1000
		Alexa647	Invitrogen (S21374)	1:1000

4 Results

4.1 Establishing the method of the clonal lineage tracing

Fate mapping is a method that has been used in biology for decades. By marking a specific cell type with viruses, dyes or by using a transgenic mice, it is possible to trace the progeny that the cell produced (Legue and Joyner, 2010). With the introduction of inducible transgenic mice, the hurdle of researching the adult brain with transgenic animals was overcome, because it allows the recombination of the reporter and hence the labelling of cells at a certain time point (Ninkovic and Gotz, 2013). Fate mapping can be performed at the population level, for example by using GLAST^{CreERT2} (Ninkovic et al., 2007) or Nestin-XFP and Nestin-CreER/Z/EG mice (Encinas et al., 2011) in the SEZ or the dentate gyrus. But it can also be used to trace the lineage of a single aNSC.

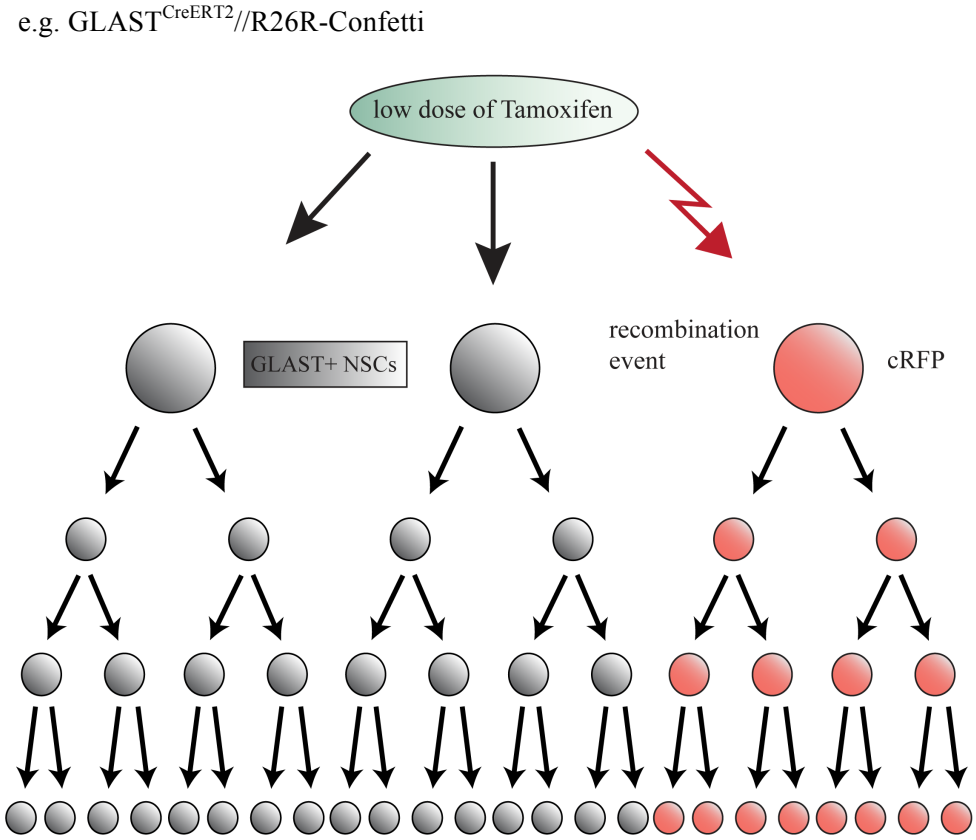

Figure 4-1. Clonal lineage tracing.
Double heterozygous mice for the inducible CreERT2 driven by a specific promoter (e.g. GLAST^{CreERT2}) and a reporter cassette (e.g. Confetti) are induced by low doses of TAM. Very sparse recombination of the reporter occurs. In this case the Confetti cassette recombined to result in the expression of cRFP in the GLAST+ cell. This labelling is inherited by the cell's progeny and enables tracing of these cells over time.

The theory behind the lineage tracing is, that by combining an inducible CreERT2 mouse with a floxed reporter mouse line, it is possible to cause recombination only in the cells that express the promoter driving the CreERT2 construct. Once the Cre recombinase is being induced with TAM (Fig. 4-1), it can catalyse recombination in between the floxed reporter cassettes and enable the expression of fluorescent proteins, labelling the respective starting cell (Fig. 1-3). This label is inherited by the progeny of the induced cell (expressing the promoter) after division (Fig. 4-1, small red cells), enabling to trace these

cells. With the titration of the TAM, it is possible to label few up to single cells, as it has been shown, for example in the intestine (Ritsma et al., 2014; Snippert et al., 2010) or the dentate gyrus (Bonaguidi et al., 2011).

4.1.1 R26R-Confetti reporter

In order to establish an analysis to investigate the behaviour of aNSCs, the new "Confetti" multicolour reporter (Snippert et al., 2010) was used. In contrast to existing monochromatic reporters like EGFP (Mao et al., 2001), the Confetti reporter encodes four different fluorescent proteins: cytoplasmic YFP, cytoplasmic RFP, membranous CFP and nuclear GFP. The construct consist of a loxP flanked neomycin resistant roadblock and the original Brainbow 2.1 cassette (Livet et al., 2007) which is inserted downstream of a CAGG promoter into the Rosa26 locus (Fig 4-2). Under the influence of a Cre recombinase, inversion and excision occurs, leading to the stochastic expression of a single colour protein.

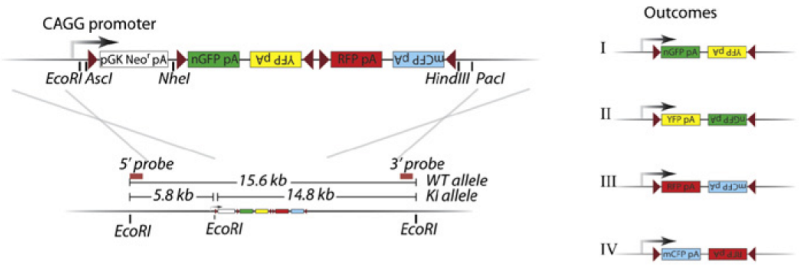

Figure 4-2. Confetti reporter.
A cassette, encoding for four different fluorescent proteins (nuclear GFP, cytoplasmic YFP, RFP and membrane CFP, Brainbow 2.1 (Livet et al., 2007)) was inserted downstream of a strong CAGG promotor and a Neomycin cassette. LoxP sites frame the sequences encoding the fluorescent proteins. A Cre recombinase can catalyse recombination in between these sites creating 4 different, exclusive outcomes: expression of (I) nGFP, (II) cYFP, (III) cRFP and (IV) mCFP. *Modified from Snippert et al., 2010* (Snippert et al., 2010).

4.1.1 Emx1^{Cre}//Confetti mouse

The Confetti reporter mice had not been studied in this lab before. Therefore the Emx1^{Cre} mouse line (Iwasato et al., 2000) was used to test this new line. Emx1 is a homebox gene which is exclusively expressed in the dorsal telencephalon (Iwasato et al., 2000) starting at E10 (Gulisano et al., 1996). The advantage of the continuously active and non-inducible Cre recombinase in this (conditional transgenic) mouse line facilitated an analysis of the Confetti reporter. 8-10 week old, double heterozygous Emx1^{Cre}//Confetti mice were transcardially perfused, the brains were sectioned and without further treatment mounted on glass slides. The visualisation of the native sections was performed with the Leica confocal microscope, because it can detect 5 channels simultaneously, in contrast to the Olympus FV1000, which allows the detection of 3 channels (3 PMT detectors) at the same time.

Fig. 4-3 shows an overview of different regions in the murine brain expressing all four fluorescent proteins.

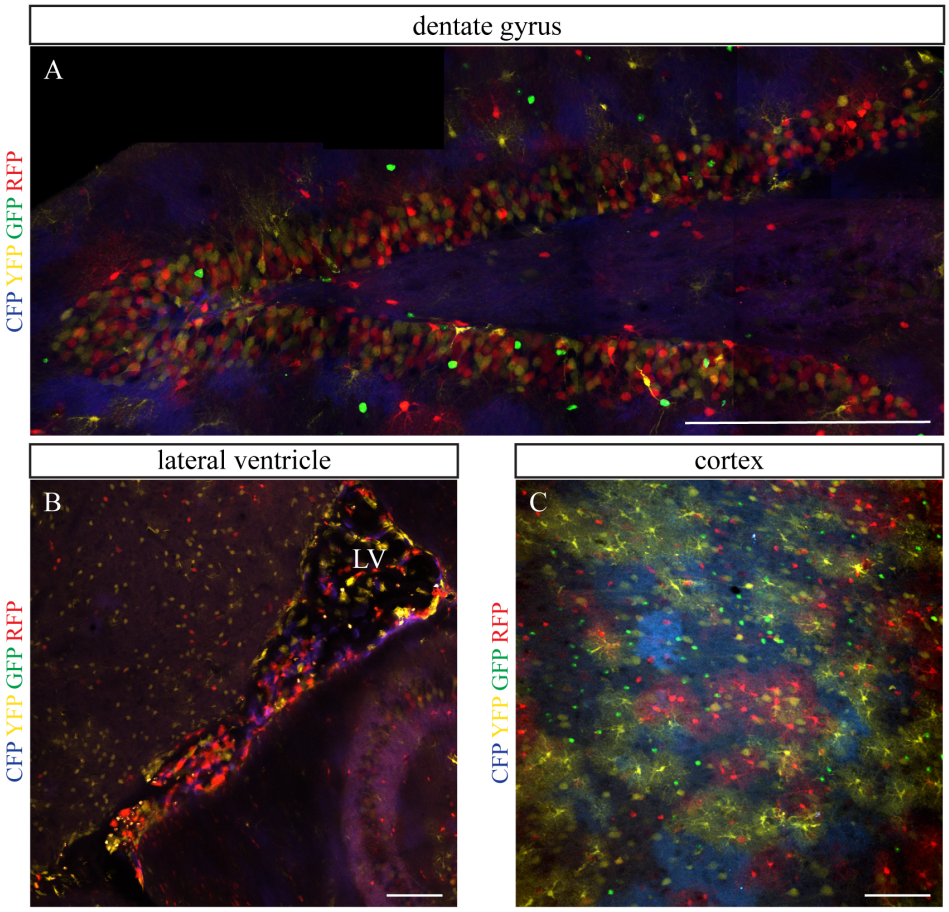

Figure 4-3. Recombination in different areas in the brain of an Emx1^{Cre}//Confetti mouse
(A) shows an overview of the dentate gyrus, of the LV with choroid plexus (B) and an overview of the cortex (C).
Images (A) and (B) were taken with the Leica TCS SP5. Image (C) was taken with a Leica LSM710 confocal and is courtesy of Dr. Sophia Bardehle. Scale bars represent 200 µm in (A) and 100 µm in (B) and (C).

The membrane-bound CFP was problematic on visualisation. First of all, its intensity was very weak in its natural spectrum, making it very hard to visualise with the confocal, let alone with epifluorescence microscopy. Since the goal of this thesis was to establish a method for clonal analysis of aNSCs and therefore the visualisation of single cells is a key point of analysis, a different approach needed to be established. Among other things, immunohistochemistry is also used to amplify the endogenous expression of the fluorophores. This method was adopted here and antibodies against RFP and GFP were used to enhance the signal. Since the proteins YFP and CFP are mutations derived from GFP isolated from *Aequorea victoria* jellyfish (Kremers et al., 2011) they can be detected by the anti-GFP antibody as well. Because these three proteins differ in their localisation within the cell, with GFP being localised in the nucleus, YFP distributed in the cytoplasm and CFP being membrane-bound, these could readily be discriminated. Fig. 4-4 shows a schematic drawing of cells expressing the four different fluorophores before and after staining.

Using a multicolour reporter for the clonal analysis has certain advantages. However, the nature of the reporter also holds some problems. Even after using the GFP-antibody, which reduces the needed channels for imaging from four (CFP, GFP, YFP and RFP) to two (GFP (CFP and YFP) and RFP)

channels, the number of channels left for a staining with other antibodies is limited. Hence the markers used to distinguish between different cell populations have to be chosen with care.

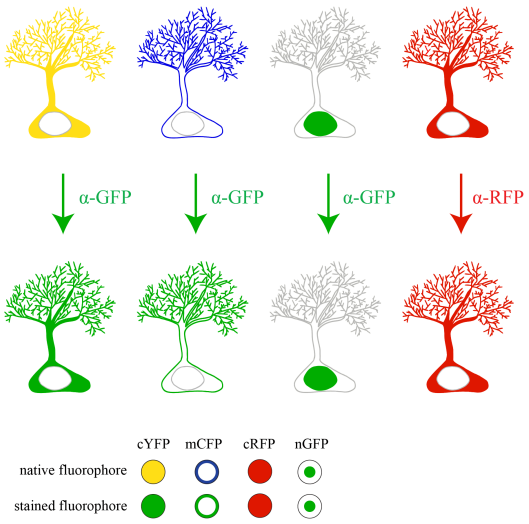

Figure 4-4. Immunohistochemistry of the Confetti reporter.
Schematic drawing of cells expressing the four different fluorophore proteins of the Confetti reporter before and after the treatment with anti-GFP and anti-RFP primary and fluorophore-coupled secondary antibodies.

An example of the visualisation of all four fluorophores in Emx1^{Cre}//Confetti mice can be seen in Fig. 4-5A1-A5 which shows an image of a native dentate gyrus taken with the Leica confocal. A similar section (Fig. 4-5B1-B4) was scanned with the Olympus FV1000 that only allows the detection of 3 channels simultaneously and hence did not easily enable the differentiation between the GFP and YFP channel.

native sections
stained sections
Leica SP5
Olympus FV1000
Olympus FV1000
merge
RFP
CFP
YFP
GFP
YFP/GFP
CFP/YFP/GFP
A1
A2
A3
A4
A5
B1
B2
B3
B4
C1
C2
C3

Figure 4-5. Comparison of visualisation of native and with anti-GFP stained sections in an Emx1^{Cre}//Confetti mouse.
(A1-A5) show images of a native, non-stained dentate gyrus. The image was taken with the Leica confocal, enabling the detection of up to 5 channels simultaneously, whereas the Olympus confocal can only detect 3 channels at the same time (B1-B4), resulting in YFP and GFP to appear in one channel. (C1-C3) show a part of a dentate gyrus that was stained with an anti-GFP antibody, the expression of RFP is endogenous. Different coloured arrows show mark cells expressing the different fluorophores. Scale bars in all images represent 100 µm.

Fig. 4-5C1-C3 shows the same brain now stained against the GFP protein, which, as stated before, also recognises CFP and YFP, hence all three proteins will be visualised by the same secondary antibody. Also in sections, it is possible to differentiate between the different sub-localisations.

In order to also enhance the signal of the endogenous RFP expression, different antibodies against RFP were used. Especially the combination of the anti-RFP antibody raised in rabbit and the anti-GFP antibody (Fig. 4-6) raised in chick worked well and were used for further studies.

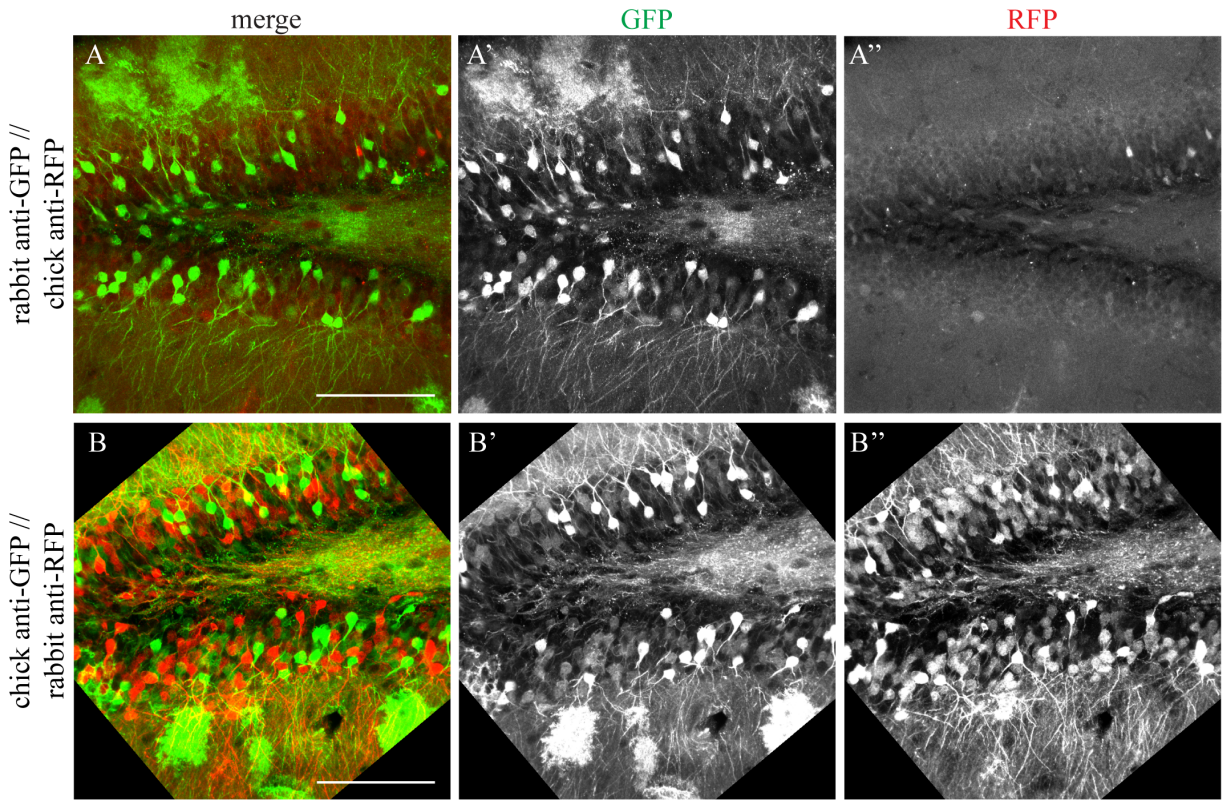

Figure 4-6. Comparison of different anti-RFP and -GFP antibodies in an Emx1^{Cre}//Confetti mouse.
(A) shows a part of a dentate gyrus stained with anti-GFP (raised in rabbit) and anti-RFP (raised in chick). (B) was treated with primary antibodies for chick anti-GFP and rabbit anti-RFP, the latter working the best. Scale bars represent 100 µm.

4.1.2 GLAST^{CreERT2}//Confetti mice

Since the analysis of the behaviour of aNSCs was the goal of this thesis, we used the GLAST^{CreERT2} mice (Mori et al., 2006), which have previously been generated in this lab. GLAST is a marker which is highly expressed, not only in radial glia cells and astrocytes before and after injury, but also in the aNSCs in the adult mammalian brain as already described in the introduction chapter (Mori et al., 2005). In this mouse line, a TAM-inducible form of the Cre recombinase was inserted into the GLAST locus (Mori et al., 2006). This mouse line was shown to recombine with high efficiency in the aNSCs of the adult SEZ as well as the SGZ of the dentate gyrus (DeCarolis et al., 2013; Mori et al., 2006; Ninkovic et al., 2007).

Therefore it is evident that the crossing of this mouse line with multicolour Confetti reporter mice, would result in a very good approach for clonal analyses. The areas of interest are the SEZ of the lateral ventricles as well as the dentate gyrus of the hippocampus.

4.1.2.1 Titration of the Tamoxifen

Before starting to titrate the TAM, GLAST^{CreERT2}//Confetti mice were tested by injection of 40 µg/g body weight TAM twice a day for 5 consecutive days (total dose of TAM of 320 µg/g body weight) (Fig. 4-7A). The same problem of the weakness of the endogenous expression of the fluorescent proteins as with the Emx1^{Cre}//Confetti animals occurred and therefore the signal had to be enhanced by immunohistochemistry as well.

For the titration analyses 8-10 week-old animals were used. The following formula (Formula 4-1) describes the calculation of the different doses per gram body weight of animals when using TAM at a concentration of 1 mg/ml (=1 µg/µl).

$$V_{Tamoxifen}\left(TM\ concentration\ of\ 1\frac{\mu g}{\mu l}\right) = (m_{animal}) * \frac{(c_{TM}\ per\ mass\ of\ animal)}{(c_{TM})}$$

$$V_{TM}\left(1\frac{\mu g}{\mu l}\right) = (20g) * \frac{(10\mu g\ per\ g\ animal)}{\left(1\frac{\mu g}{\mu l}TM\right)}$$

$$V_{TM}\left(1\frac{\mu g}{\mu l}\right) = 200\ \mu l$$

Formula 4-1. Calculation of the volume of TAM of a certain concentration needed, to induce animals of a certain weight.

The mice were all sacrificed 7 days after their first injection with TAM. Their brains were perfused and serially sectioned, before every other section was stained against GFP and RFP proteins and mounted. The two areas of interest, the dentate gyrus of the hippocampus and the SEZ of the lateral ventricles, were then analysed by using an epifluorescence microscope. Labelled cells (also including parenchymal astrocytes) in the respective regions were counted. Tab. 4-1 shows the different doses of TAM that were used to establish the correct clonal TAM-concentration.

Table 4.1. Overview of different doses of TAM used.

Doses of TM/g body weight
2x80 µg/g
1x40 µg/g
1x30 µg/g
1x20 µg/g
1x10 µg/g
1x5 µg/g

The first concentration used was 80 µg/g body weight TAM once daily for two consecutive days (total of 160 µg/g body weight). It showed a great number of cells in the SEZ as well as the dentate gyrus (Fig. 4-7B). The number of cells varied also in animals induced with the same doses, which could be

explained by progeny being produced within the 7 days (e.g. 1x 40µg/g body weight: animal 1: a total of 6 labelled cells compared to animal 2: 22 labelled cells counted in the SEZ).

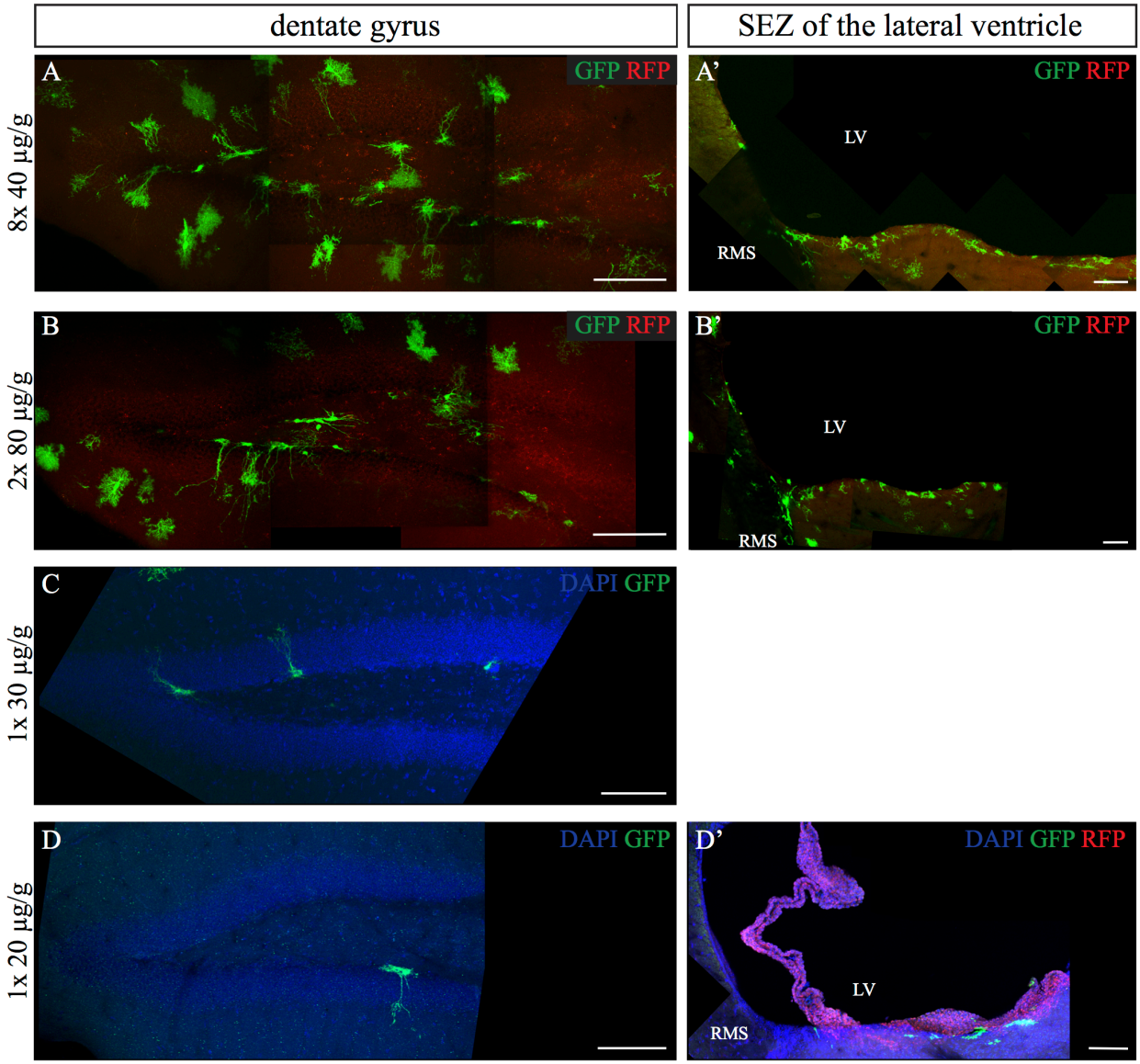

Figure 4-7. Different doses of TAM result in different recombination densities.
Images of dentate gyrus and SEZ of the lateral ventricle of mice induced with different doses of TAM are depicted. (A) 8x40 µg/g, (B) 2x80 µg/g, (C) 1x30 µg/g and (D) 1x20 µg/g. Sections were all stained for anti-GFP and anti-RFP. Scale bars represent 100 µm. All sections are merged stacks of 25 µm.

As expected, a decrease in number of labelled cells could be observed with reduced doses. A suitable dose for clonal analysis would be a dose where only one or maximum two aNSCs are being labelled at the time point of induction. Like this it can be assured that a cluster of cells observed at a certain time after the induction and expressing the same reporter are really the progeny of a single aNSC as shown in Fig. 4-1. Such a cluster of cells expressing the same fluorescent protein would the be referred to being "a clone" of said aNSC. This cluster would be then called as being the clone of a single aNSC. This holds true for two reasons: Firstly, even if two aNSCs are labelled at the same time, the probability that both of them expressing the same marker is low (taken into account that GFP was not observed in any of the

clones) and secondly because the progeny of a aNSC especially in the dentate gyrus does not travel a long distance.

In the dentate gyrus such a dose would be 20-30 µg/g body weight, because after 7 days only 0-2 (1, 2, 1, 0, 1 cells) labelled cells could be found in the five respective hemispheres.

For the analysis of the SEZ, on the other hand, a dose of 5-10 µg/g body weight (10 µg/g: (no.1) - no cells, (no.2) - 1 cell and (no.3) - 5 cells observed and for 5 µg/g: twice no cells observed) was the best, because in contrast to the dentate gyrus, the SEZ has a very complex anatomical structure and also the NBs migrate a long way along the lateral wall before they reach the OB. Therefore, it is even more important to sparsely label aNSCs in order to argument that a cluster of cells expressing the same reporter really belong to the same precursor even taking into account that in some hemispheres no aNSCs were labelled at all.

After having established the correct titrations of TAM, the analysis was focused on the SEZ. To test the concentration of 10 µg/g body weight for the SEZ further, the animals were induced with that dose and sacrificed 21 days later and their OBs were analysed for clones. In six out of seven cases mono-coloured cluster of cells were found in the OB (maximum of 10 cells in one hemisphere). All the cells expressed the same fluorescent protein thus suggesting that all of them are the progeny of the same aNSC. In these cases and with that dose, the cluster of cells never expressed more that one reporter hence confirming the finding of the 7 days post induction (dpi) experiment that with 10 µg/g one labels a single aNSC at the time point of induction.

After further analysis of experiments with the dose of 10 µg/g body weight especially at the longer survival times, cluster of cells expressing up to two different reporters were observed. As explained further above, even though it is less likely that two aNSCs were induced to express the same rather than two different reporters, it was decided to also use the dose of 5 µg/g body weight to confirm the results of the larger dose. Further statistical analyses to affirm this were performed by Dr. F. Calzolari and can be studied in detail in Calzolari et al., 2015 (Calzolari et al., 2015).

4.1.3 Recombination in GLAST^{CreERT2}//Confetti mice

To test if recombination may also take place in some cells of the progeny of NSCs, e.g. TAPs and NBs in the SEZ of GLAST^{CreERT2}//Confetti mice, they were induced with a high dose of TAM (40-50 µg/g bodyweight) and sacrificed 32 hours later for analysis. A short pulse of BrdU, which incorporates into newly synthesised DNA and hence labels fast-proliferating cells, was administered 1 hour before the sacrifice. Multiple sections of three different animals were stained with anti-GFP, anti-RFP and anti-Dcx (NBs) or anti-BrdU and -GFAP. The last two antibodies were labelled with a secondary antibody coupled with the same fluorophore. Since the localisations of the recognised antigens (BrdU being nuclear and GFAP an intermediate filament, they can still be differentiated. BrdU-only cells were regarded and analysed as fast proliferating cells (TAPs) and GFAP-only cells as astrocytes.

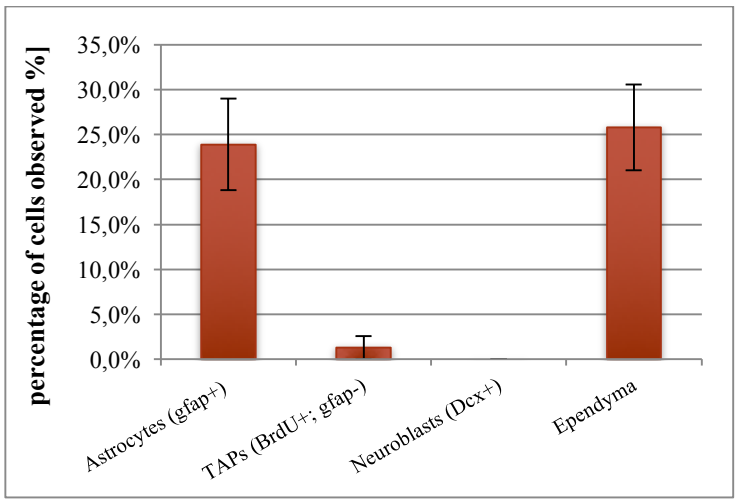

Figure 4-8. Recombination of cells at 32hpi.
Cell type distribution of recombined cells at 32hpi with a single induction of 40-50µg/g body weight TAM per animal. Mice were treated with a short pulse of BrdU IP 1 h prior to perfusion. Immunohistochemistry was performed with anti-Dcx (n=3, total of 207 analysed cells), as well as anti-GFAP and -BrdU with secondary antibody being the same fluorescent protein (n=3, total of 102 analysed cells). Thus a TAP was defined by the presence of BrdU and absence of GFAP. Ependymal cells where identified by their typical morphology (cuboidal and multiciliated) and localisation (lining the ventricles) (Spassky et al., 2005) (n=6, total of cells 309). An average of 25.8% of cells were of ependymal morphology (Fig. 5-11C). In the sections stained for Dcx, no cell was found to co-localise with Dcx. In two cases BrdU+ only cells with TAP morphology were found.
Error bars depict the standard error of the mean (SEM).

Analyses of sections stained for BrdU and GFAP of 3 different animals showed an average of 23.9% (total of 102 cells) being GFAP+ astrocytes (Type B1 and B2) (Fig. 4-8 and 4-9A-B) and 2.6% being double positive for BrdU and GFAP (data not shown). Twice a BrdU+ GFAP- cell like the one depicted in Fig. 4-9D, was observed. In the sections stained against Dcx, no co-localisation with that marker was found (out of 207 cells), suggesting that recombination at the NB and TAP level is a very rare event.

Fig. 4-9C shows an example of an ependymal cell (cuboidal and multiciliated and lining the ventricle (Spassky et al., 2005)), a cell type that was very frequently (25.8%) observed.

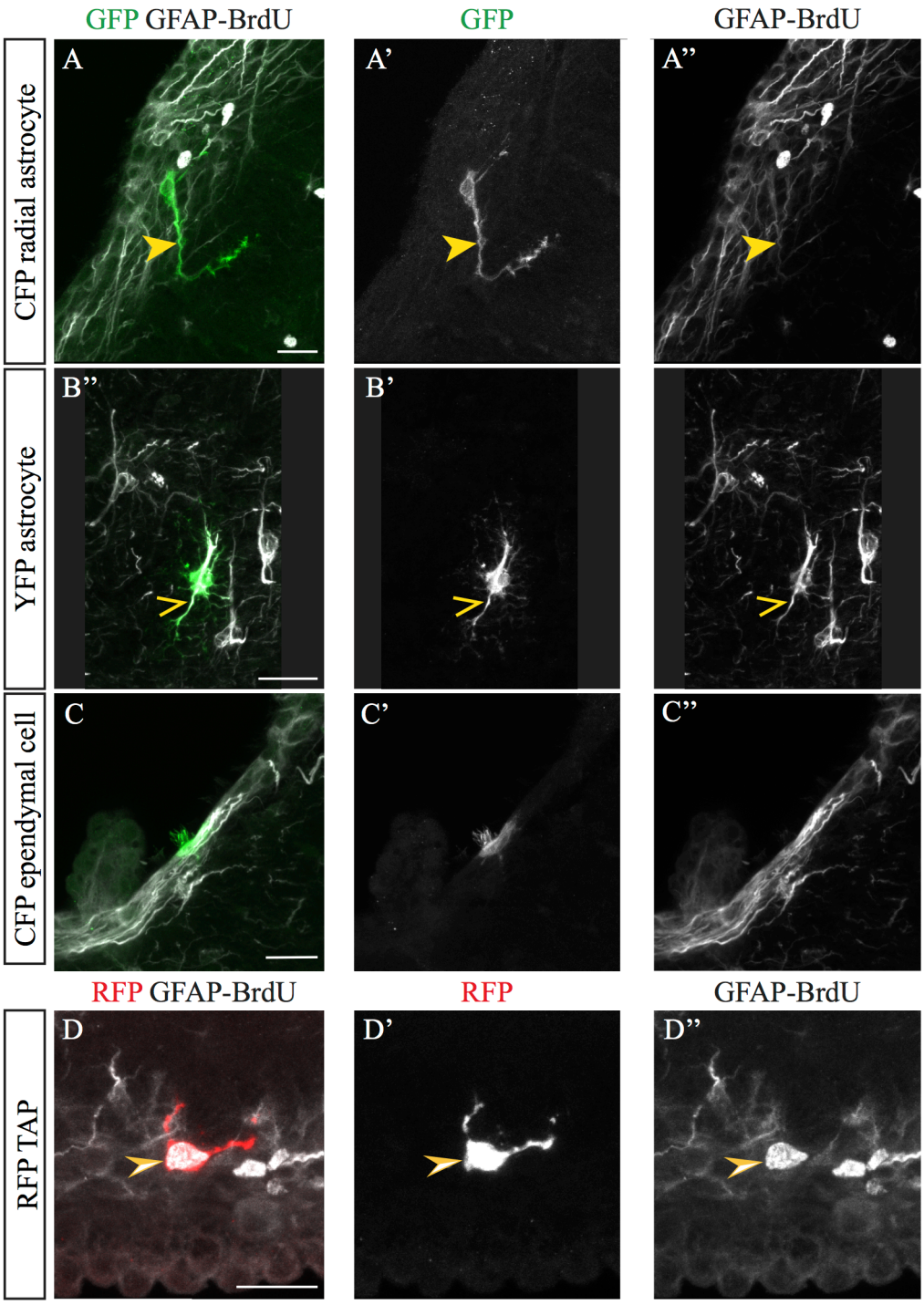

Figure 4-9. Overview of cells types observed at 32hpi.
In the dorsal and lateral wall of mice induced with 40-50 µg/g TAM body weight and sacrificed 32h later, different cell types can be observed: (A) radial astrocytes aNSCs, (B) astrocytes and (C) ependymal cells. Only twice a BrdU+/GFAP- single cell, classified as a TAP could be observed (D). Yellow arrows heads in (A) and (B) indicate co-localisation with GFAP and orange arrow heads in (D) show the co-localisation with BrdU.
Scale bars represent 20 µm. BrdU was IP injected 1h before sacrificing the animals.

4.2 Clonal lineage tracing

4.2.1 General clonal analysis

For the clonal analysis of aNSCs of the SEZ of the lateral ventricles, 8-10 week-old mice were injected with either 10 or 5 µg/g TAM and sacrificed at 3, 7, 21 or 56dpi.

Since it cannot be known which subtypes to expect in the hemispheres and under the background of limited imaging channels as mentioned above, a compromise of markers used had to be made. GFAP, which labels aNSCs, was an invaluable marker to identify the radially shaped aNSCs in the SEZ. Therefore it was used in combination with a secondary antibody in the far-red wavelength (A647). Dcx was used as a second marker, because even though NBs have a typical morphology, it can be hard to distinguish them from TAPs in the SEZ. Furthermore it was an important marker for cells in the OB. It enables the discrimination of neurons (mature morphology and/or Dcx-) and still immature NBs (Dcx+). DAPI is an invaluable counterstaining for the visualisation of nuclei. Since the other channels are already blocked for the fluorophores coupled with the antibodies against RFP, GFP/CFP/YFP and GFAP, only the A405-channel was left for imaging without the danger of overlapping of signals. That was why the anti-Dcx antibody had to be visualised by a secondary antibody in the ultraviolet spectrum (A405) that superimposes with DAPI. Since their morphology is so different (DAPI: nuclei and Dcx: microtubule-associated) the differentiation between these two markers was no problem. Dcx and GFAP in combination with DAPI, GFP and RFP posed a very good compromise and enable the identification of aNSCs as well as NBs and neurons. TAPs on the other hand were identified by their distinct morphology (big and round cell body) as well as their close proximity to NBs and/or radial GFAP+ cell (aNSCs) and their behaviour to amplify in clusters. Hence, the sections were prepared as stated in the methods part, stained against GFP (A488), RFP (A546), GFAP (A647) and Dcx (A405) as well as DAPI and serially mounted on glass slides for microscopic analysis.

Furthermore a clone was defined as cells ($n \geq 2$ cells) that are in close proximity to each other and are expressing the same colour reporter. Therefore cells of a monochromatic clone were most likely derived from the same progenitor/ aNSC. In total 30 hemispheres were analysed for this thesis. Tab. 4-2 shows an overview of the number of hemispheres per dose and time point.

Table 4.2. Overview of time points and concentrations for the clonal analysis.

Time points					
3 dpi	**7 dpi**	**21 dpi**		**56 dpi**	
10 µg/g	10 µg/g	10 µg/g	5 µg/g	10 µg/g	5µg/g
n=6	n=7	n=6	n=5	n=2	n=4

4.2.2 Frequency of fluorescent proteins

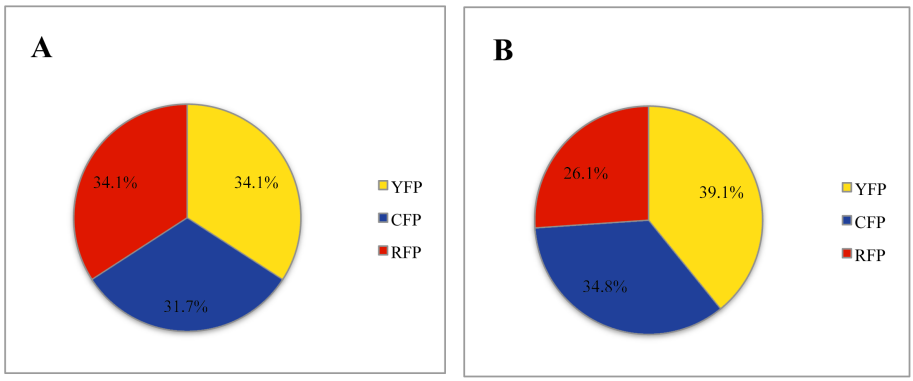

Figure 4-10. Distribution of fluorophores observed.
(A) depicts the distribution of the fluorophores among all cells observed at 3, 7, 21 and 56dpi, including radial GFAP+ astrocytes or only of clones (>1 cell, excluding GFAP+ only clones) (B). A clone consisting of nGFP labelled cells was never observed in the analysis of GLAST^{CreERT2}//Confetti mice. (A) n=41, (B) n=23.

Theoretically the probability of the Cre-mediated recombination of the Confetti-cassette should be the same for each of the four fluorescent proteins. However, also in combination with the GLAST^{CreERT2} mouse line, the nuclear GFP was highly underrepresented and could never be observed in a clone in this dataset. This observation has already been reported in the intestine using a different Cre line (Snippert et al., 2010) . The colour distribution among all hemispheres with recombined cells (also including GFAP+ only cells, total of 41 clones) is depicted in Fig. 4-10A. It shows an equal distribution of RFP and YFP (34.1%) and a slightly smaller proportion of CFP (31.7%). A slightly different picture occurs if the distribution is calculated among the actual clones (>1 cell, therefore excluding the GFAP+ only clones, total of 23 clones) with YFP being the most abundant of all three observed colours (39.1%), followed by CFP (34.7%) and RFP (26,1%) as shown in Fig. 4-10B. Although the numbers are very low, it is evident that the recombination of the three observed colours is nearly equally contributed.

4.2.3 Frequency of occurrence of clones

Out of the 30 hemispheres analysed, the majority of them (43.3%, 13 hemispheres) did not contain any clone at all (Fig. 4-11A). However in 20% of all cases, separate cluster of cells expressing two different fluorophores, hence two clones, were observed in the same hemisphere.

For the early time points 3 and 7dpi, the frequency of clones observed was even lower. At 3dpi 83.3% (5 hemispheres) of hemispheres did not contain any clones at all and only one harboured a cell doublet (Fig. 4-11B). At 7dpi, also the majority of hemispheres did not contain any clone, however in two hemispheres two differently coloured cluster of cells (28.6%) could be observed.

For the later time points, namely 21dpi and 56dpi of the 10 µg/g dose, the abundance of multiple clones per hemisphere was bigger (33.3% and 50%, data not shown here).

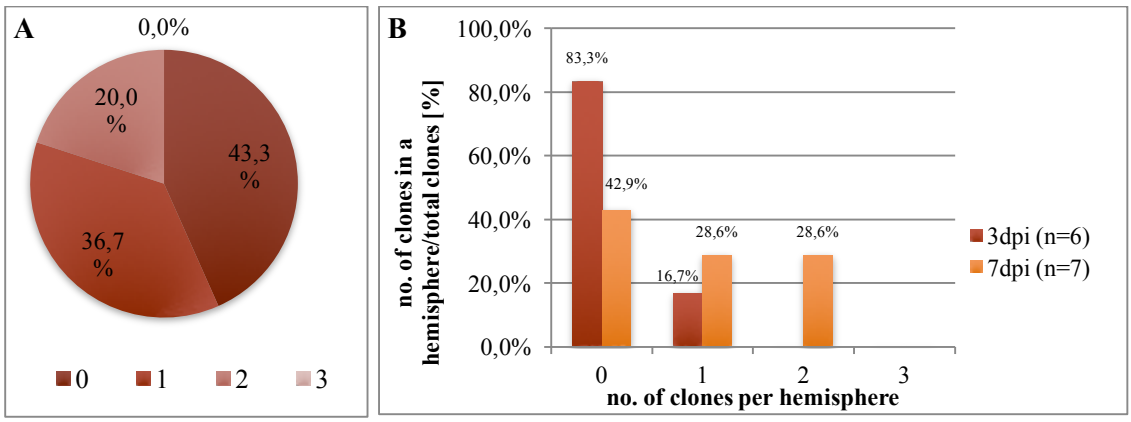

Figure 4-11. Occurrence of clones per hemisphere.
(A) shows the number of clones (>1 cell) per hemisphere at all time points (3-56dpi). The majority of hemispheres (43.3%) did not contain any clones. However in 20.0% of cases (6 out of 30 clones), clones of two different colours were observed. (B) depicts the number of clones per hemispheres at 3dpi and 7dpi. N represents number of hemispheres counted.

This is why, to assure clonality for future analysis, a dose of 5 µg/g TAM was used for later time points. Fig. 4-12 shows that, with the decreased dose of 5 µg/g TAM, the frequency of two clones per hemisphere decreases from 37.5% to 11.1%.

The already analysed data for these two time points was still used, since in none of these brains three clones in one hemisphere were observed. The same holds true for 3 and 7dpi time point. This strengthens the proposition that with the concentration of 10 µg/g and 5 µg/g for the later time points, clonal labelling of a GLAST+ aNSC had occurred. From now on, the data obtained for 5 and 10 µg/g will be pooled into one data set if not stated otherwise.

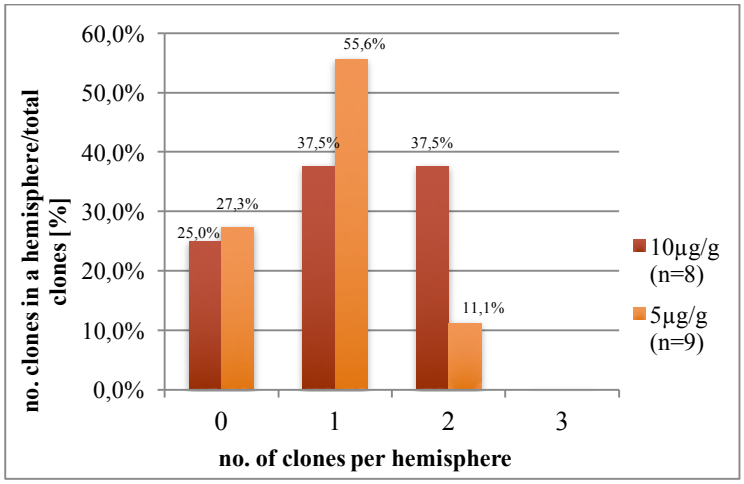

Figure 4-12. Lower TAM concentration results in smaller abundance of clones per hemisphere.
The figure shows the number of clones per hemisphere for the doses of TAM of 10 and 5 µg/g. Time points 21dpi and 56dpi are pooled.

4.2.4 Clone size

A total of 22 clones (3dpi: 1 clone; 7dpi: 6 clones; 21dpi: 8 clones; 56dpi: 7 clones) could be analysed in more detail. Fig. 4-13 shows the distribution of clone sizes at different time points. An increase in the average and mean clone size can be seen over time, with a huge increase in cell number between 3 and 7dpi. The differences between 7, 21 and 56dpi are smaller, with the majority of clones ranging in between clone sizes of 2-82 cells. However, both at 21 and 56dpi one large cell clone (141 and 217 cells) was

observed which indicates fast cell proliferation. Furthermore this data shows a very heterogeneous clone size at each time point.

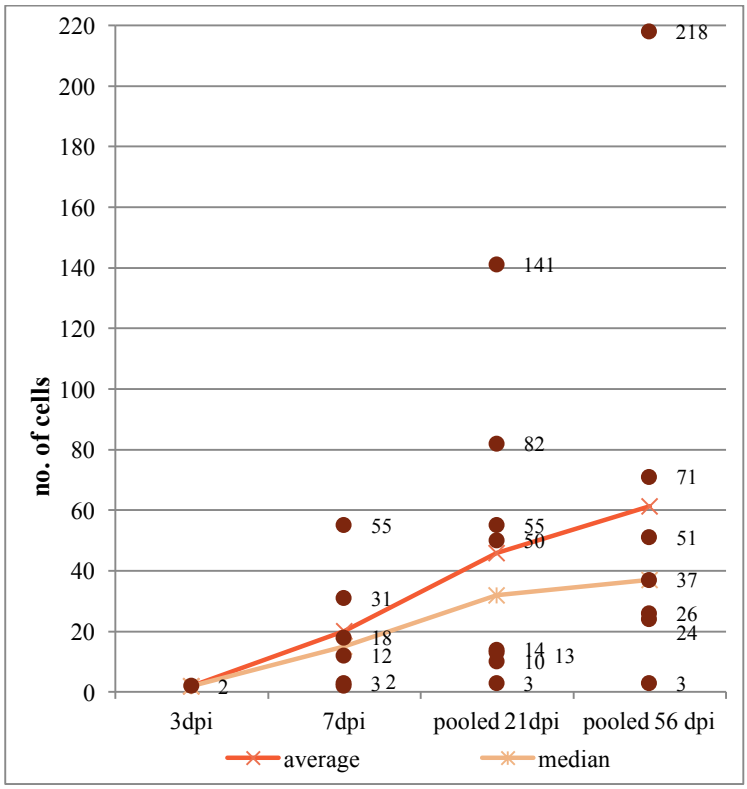

Figure 4-13. Distribution of clone sizes at different time points.
Clone sizes vary between 2 and 217 cells (at 56dpi). Averages (3dpi: 2; 7dpi: 20.2; 21dpi: 46.0; 56dpi: 61.4) and median (3dpi: 2; 7dpi: 15.0; 21dpi: 32.0; 56dpi: 37.0) for each time point are shown. For 21 and 56dpi 5 and10 µg/g doses are pooled.

4.2.5 Clone properties

In the following analysis, the number and identity of cells were analysed for each clone. GFAP+ cells of the same colour of the clone were only regarded as belonging to the clone, if they were in close proximity to a cell cluster. For better statistical evaluation the number of GFAP+ cells and TAPs were summed up within a clone. The areas that were distinguished were SEZ (GFAP+ and TAPS; NBs), RMS, RMS in the core of the OB (NBs) and OB (NBs and neurons). Clones induced with 5 µg/g are marked with an apostrophe. The asterisk indicates that the sections were cut in a coronal and sagittal orientation as it was describes in Fig. 3-2A.

For further discussion, clones were categorized according to the most distant location of the majority of its cells. A “newborn clone”, is restricted to the SEZ, whereas in a “juvenile clone” a great number of NBs are already migrating in the RMS. In order to be categorised as a “mature clone” the majority of cells have to have reached to OB and if the greater number of these have already differentiated into neurons, the clone will be called “senior”.

4.2.5.1 *Spatial distribution of cells at 3dpi*

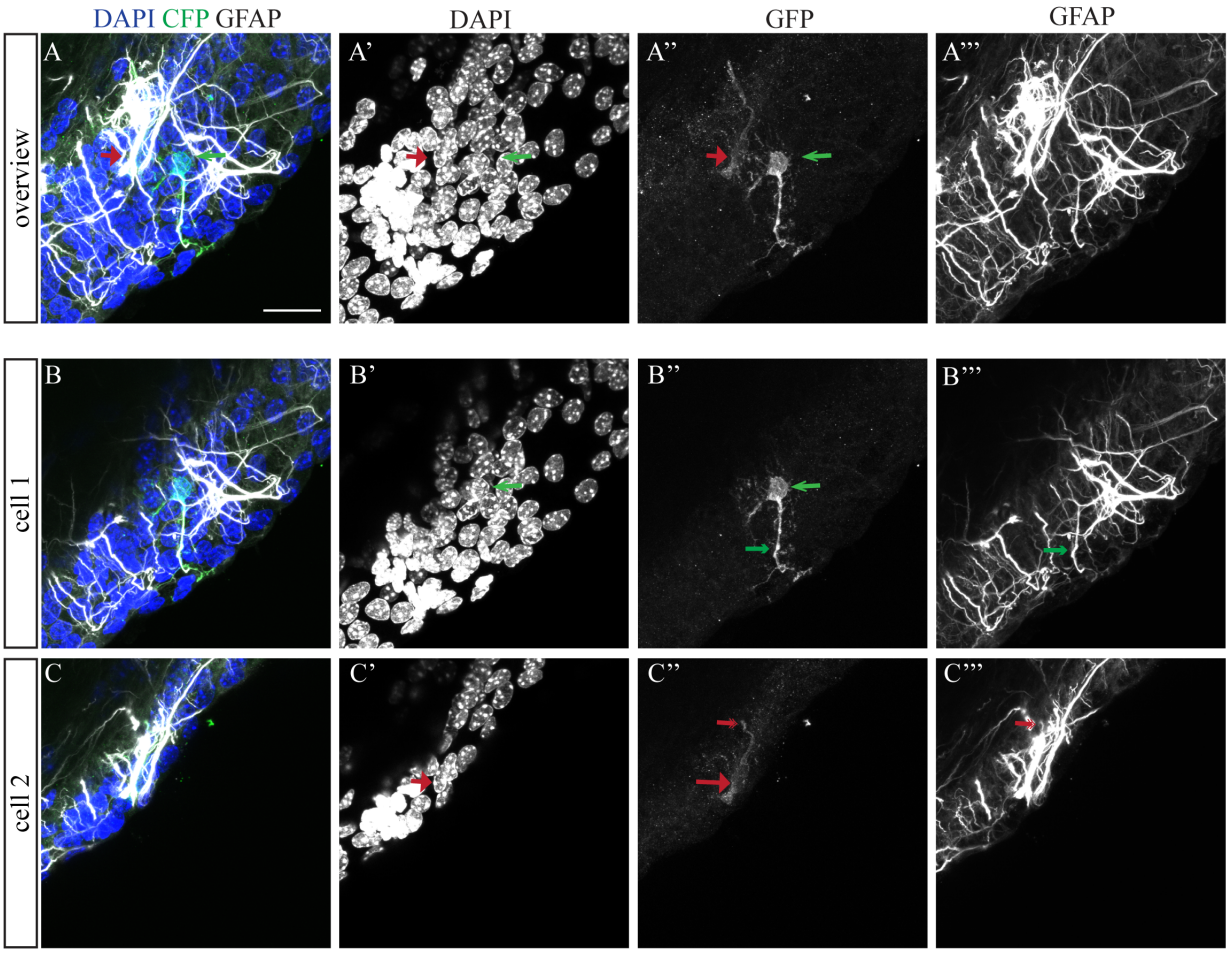

Figure 4-14. Example of a clone at 3dpi: A doublet of radial GFAP+ CFP cells in the SEZ.
(A) shows a merged image of a GFAP+ doublet at 3dpi. The green arrows indicate the cell body and GFAP+ process of cell 1 (B), whereas the colour red indicates the same for the weaker cell 2 (C). Processes of both cells co-localise with GFAP. Scale bar represents 20 µm. Confocal image of overview: z-stack of 76 µm, of cell 1: z-stack of 42 µm and cell 2: z-stack of 14 µm thickness.

Of all 6 hemispheres analysed at 3dpi, only one showed a cluster of cells of the same colour. This cluster consisted of 2 radial GFAP+ CFP cells in very close proximity, thus they seem to be derived from a symmetric division of an aNSC. Fig. 4-14 shows confocal collapsed z-stack images of this "newborn clone" and individual stacks of each cell.

4.2.5.1 *Spatial distribution of cells at 7dpi*

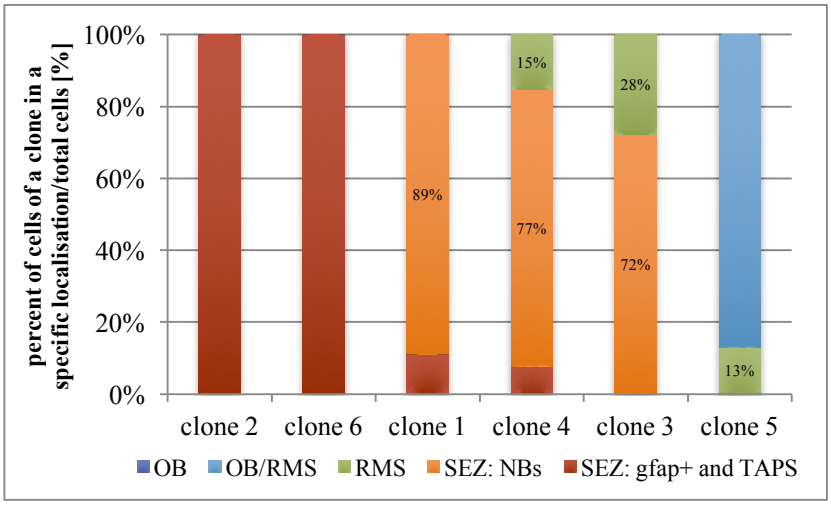

Figure 4-15. Spatial distribution of clones at 7dpi.
Each bar graph represents a single clone at 7dpi. The percentage of cells at each location of the overall number of cells of this clone was calculated. The OB was subdivided into the RMS core (RMS/OB), where NBs are still migrating and the rest of the OB. In the SEZ GFAP+ cells were only considered part of the clone when they were in close proximity to a cluster of progeny (TAPs or NBs). For the SEZ the amount of GFAP+ cells, combined with TAPs as well as the number of NBs were counted.

At 7 days after a single dose of 10 µg/g TAM, all the clones are still spatially very restricted. One half of clones analysed, was still found in the SEZ (Fig. 4-15). Clones 2 and 6 consisted only of GFAP+/TAPs and had not yet produced any NBs, whereas clones 3 and 4 possess a large proportion of NBs in the SEZ, some of them already migrating towards the OB in the RMS. Clone 5 on the other hand, consisted only of 4 NBs migrating in the RMS and 27 NBs that had already reached the RMS in the core of the OB. No NBs, TAPs or corresponding GFAP+ cells in the SEZ could be found, suggesting that their ancestor aNSC got depleted or went back to quiescence.

Fig. 4-16 shows an example of one sagittal section of the hemisphere of clone 1 at 7dpi. In the lateral wall of the lateral ventricle of that section 33 Dcx+ (NBs) and 2 marker negative (mk-) cells (TAPs) were found. (Fig. 4-16B1-B2; TAPs marked by arrows in B1). In total this clone consists of 55 cells and had no associated GFAP+ cell, but 8 TAPs and 47 NBs, all of them still localised within the SEZ. This clone can be viewed as an example for the clones at 7dpi, since most of them were restricted to the SEZ, hence being “newborn clones”. The clone size of this particular clone, however, is by far greater than the average clone size at 7dpi (20.2 cells).

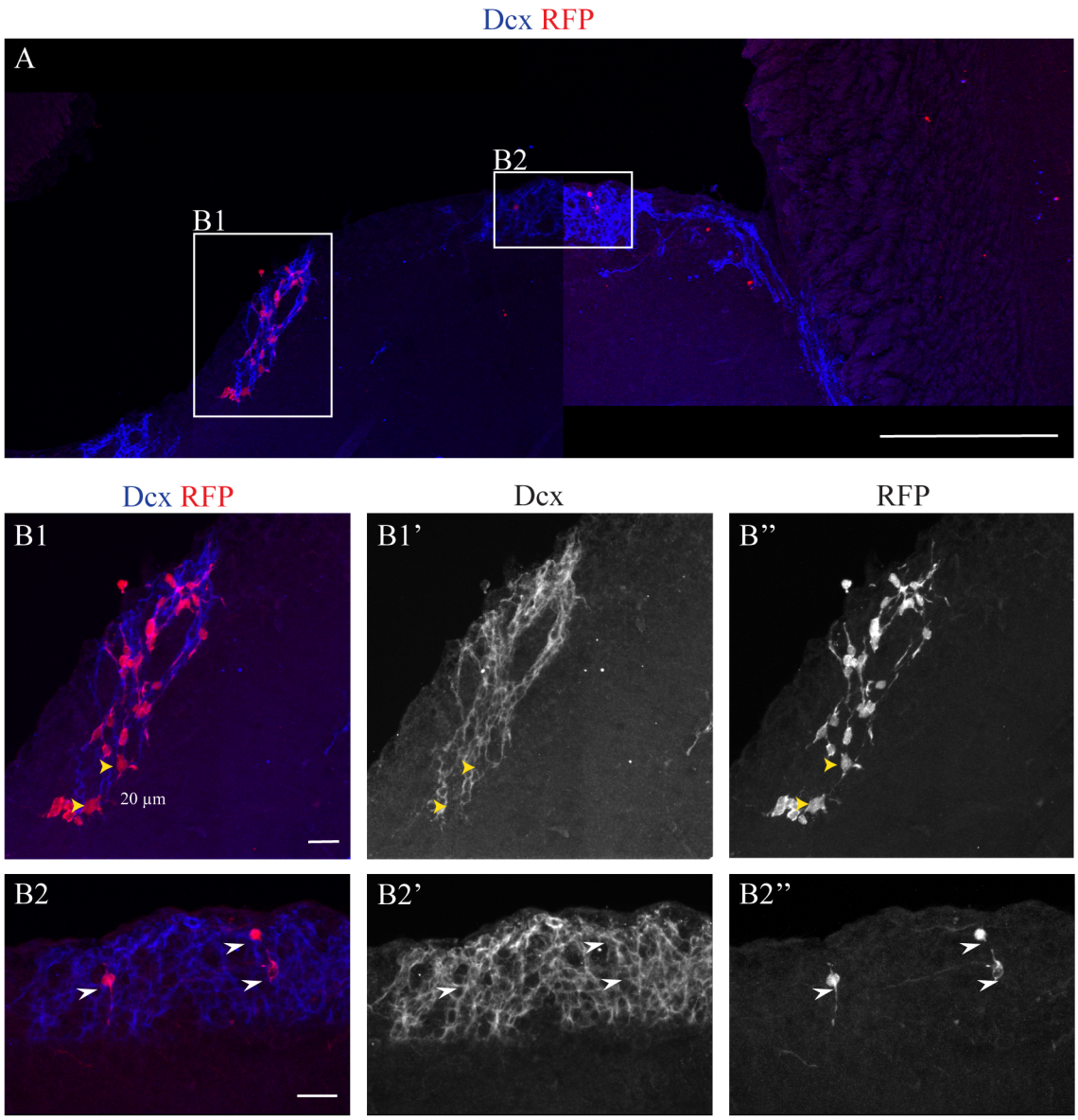

Figure 4-16. Example of a clone at 7dpi.
(A) shows an overview of the SEZ of the lateral wall of the lateral ventricle of one brain section with two cell clusters. The first cluster (B1) consists of 30 NBs and, marked by the two yellow arrows 2 mk- cells (TAPs). (B2) shows 3 NBs, marked by the three white arrows. The total number of cells of that clone is 55 cells.
Scale bars represent 200 µm in (A) and 20 µm in (B1)-(B2).

4.2.5.1 *Spatial distribution of cells at 21dpi*

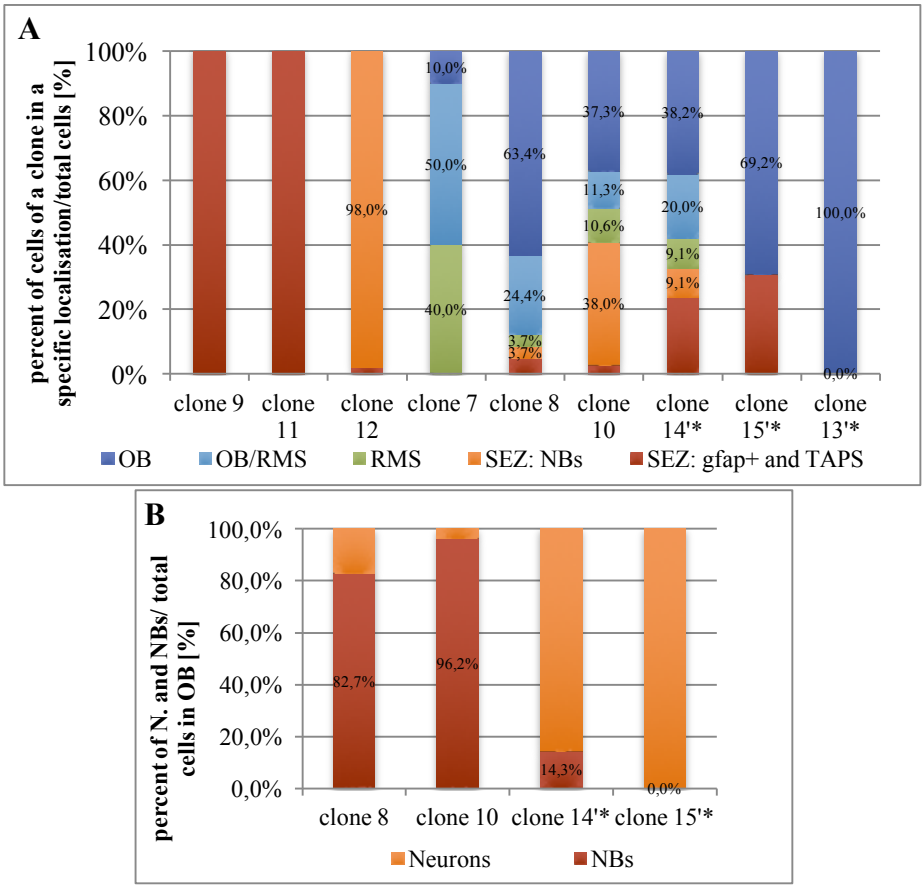

Figure 4-17. Spatial distribution of cells at 21dpi shows heterogeneity.
Each bar graph in (A) represents a single clone. The percentage of cells at each location of the overall amount of cells of a clone was calculated. The OB was subdivided into the RMS core where NBs are still migrating and the rest of the OB. It shows newly generated clones (clones 9, 11 and 12) with high abundance in the SEZ and a juvenile clone (clone 7), whose cells are already migrating in the RMS as well as more mature clones (clones 13'*, 14'* and 15'*). Cells of clone 10 have already reached the OB, but at the same time new NBs are being generated in the SEZ.
The distribution of NBs and neurons in the OB of the mature clones are shown in the histogram (B). The total number of cells in the OB is the reference.
The asterisk indicates that the OBs were cut coronally, the clones labelled with an apostrophe were induced with a dose of 5 µg/g TAM. N.: neurons.

For the 3 weeks time point, 9 clones were analysed. Their average clones size was 46.1 cells. Fig. 4-17A depicts the location of cells in newborn clones and a juvenile clone (clones 9, 11 and 12; clone 7). Clone 9 for example consisted of a doublet of radial GFAP+ cells, whereas clone 11 consisted of a cluster of 14 TAPs and one adjacent radial GFAP+ cell. Clone 7 on the other hand is an example for a juvenile clone, because most of its NBs are migrating in the RMS. The cells of the other clones depicted in Fig. 4-17A have already reached the OB. They are therefore summarised under the category "mature clones". What is very obvious from the shapes of the graphs of clones 10, 14'* and 15'* is, that they have a high percentage of cells in the SEZ as well as the OB. Therefore it seems that after the first cells have reached the OB, a new "wave" of cells was generated.

By looking at the identity of cells in the OB, hence NBs or neurons (Fig. 4-17B), it is possible to further distinguish more "senior clones" with a higher proportion of neurons from the group of "mature clones". The clones 13'*, 14'* and 15'* consisted of 85-100% of neurons, whereas the proportion in clones 8 and 10 in the OB was relatively low (17.3 and 3.8%).

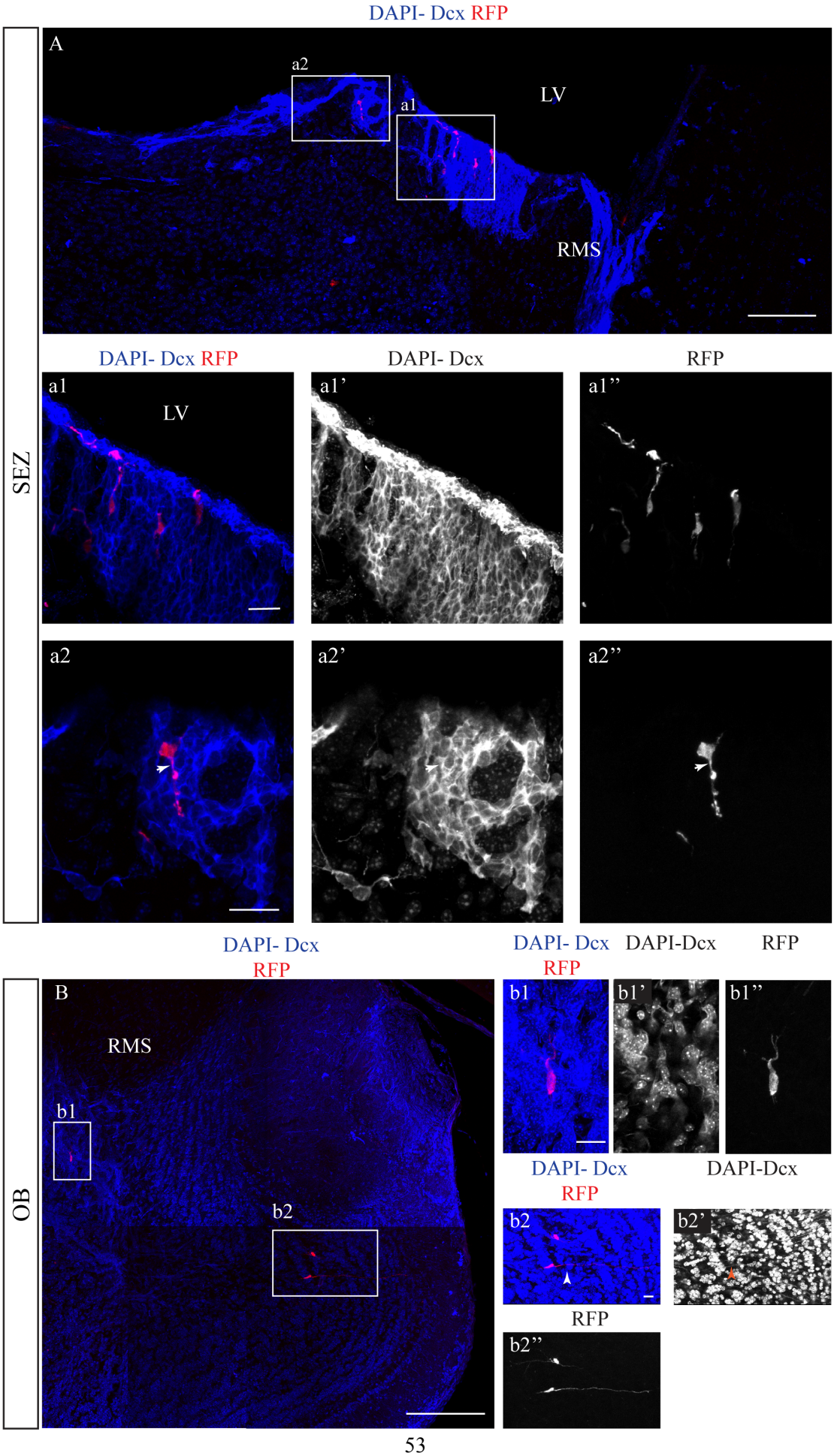
DAPI- Dcx RFP
A
a2
a1
LV
RMS
SEZ
DAPI- Dcx RFP
DAPI- Dcx
RFP
a1
LV
a1'
a1''
a2
a2'
a2''
DAPI- Dcx
RFP
DAPI- Dcx
RFP
DAPI-Dcx
RFP
B
RMS
b1
b2
OB
b1
b1'
b1''
DAPI- Dcx
RFP
DAPI-Dcx
b2
b2'
RFP
b2''

Figure 4-18. Example of clone at 21dpi.
(A) shows an overview of the SEZ of one section with a cluster of 7 NBs. Images (a1-a1'') and (a2-a2'') are magnifications from the areas highlighted in (A). (B) depicts a cropped image of the OB of the same section with one NB (b1-b1'') and two more mature, but still Dcx+ sGCs (b2-b2''), the upper cell being very weakly positive for Dcx.
(B) The arrows in (a2-a2''), (b1-b1'') and in (b2-b2'') indicate the Dcx-co-localisation. Scale bars represent 200 µm in (B), 100 µm in (A), 20 µm in (a1-a2) and (b1-b2).

Images taken of clone 10 with a total clone size of 142 cells are depicted in Fig. 4-18. This clone is a good example of a mature clone with NBs and neurons already localised in the OB (2 neurons and 51 NBs), but also a second wave of new neurons being generated in the SEZ (54 NBs and 1 GFAP+ cell and 3 TAPs). Fig. 4-18A shows an overview of the SEZ with a big cluster of NBs (Fig. 4-18a1-a1'', as well as a2-a2''), whereas Fig. 4-18B shows a piece of the OB with 3 Dcx+ cells. Two of these cells (b2) were located in the deep GCL, whereas the third (b1) was still a migrating NB in the RMS of the OB.

4.2.5.1 Spatial distribution of cells at 56dpi

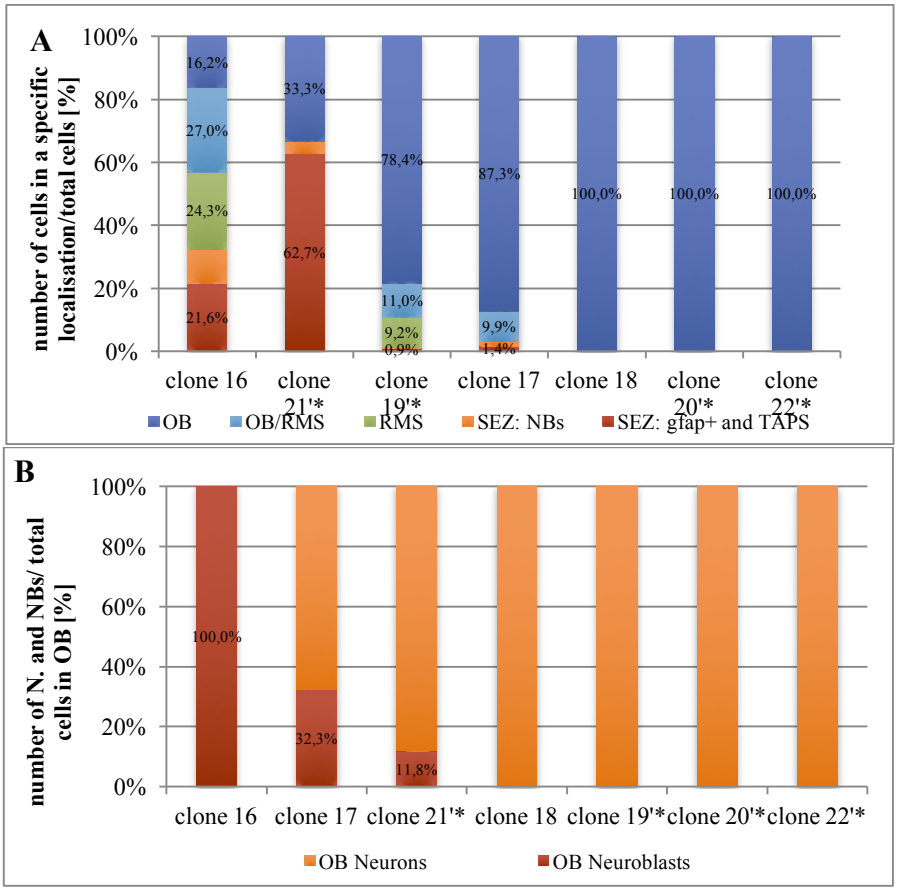

Figure 4-19. Spatial distribution of clones at 56dpi.
(A) depicts bar graphs of clones at 56dpi. Clone 18, 20'* and 22'* and clones 17 and 19'* were categorised as "mature clones", because either all cells were distributed only in the OB (100%) or the majority of them. Clone 21'* is an exception, since most of the cells were still localised in the SEZ, however almost 90% of cells in the OB were already neurons. That was why this clone was also categorised as being a mature clone. Clone 16 is a juvenile clone, because most of the cells are still in the RMS. (B) depicts the proportion of NBs and neurons of all cells in the OB of the mature clones from (A). The asterisk indicates that the OBs were cut coronally, the clones labelled with an apostrophe were induced with a dose of 5 µg/g TAM.

A total of 7 clones could be analysed at 8 weeks post induction. Their average clone size was 61.3 cells (Fig. 4-13). Only one of the clones, clone 16, was still a "juvenile clone" (Fig. 4-19A), with the majority of cells still migrating in the RMS and the few cells in the OB still being NBs (6 cells). The remaining clones, depicted in Fig. 4-19A, were all "mature clones" with their majority of cells already located in the

OB. Since most of those cells were already neurons (Fig. 4-19B), they can be even further categorised to being “senior clones” (clones 17-22’*).

4.2.5.2 Example of a transit-amplifying progenitor clone

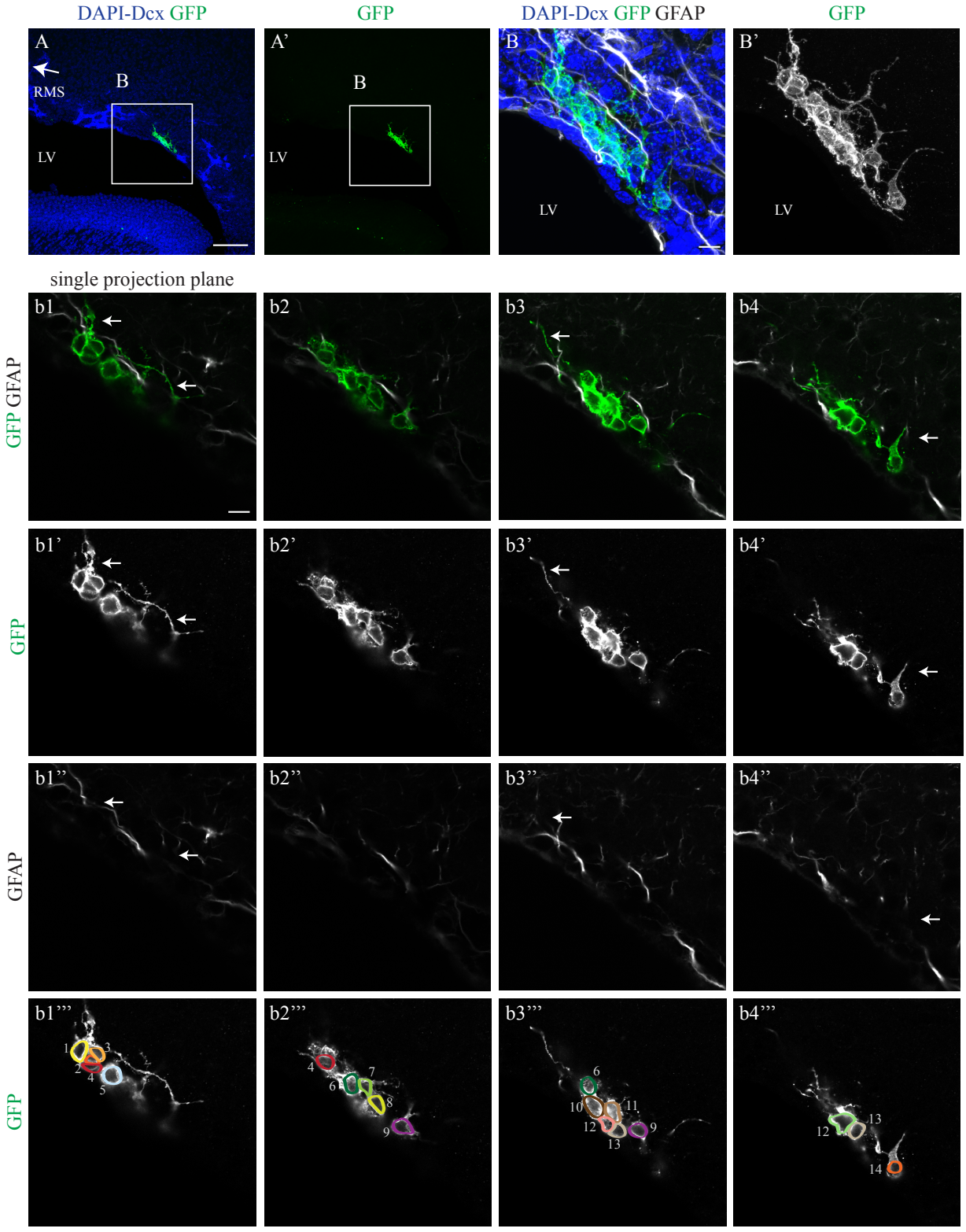

Figure 4-20. Example of a TAP clone at 21dpi.
(A) shows an overview of a CFP TAP clone in the SEZ. (B) represents the magnification of the area marked in (A). The cells were not in a Dcx-co-labelled area and none of the processes were positive for GFAP (b1’’-b4’’; arrows). In total there were 14 TAPs (b1’’’-b4’’’). Scale bars represent 100 µm in (A) and 10 µm in (B) and (b1-b4). (b1-b4) are single plane projections of different z-positions (z=1 µm) of the image depicted in B’.

Fig. 4-20 shows an example of a cluster of mk- cells with a distinct morphology (big cell bodies, clustering together), which were classified as TAPs. These cells were the only ones that belonged to that CFP clone, no NBs were observed yet which suggests that a big amplification step is being performed at the TAP level.

4.2.6 General clone properties

4.2.6.1 Temporal clone composition

After looking at each clone individually, it is interesting to see whether general features can be derived from these clones. The mean of the composition of all clones at each time point validates what can be seen on the single cell level (Fig. 4-21A). At 3dpi the stem cell did not produce any NB progeny yet, whereas at 7dpi the majority of cells (63.6%) were already NBs. As expected after 3 weeks a small proportion (23.8%) of cells have already differentiated into neurons in the OB and this proportion of neurons observed at this time point is even greater (66.7%) at 56dpi. However, in all three of the later time points (7, 21 and 56dpi), a small but decreasing proportion (36.4%, 29.3% and 12.4%) of cells were still GFAP+ cells and/or TAPs, which suggests that overall there still is production of new progeny, even though it is decreasing.

In comparison to Fig. 4-21A, Fig. 4-21B shows a population analysis of the same original data set. For this analysis, cell numbers of each clone at a time point were summed up as if many aNSCs were labelled in the first place as it is done with population analysis. The proportion of the different cell types was then calculated, hence showing the picture of an artificial small number-population analysis.

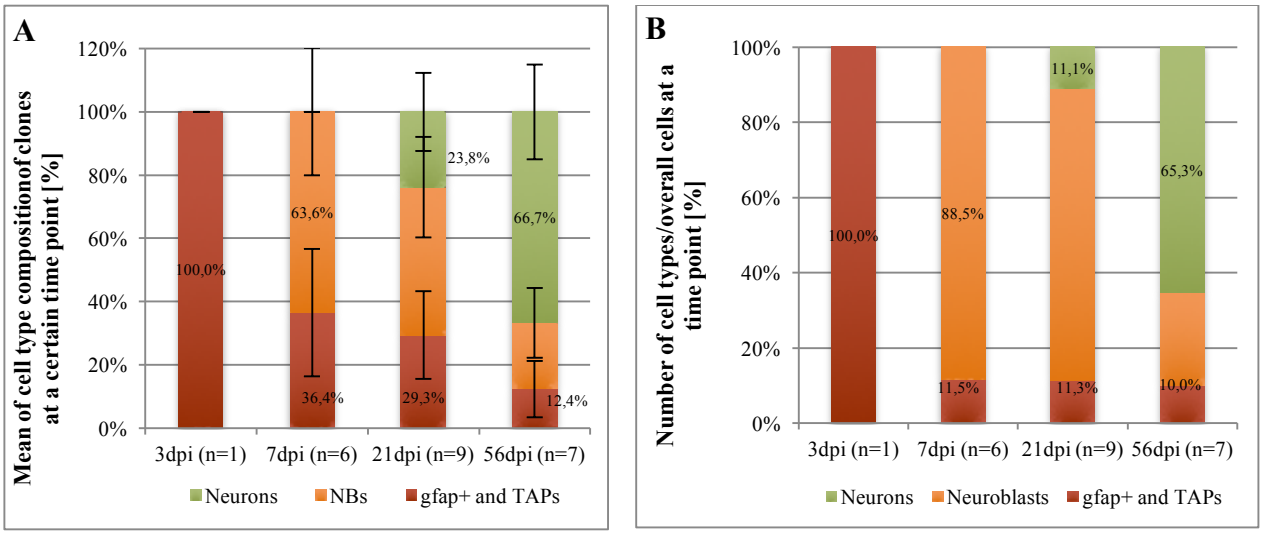

Figure 4-21. Mean clone and population composition at different time points.
(A) depicts the mean of the composition of the clones at each time point whereas figure (B) shows the composition of cells per time point at the population level. All cells of the mentioned cells types were summarised and then their percentage of the total number of cells at this time point were calculated. The only clone at 3dpi consisted of two GFAP+ cells (see Fig. 4-16). At 7dpi 88.5% of all cells at that time point were also NBs, whereas at 21dpi already 11.1% were neurons. The majority (65.3%) of cells at 56dpi were neurons. Error bars depict the SEM.

What can be seen in Fig. 4-21B is that at the population level a small but seemingly constant proportion (10.0-11.5%) of cells are still precursors in the SEZ whereas at the clonal level this proportion is actually decreasing.

4.2.6.2 *Spatial distribution of all clones*

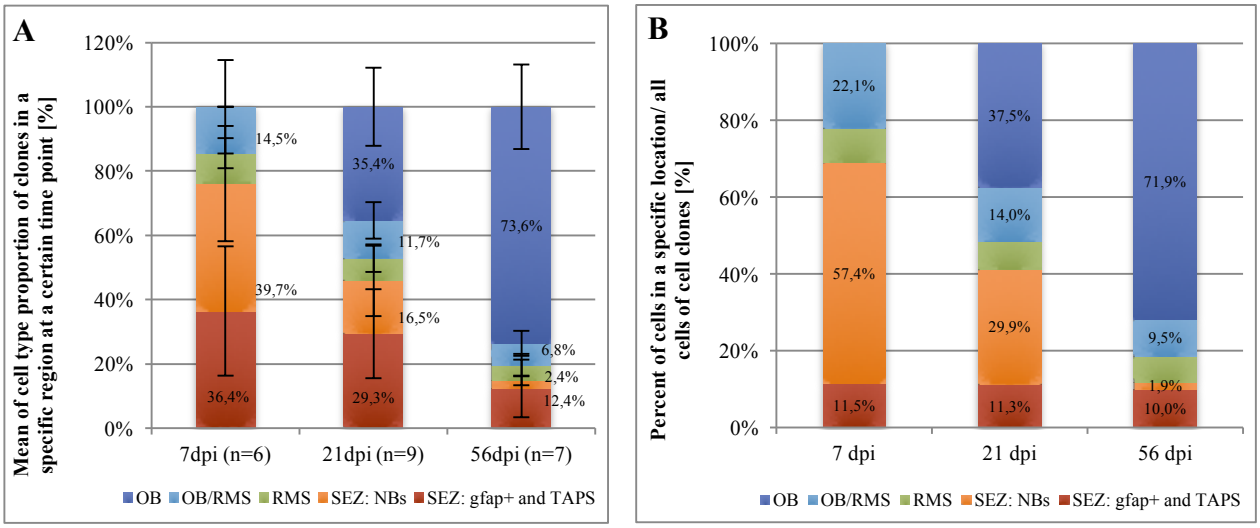

Figure 4-22. Mean clone and population spatial distribution.
(A) depicts the mean of the proportion of cells of clones at a specific time point (7, 21 and 56dpi) in a specific region whereas (B) shows the spatial distribution of all cells of clones of a time point and their (population) spatial distribution. At 7dpi the majority of cells were still localised in the SEZ, whereas at 21dpi the cells have already reached the OB. At 56dpi about 71.9% of all cells were NBs or neurons in the OB. Error bars depict the SEM.

For each individual clone the spatial distribution has been extensively discussed. However, for each time point the overall distribution of cells was calculated. The findings make it possible to conclude general principles and sum up the observations already made at the single clone level (Fig. 4-22A). At 7dpi the majority of cells were still localised in the SEZ. As time passes the cells migrate as expected and at 56dpi the majority of cells are located in the OB. Also here the difference to population analyses can be observed as in Fig. 4-21.

4.2.6.1 *Temporal distribution of all clones*

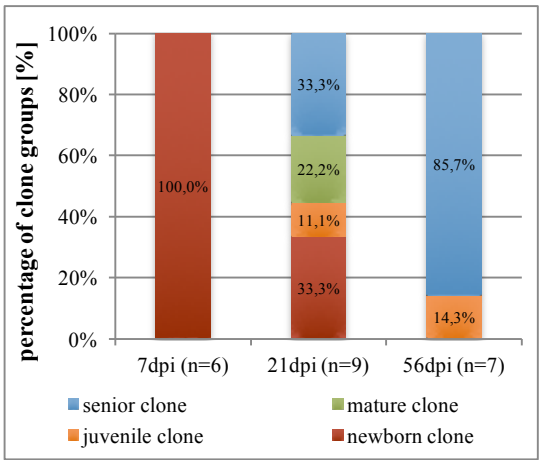

Figure 4-23. Temporal distribution of different clone subgroups.
The clones were categorised into four different groups: “newborn”, “juvenile”, “mature” and “senior” clone. At 21dpi all four subtypes can be observed. At 56dpi the majority (85.7%) of clones are already senior clones.

Fig. 4-23 shows the proportion of clone groups for each time point. It summarises the observations made at the individual level. As expected, at 7dpi all clones were “newborn”, whereas at 21dpi the clones were

more heterogeneous. Interestingly one “juvenile clone” was observed at 56dpi, which suggests that this clone was later generated in time, maybe by a quiescent aNSC.

4.2.7 Neuron diversity

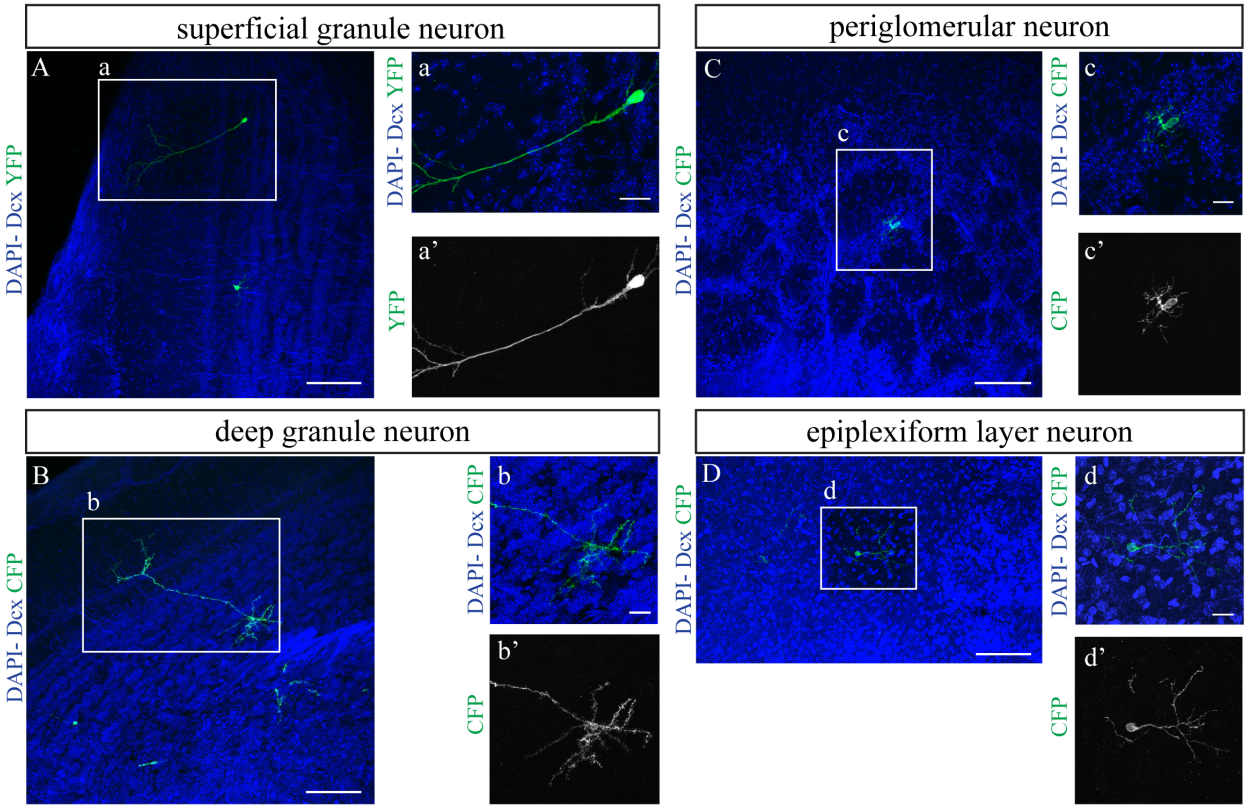

Figure 4-24. Diversity of interneurons observed in the OB.
(A) shows an example of a sGC and (B) a differentiated dGC, with many spines in the deep GCL. (C) and (D) depict a PGN as well as a neuron located in the epiplexiform layer. Scale bars represent 100 µm in A-D and 20 µm in a-d’. The confocal images depicted in (A)-(d’) were taken by Dr F. Calzolari.

The neurons of the clones depicted in Fig. 4-24 were categorised according to their morphology and/or their location in the OB. Interneurons observed were sGCs, dGCs Fig. 4-24A-B as well as neurons located in the middle of the granule cell layer (midgn). Neurons in the epiplexiform layer and PGNs (Fig. 4-24C-D) could also be seen. The latter cell had to be excluded from the analysis because they were also found in the corn-oil-only controls (data obtained by Dr F. Calzolari, not shown).

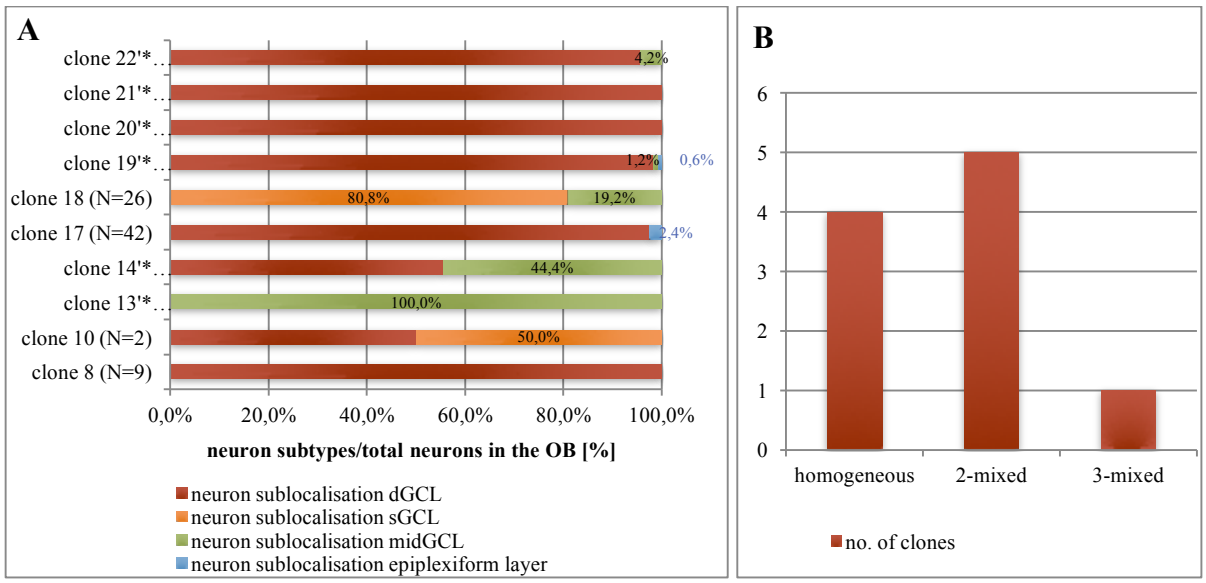

Figure 4-25. Diversity of neuron subtypes observed in a single clone.
(A) For all clones that harboured neurons, the proportion of each type was calculated over the total number of neurons in that clone. 5 clones consisted of two different subtypes (clones 10, 14'* 17, 18 and 22'*) and 1 clone harboured 3 different neuron subtypes (clone 19'*) (B).
The asterisk indicates that the OBs were cut coronally, the clones labelled with an apostrophe were induced with a dose of 5 µg/g TAM. dGCL: deep granule cell layer; sGCL: superficial granule cell layer; midGCL: mid granule cell layer.

4 of the 12 clones were homogeneous and consisted of deep granule or in one case of mid-granule cells (localised in the middle of the granule cell layer) only (Fig. 4-25A; clones 8, 13'*, 20'* and 21'*). Clones 10 and 18 were the only clones that consisted of sGCs. The other proportion of cells was made up of either deep or mid-granule cells. Two other clones (clone 14'* and 22'*) harboured mid and deep granule cells. Furthermore in the OB of clone 17 two neurons were located in the epiplexiform layer.
Only once a clone with 3 different neuron subtypes was detected (Fig. 4-25B; clone 19'*). Interestingly the majority (97.6%) of neurons were found in the deep, only two cells were located in the mid granule cell layer and one in the epiplexiform layer. This clone was also the largest one observed with 218 cells. Also the other clones that consisted of more than one neuron subtype in the OB were mostly big cell clones.

The clones 5, 6, 13', 14'*, 15'*, 17-22'* were analysed at the microscope by Dr F. Calzolari, but provided for this thesis, since the animals utilised for this analysis were prepared, induced and perfused by the author.*

5 Discussion

Until now, an analysis of single aNSCs in the SEZ of the adult mouse has not been performed. Everything that is known about these cells and their progeny has either been derived from experiments performed *in vitro*, which cannot model the complexity observed in the aNSC niche, or the findings depend on analyses performed on the population level *in vivo*.

The method that was established in this thesis was primarily aimed to trace the lineage of a single aNSC in that niche. The findings presented in this thesis are a first insight of the behaviour of aNSC in the SEZ. Since then further analyses to investigate the lineage of a single aNSC have been performed by Dr. Calzolari who continued the analyses and will be referred to further down.

Moreover, this sparse labelling method was also used to verify results that were obtained by imaging the behaviour of astrocytes after an induced injury (Bardehle et al., 2013) as well as to confirm live imaging data of the radial glia cells in the embryonic telencephalon (Pilz et al., 2013).

5.1 Technical considerations of clonal analysis

As already described before, clonal analysis has been performed in the dentate gyrus of the murine hippocampus (Bonaguidi et al., 2011). With this technique these collegues could show that in this region, cells of the neurogenic and astrocytic lineage could be produced by a single aNSC. Also these cells were found to be able to self-renew.

In this thesis, GLAST^{CreERT2}//Confetti mice were used and TAM doses were titrated to receive a sparse labelling of aNSCs in the dentate gyrus and SEZ. This enabled the lineage tracing of the progeny of an aNSC over a certain time period. This means that because of the very sparse labelling, all the cells expressing the same reporter were regarded as being derived from the same aNSC. Such a cell cluster was called a clone of that aNSC. The expression of fluorophores was enhanced by immunohistochemistry and also cell specific markers (GFAP, Dcx) were used for the identification of cell identity. Further analysis of the aNSCs was, however, was focused on the SEZ.

The neurogenesis of the SEZ differs massively from the dentate gyrus. Not only are the aNSCs in contact with the CSF of the ventricle (Mirzadeh et al., 2008), also the neurons produced by aNSCs of the SEZ are much more diverse (Weinandy et al., 2011). Another caveat of the clonal analysis of aNSCs in the SEZ is, that unlike in the dentate gyrus, the progeny of these cells migrates a long distance towards the OB. Only there, the cells differentiate into neurons and integrate into the circuit. By using a mono-colour reporter, it is very difficult to recognise neurons in the OB and a cluster of NBs in the SEZ/RMS belonging to the same clone. This problem was overcome by the use of the multicolour reporter line Confetti (Snippert et al., 2010) in this thesis. It theoretically allows stochastic expression of four exclusive fluorescent proteins. Therefore cells labelled with the same fluorophore are more likely to belong to the same clone and are hence derived from the same progenitor cell. The combination of this reporter with the inducible GLAST^{CreERT2} mouse line (which recombines in astrocytes and more importantly in the radial-like

astrocytes which are thought to label the neural stem cell population in the dentate gyrus and the SEZ (DeCarolis et al., 2013; Mori et al., 2006; Ninkovic et al., 2007)) made a good tool for the clonal analysis of the aNSCs in the SEZ.

Whereas in the study of Bonaguidi *et al.*, 2011 (Bonaguidi et al., 2011) about 8 aNSCs per dentate gyrus were labelled with a single injection of 62 mg/kg body weight, the titration of the TAM for the analysis in the SEZ had to be done more sparsely due to the long distance of migration of the progeny and because of the complex structure of the lateral ventricle as described before. In the first set of experiments of this thesis, the concentration of 10 µg/g TAM bodyweight only showed single-coloured clusters of cells in the OB/RMS of adult mice consistent with their clonal identity. With increasing analyses it became clear that for longer time points a concentration of 5 µg/g TAM would be safer to use since it reduces the probability of a clone being the product of two aNSCs expressing the same fluorophore Fig. 4-12.

Since recombination in these mice did not only occur in (radial) aNSCs in the SEZ but also in parenchymal astrocytes, the analysis had to be limited towards the neuronal lineage differentiation. In this aspect, it had to be assured that the $GLAST^{CreERT2}$//Confetti mice did not recombine in the neurogenic progeny of the aNSCs, namely TAPs and NBs. Shortly after induction (32hpi), no fluorophore positive cells were co-labelled with Dcx in over 200 cells analysed and only in two cases TAPs (BrdU-only cells) were observed. Especially for the TAPs, it is still likely that these cells were already the progeny of a division of an aNSC, which could have occurred in the 32h after induction (the cell cycle for the aNSC being less than 17h (Ponti et al., 2013b)), like it was seen in Fig. 4-9. In summary, since the probability that recombination also takes place in the neuronal progeny is very low, these animals can be used without a problem for clonal analysis of the progeny of single aNSCs.

5.2 Clonal lineage tracing

5.2.1 Cell expansion

The size of the progeny of a single aNSC in the SEZ of the adult murine brain has not yet been described. Consistent with recent cell cycle analyses, it takes 4-6 days until the first post mitotic neuron can be observed (Ponti et al., 2013b). The same can be seen with this clonal analysis. At 3dpi the only clone that was observed, consisted of two GFAP+ radial astrocytes. At 7dpi the clone sizes increased massively to a mean of 20.2 cells and the first NBs had already left the SEZ and migrated in the RMS towards the OB (Fig. 4-15). In one clone the cells had even already reached the OB (clone 5), which also conforms to the finding of Petreanu *et al.* that it takes NBs approximately 7 days to reach the OB and another 15 and 22 days for the NBs to mature (Petreanu and Alvarez-Buylla, 2002).

This can be observed at the time point of 21dpi. NBs had reached the OB in most of the clones and had already matured to neurons (Fig. 4-17. A further expansion in clone size could be seen at 56dpi with an average clone size of 61.4 cells with the majority of clones being senior and consisting of neurons (Fig. 4-19). These findings show that aNSCs are capable of producing a large progeny in a short period of time

(at 21dpi a maximum clones size of 141 and at 56dpi 218 cells) and that it takes about 4 weeks for the first neurons to have matured in the OB (Belluzzi et al., 2003; Carleton et al., 2003).
Interestingly, the clone sizes produced by aNSC of the SEZ is much larger than the ones observed in the SGZ. By using a different mouse line (Nestin-CreER^{T2}, Z/EG) the maximum clone size observed at one month post induction was up to 20 cells (Bonaguidi et al., 2011). This leads to the conclusion that aNSCs and their progeny in the SEZ are different from the aNSCs observed in the dentate gyrus.

5.2.2 Amplification modes

Furthermore, it is known that stem cells themselves divide slowly (Whitman and Greer, 2009) even though a subpopulation seems to have a very short cell cycle (Ponti et al., 2013b) and that the TAPs generated are capable of fast amplification. In literature a total number of three division of these cells could be estimated (Ponti et al., 2013b). An example of a clone that only consisted of TAPs was shown in Fig. 4-20. These 14 TAPs clustering tightly together could be the product of four or more subsequent symmetrical divisions within 21 days. Since no NBs were observed at this stage, it strengthens the hypothesis that that a big amplification step occurs at the TAP level. This however, is only a single example. Further analyses were performed by Dr. Calzolari who could verify the number of amplification steps at the TAP stage as well as add more dimension to the analysis by estimating that an additional division round also occurred at the NB level as it has been reported in literature (Calzolari et al., 2015; Ponti et al., 2013b).

5.2.3 Division modes, quiescence and exhaustion

What can also be seen by looking at clones, especially at 3 weeks post induction is, that there seem to be waves of new cells that are being generated. For example in clone 14'* (Fig. 4-17) NBs had already reached the OB and matured to neurons, but at the same time new TAPs/NBs were generated in the SEZ. The cells of that clone however were most of the time in close proximity to each other. Further analysis of this phenomenon lead to the conclusion that these "sub clones" were indeed produced by an aNSC that divided repeatedly (Calzolari et al., 2015).
This goes in accordance to findings by Costa *et al.* who could show by continuous imaging that the sequence of the lineage progression was reproducible with a rather quiescent aNSC that symmetrically divides and gives rise to a fast proliferating cell of astroglia nature which in turn produce fast-proliferating astroglia and TAPs or only TAPs. This division sequence although observed *in vitro* could explain the multiple rounds of divisions observed in this thesis (Costa et al., 2011).
Interestingly, also very "young" clones compared to the time of induction could be observed. In clone 16 at 56dpi (Fig. 4-19B) for example, NBs had reached the OB, but were still immature, therefore suggesting that the aNSC did not divide at the time point of induction but only later. This could be explained by the hypothesis that this aNSC was quiescent at the time point of induction and became activate only later like the other estimated 699 aNSCs in the SEZ that proliferate daily (Ponti et al., 2013a).

In the neurogenic regions it is believed that a large proportion of aNSCs is quiescent (Doetsch et al., 1999a; Morshead et al., 1994; Seri et al., 2001) before being activated and producing new neurons (Ming and Song, 2011). As it has been discussed before, with retroviruses and BrdU only dividing cells can be labelled. Hence by using transgenic mouse lines, also aNSCs that were quiescent at the time point of induction (Bonaguidi et al., 2011) and got activated at a later time point, can be labelled. This was also observed in this thesis. This can however can be an explanation of the different observations between analyses performed by labelling only the proliferating or also a quiescent subpopulation aNSCs (Bonaguidi et al., 2011; DeCarolis et al., 2013; Encinas et al., 2011).

The same applies for experiments that target the understanding of the role of aNSC in aging. Encinas *et al.* propose a "disposable stem cell" model in which the aNSC terminally differentiates into a non-neurogenic astrocyte after several rounds of division in the dentate gyrus whereas analyses of the progeny of single aNSC in the same region could show that even though many of aNSCs were depleted over time, some of them survived and could be analysed up to one year later. These results seem contradictory. However, one should not forget that the aNSC labelled in these analyses could be different subpopulations with different properties. By extending the clonal analysis established in this thesis, it could be shown that also in the SEZ the aNSC are exhausted (Calzolari et al., 2015) supporting the findings in the dentate gyrus (Bonaguidi et al., 2011; Encinas et al., 2011). Also in this thesis, analyses showed that the percentage of newborn clones reduces with time that goes along with the findings mentioned above.

What has to be taken into account is, that the analysis methods used in these studies mentioned above are different and target at different conclusions. Analyses performed at the single cell level (Bonaguidi et al., 2011; Calzolari et al., 2015) will show the properties of an individual aNSC whereas analyses at the population level (DeCarolis et al., 2013; Encinas et al., 2011; Imayoshi et al., 2008; Ninkovic et al., 2007) will show the overall properties of the whole heterogeneous aNSC population.

5.2.4 Population and clonal analysis

The difference of population and single cell properties mentioned above can also be seen in (Fig. 4-21B). By pooling the numbers of cell populations for each time point and therefore "creating" an artificial population analysis, it can be observed that the percentage of neurons increases with time, as expected. The proportion of TAPs/GFAP+ cells stays approximately the same for all time points (7, 21 and 56dpi). This however does not represent what was observed for the single clones. Especially at 56dpi, in 3 out of the 7 clones 100% of cells were located in the OB without any TAP or NB progeny left in the SEZ (Fig. 4-19A). Fig. 4-21A summarises this. At the individual cell level the percentage of TAPs/GFAP+ cells decreases with time whereas at the population level, it looks like that there is still proliferation in the SEZ up to 8 weeks post induction. This example makes the difference of population and clonal analysis very clear and shows that adult neurogenesis is maintained at the population level and single aNSCs are

only activated over a short period. This also supports the data that the majority of cells in the murine OB are being replaced (Imayoshi et al., 2008; Ninkovic et al., 2007).

5.2.5 Neuronal heterogeneity

The concept of regional specification of aNSCs has been proposed in the past (Merkle et al., 2007). Depending on their site of origin only certain subsets of interneurons are generated. GCs were produced all over the SEZ of the lateral ventricle. More precisely, sGCs were derived from stem cells located in the dorsal regions and dGCs mostly in the ventral region. This analysis, however did not answer the question whether a single aNSC is capable of producing multiple interneuron types or whether the fate of the aNSC is set and therefore enabling it only to produce a certain subtype of neuron. This is a key question since it defines the potential of the aNSC.

Interneurons, which were observed in this thesis were deep, mid and superficial GCs as well as neurons in the epiplexiform layer and PGNs. Since the last cell type was also observed in corn oil controls, it had to be excluded from the analysis (data by Dr F. Calzolari, not shown). The cells observed in the epiplexiform layer have also recently been described however their function is still under debate (Merkle et al., 2014).

In total, 10 clones could be analysed for their interneuronal subtypes and it was found that the majority (4 clones) were homogeneous and consisted of deep or once of mid granule cells. The other five clones consisted of two subtypes, either deep-superficial (clone 10), deep-epiplexiform (clone 17), deep-mid (clones14'* and 22'*) or mid-superficial granule cells. There was only one clone that consisted of three subtypes: deep-mid-epiplexiform neurons. The dGCs however composed the majority.

This is a general finding, because over all clones analysed the most abundant neuron type was the dGC. This observation is in agreement with the finding that in older animals the majority of interneurons produced are dGCs (Lemasson et al., 2005). It seems that the majority of aNSCs were heterogeneous, hence are capable of producing more than one neuronal subtype.

Further analysis performed could strengthen this observation and show that this heterogeneity was largely found in big cell clones. Whether this is due to the aNSC self-regeneration and therefore the production of a different subsets of aNSC which then each produce a certain subset of interneurons (Calzolari et al., 2015) or whether this heterogeneity is caused at the TAP or NBs level will need further analyses.

Regarding the question of when the heterogeneity of interneurons produced is established, a homologue clonal lineage tracing could be done. By using inducible mice expressing TAP- or NB-markers, their progeny and therefore their potential could be evaluated. This analysis would also answer the question more thoroughly, at which point the biggest amplification takes place.

5.3 Outlook

The findings, which are described in this thesis, are only a first step of the characterisation of the behaviour of aNSCs in the SEZ and their progeny.

For further analyses, it would be interesting to see whether the usage of a different inducible transgenic mouse lines in similar clonal lineage analysis, for example Nestin-CreER^{T2} (Bonaguidi et al., 2011) would result in the observation of a different aNSC properties compared to the GLAST^{CreERT2} mice used in this thesis.

Another interesting aspect would be the lineage tracing of aNSCs in the aging murine brain. Are the aNSCs of an old mouse brain still capable of producing the same amount of progeny or does this capability decrease? And do aged aNSC still produce the same interneuronal heterogeneity as their younger equivalents?

Regarding the question of when the heterogeneity of interneurons produced is established, a homologue clonal lineage tracing could be done as described before. By using inducible mice expressing TAP- or NB-markers, their progeny and therefore their potential could be evaluated. This analysis would also answer the question more thoroughly, at which point the biggest amplification takes place.

5.4 Conclusion

This thesis provided an analysis method which allowed sparse spatial as well as specific temporal analyses of single aNSC in the neurogenic regions but also the analysis of astrocytes in the murine cortex and of radial glia cells in the embryo.

With this method it is now possible to analyse the progeny of a single aNSC in the SEZ. Key findings of this thesis were the size of the progeny derived from such a single aNSC and at which cell level and time point this occurs. Furthermore first insights into the temporal profile (quiescence and exhaustion) of such cells could be gained. It was found that adult neurogenesis is maintained at the population level and that the heterogeneous individual aNSCs are only active for a short time.

Therefore it seems that aNSCs in the SEZ are a heterogeneous population, a hallmark that they share with their sisters in the dentate gyrus as well as their limited self-renewal (Bonaguidi et al., 2011; Calzolari et al., 2015; Encinas et al., 2011). However in their property to generate a big progeny (in the SEZ) the aNSCs of the two different regions differ.

They ability of endogenous aNSC to produce different neuron subtypes could at some point be used in the regenerative medicine research as an alternative to embryonic or induced pluripotent stem cells (Lepousez et al., 2015). Until then, further research on the lineage and behaviour of murine aNSCs as well as the translation of that knowledge to human neurogenesis has to be performed. This knowledge may one day help to find a treatment for the very common neurodegenerative diseases of the human.

References

Alonso, M., Ortega-Perez, I., Grubb, M.S., Bourgeois, J.P., Charneau, P., and Lledo, P.M. (2008). Turning astrocytes from the rostral migratory stream into neurons: a role for the olfactory sensory organ. J Neurosci *28*, 11089-11102.

Altman, J. (1962). Are new neurons formed in the brains of adult mammals? Science *135*, 1127-1128.

Altman, J. (1969). Autoradiographic and histological studies of postnatal neurogenesis. IV. Cell proliferation and migration in the anterior forebrain, with special reference to persisting neurogenesis in the olfactory bulb. J Comp Neurol *137*, 433-457.

Altman, J., and Das, G.D. (1965). Autoradiographic and histological evidence of postnatal hippocampal neurogenesis in rats. The Journal of Comparative Neurology *124*, 319-335.

Alvarez-Buylla, A., Garcia-Verdugo, J.M., and Tramontin, A.D. (2001). A unified hypothesis on the lineage of neural stem cells. Nat Rev Neurosci *2*, 287-293.

Alvarez-Buylla, A., and Nottebohm, F. (1988). Migration of young neurons in adult avian brain. Nature *335*, 353-354.

Bardehle, S., Kruger, M., Buggenthin, F., Schwausch, J., Ninkovic, J., Clevers, H., Snippert, H.J., Theis, F.J., Meyer-Luehmann, M., Bechmann, I.*, et al.* (2013). Live imaging of astrocyte responses to acute injury reveals selective juxtavascular proliferation. Nat Neurosci *16*, 580-586.

Beckervordersandforth, R., Deshpande, A., Schaffner, I., Huttner, H.B., Lepier, A., Lie, D.C., and Gotz, M. (2014). In vivo targeting of adult neural stem cells in the dentate gyrus by a split-cre approach. Stem cell reports *2*, 153-162.

Beckervordersandforth, R., Tripathi, P., Ninkovic, J., Bayam, E., Lepier, A., Stempfhuber, B., Kirchhoff, F., Hirrlinger, J., Haslinger, A., Lie, D.C.*, et al.* (2010). In vivo fate mapping and expression analysis reveals molecular hallmarks of prospectively isolated adult neural stem cells. Cell Stem Cell *7*, 744-758.

Belluzzi, O., Benedusi, M., Ackman, J., and LoTurco, J.J. (2003). Electrophysiological differentiation of new neurons in the olfactory bulb. J Neurosci *23*, 10411-10418.

Bergmann, O., Liebl, J., Bernard, S., Alkass, K., Yeung, M.S., Steier, P., Kutschera, W., Johnson, L., Landen, M., Druid, H.*, et al.* (2012). The age of olfactory bulb neurons in humans. Neuron *74*, 634-639.

Bonaguidi, M.A., Song, J., Ming, G.L., and Song, H. (2012). A unifying hypothesis on mammalian neural stem cell properties in the adult hippocampus. Curr Opin Neurobiol *22*, 754-761.

Bonaguidi, M.A., Wheeler, M.A., Shapiro, J.S., Stadel, R.P., Sun, G.J., Ming, G.L., and Song, H. (2011). In Vivo Clonal Analysis Reveals Self-Renewing and Multipotent Adult Neural Stem Cell Characteristics. Cell.

Braun, S.M., and Jessberger, S. (2014a). Adult neurogenesis and its role in neuropsychiatric disease, brain repair and normal brain function. Neuropathol Appl Neurobiol *40*, 3-12.

Braun, S.M., and Jessberger, S. (2014b). Adult neurogenesis: mechanisms and functional significance. Development *141*, 1983-1986.

Breton-Provencher, V., and Saghatelyan, A. (2012). Newborn neurons in the adult olfactory bulb: unique properties for specific odor behavior. Behavioural brain research *227*, 480-489.

Brill, M.S., Ninkovic, J., Winpenny, E., Hodge, R.D., Ozen, I., Yang, R., Lepier, A., Gascon, S., Erdelyi, F., Szabo, G.*, et al.* (2009). Adult generation of glutamatergic olfactory bulb interneurons. Nat Neurosci *12*, 1524-1533.

Cajal, S.R. (1928). Degeneration and Regeneration of the Nervous System. Oxford University Press, London 1928.

Calzolari, F., Michel, J., Baumgart, E.V., Theis, F., Gotz, M., and Ninkovic, J. (2015). Fast clonal expansion and limited neural stem cell self-renewal in the adult subependymal zone. Nat Neurosci *18*, 490-492.

Cameron, H.A., Woolley, C.S., McEwen, B.S., and Gould, E. (1993). Differentiation of newly born neurons and glia in the dentate gyrus of the adult rat. Neuroscience *56*, 337-344.

Carleton, A., Petreanu, L.T., Lansford, R., Alvarez-Buylla, A., and Lledo, P.M. (2003). Becoming a new neuron in the adult olfactory bulb. Nat Neurosci *6*, 507-518.

Chojnacki, A.K., Mak, G.K., and Weiss, S. (2009). Identity crisis for adult periventricular neural stem cells: subventricular zone astrocytes, ependymal cells or both? Nat Rev Neurosci *10*, 153-163.

Costa, M.R., Ortega, F., Brill, M.S., Beckervordersandforth, R., Petrone, C., Schroeder, T., Gotz, M., and Berninger, B. (2011). Continuous live imaging of adult neural stem cell division and lineage progression in vitro. Development *138*, 1057-1068.

DeCarolis, N.A., Mechanic, M., Petrik, D., Carlton, A., Ables, J.L., Malhotra, S., Bachoo, R., Gotz, M., Lagace, D.C., and Eisch, A.J. (2013). In vivo contribution of nestin- and GLAST-lineage cells to adult hippocampal neurogenesis. Hippocampus *23*, 708-719.

Dhaliwal, J., and Lagace, D.C. (2011). Visualization and genetic manipulation of adult neurogenesis using transgenic mice. The European journal of neuroscience *33*, 1025-1036.

Doetsch, F., Caille, I., Lim, D.A., Garcia-Verdugo, J.M., and Alvarez-Buylla, A. (1999a). Subventricular zone astrocytes are neural stem cells in the adult mammalian brain. Cell *97*, 703-716.

Doetsch, F., Garcia-Verdugo, J.M., and Alvarez-Buylla, A. (1997). Cellular composition and three-dimensional organization of the subventricular germinal zone in the adult mammalian brain. J Neurosci *17*, 5046-5061.

Doetsch, F., Garcia-Verdugo, J.M., and Alvarez-Buylla, A. (1999b). Regeneration of a germinal layer in the adult mammalian brain. Proc Natl Acad Sci U S A *96*, 11619-11624.

Doetsch, F., Petreanu, L., Caille, I., Garcia-Verdugo, J.M., and Alvarez-Buylla, A. (2002). EGF converts transit-amplifying neurogenic precursors in the adult brain into multipotent stem cells. Neuron *36*, 1021-1034.

Encinas, J.M., Michurina, T.V., Peunova, N., Park, J.H., Tordo, J., Peterson, D.A., Fishell, G., Koulakov, A., and Enikolopov, G. (2011). Division-coupled astrocytic differentiation and age-related depletion of neural stem cells in the adult hippocampus. Cell Stem Cell *8*, 566-579.

Episkopou, V. (2005). SOX2 functions in adult neural stem cells. Trends Neurosci *28*, 219-221.

Eriksson, P.S., Perfilieva, E., Bjork-Eriksson, T., Alborn, A.M., Nordborg, C., Peterson, D.A., and Gage, F.H. (1998). Neurogenesis in the adult human hippocampus. Nat Med *4*, 1313-1317.

Ernst, A., Alkass, K., Bernard, S., Salehpour, M., Perl, S., Tisdale, J., Possnert, G., Druid, H., and Frisen, J. (2014). Neurogenesis in the striatum of the adult human brain. Cell *156*, 1072-1083.

Ernst, A., and Frisen, J. (2015). Adult neurogenesis in humans- common and unique traits in mammals. PLoS Biol *13*, e1002045.

Faigle, R., and Song, H. (2013). Signaling mechanisms regulating adult neural stem cells and neurogenesis. Biochim Biophys Acta *1830*, 2435-2448.

Feil, S., Valtcheva, N., and Feil, R. (2009). Inducible Cre mice. Methods Mol Biol *530*, 343-363.

Feinstein, P., and Mombaerts, P. (2004). A contextual model for axonal sorting into glomeruli in the mouse olfactory system. Cell *117*, 817-831.

Gage, F.H., and Temple, S. (2013). Neural stem cells: generating and regenerating the brain. Neuron *80*, 588-601.

Garcia, A.D., Doan, N.B., Imura, T., Bush, T.G., and Sofroniew, M.V. (2004). GFAP-expressing progenitors are the principal source of constitutive neurogenesis in adult mouse forebrain. Nat Neurosci *7*, 1233-1241.

Gilyarov, A.V. (2008). Nestin in central nervous system cells. Neuroscience and behavioral physiology *38*, 165-169.

Goldman, S.A., and Nottebohm, F. (1983). Neuronal production, migration, and differentiation in a vocal control nucleus of the adult female canary brain. Proc Natl Acad Sci U S A *80*, 2390-2394.

Gotz, M., Sirko, S., Beckers, J., and Irmler, M. (2015). Reactive astrocytes as neural stem or progenitor cells: In vivo lineage, In vitro potential, and Genome-wide expression analysis. Glia.

Gould, E. (2007). How widespread is adult neurogenesis in mammals? Nat Rev Neurosci *8*, 481-488.

Gould, E., Cameron, H.A., Daniels, D.C., Woolley, C.S., and McEwen, B.S. (1992). Adrenal hormones suppress cell division in the adult rat dentate gyrus. J Neurosci *12*, 3642-3650.

Gritti, A., Parati, E.A., Cova, L., Frolichsthal, P., Galli, R., Wanke, E., Faravelli, L., Morassutti, D.J., Roisen, F., Nickel, D.D*., et al.* (1996). Multipotential stem cells from the adult mouse brain proliferate and self-renew in response to basic fibroblast growth factor. J Neurosci *16*, 1091-1100.

Gross, C.G. (2000). Neurogenesis in the adult brain: death of a dogma. Nat Rev Neurosci *1*, 67-73.

Gulisano, M., Broccoli, V., Pardini, C., and Boncinelli, E. (1996). Emx1 and Emx2 show different patterns of expression during proliferation and differentiation of the developing cerebral cortex in the mouse. Eur J Neurosci *8*, 1037-1050.

Hack, M.A., Saghatelyan, A., de Chevigny, A., Pfeifer, A., Ashery-Padan, R., Lledo, P.M., and Gotz, M. (2005). Neuronal fate determinants of adult olfactory bulb neurogenesis. Nature neuroscience *8*, 865-872.

Herculano-Houzel, S. (2009). The human brain in numbers: a linearly scaled-up primate brain. Frontiers in human neuroscience *3*, 31.

Ihrie, R.A., and Alvarez-Buylla, A. (2011). Lake-front property: a unique germinal niche by the lateral ventricles of the adult brain. Neuron *70*, 674-686.

Imayoshi, I., Sakamoto, M., Ohtsuka, T., Takao, K., Miyakawa, T., Yamaguchi, M., Mori, K., Ikeda, T., Itohara, S., and Kageyama, R. (2008). Roles of continuous neurogenesis in the structural and functional integrity of the adult forebrain. Nat Neurosci *11*, 1153-1161.

Indra, A.K., Warot, X., Brocard, J., Bornert, J.M., Xiao, J.H., Chambon, P., and Metzger, D. (1999). Temporally-controlled site-specific mutagenesis in the basal layer of the epidermis: comparison of the recombinase activity of the tamoxifen-inducible Cre-ER(T) and Cre-ER(T2) recombinases. Nucleic Acids Res *27*, 4324-4327.

Iwasato, T., Datwani, A., Wolf, A.M., Nishiyama, H., Taguchi, Y., Tonegawa, S., Knopfel, T., Erzurumlu, R.S., and Itohara, S. (2000). Cortex-restricted disruption of NMDAR1 impairs neuronal patterns in the barrel cortex. Nature *406*, 726-731.

Jankovski, A., and Sotelo, C. (1996). Subventricular zone-olfactory bulb migratory pathway in the adult mouse: cellular composition and specificity as determined by heterochronic and heterotopic transplantation. J Comp Neurol *371*, 376-396.

Johansson, C.B., Svensson, M., Wallstedt, L., Janson, A.M., and Frisen, J. (1999). Neural stem cells in the adult human brain. Exp Cell Res *253*, 733-736.

Kheirbek, M.A., and Hen, R. (2013). (Radio)active neurogenesis in the human hippocampus. Cell *153*, 1183-1184.

Kokoeva, M.V., Yin, H., and Flier, J.S. (2005). Neurogenesis in the hypothalamus of adult mice: potential role in energy balance. Science *310*, 679-683.

Kosaka, K., and Kosaka, T. (2007). Chemical properties of type 1 and type 2 periglomerular cells in the mouse olfactory bulb are different from those in the rat olfactory bulb. Brain Res *1167*, 42-55.

Kremers, G.J., Gilbert, S.G., Cranfill, P.J., Davidson, M.W., and Piston, D.W. (2011). Fluorescent proteins at a glance. J Cell Sci *124*, 157-160.

Kriegstein, A., and Alvarez-Buylla, A. (2009). The glial nature of embryonic and adult neural stem cells. Annu Rev Neurosci *32*, 149-184.

Kuhn, H.G., Dickinson-Anson, H., and Gage, F.H. (1996). Neurogenesis in the dentate gyrus of the adult rat: age-related decrease of neuronal progenitor proliferation. J Neurosci *16*, 2027-2033.

Kukekov, V.G., Laywell, E.D., Suslov, O., Davies, K., Scheffler, B., Thomas, L.B., O'Brien, T.F., Kusakabe, M., and Steindler, D.A. (1999). Multipotent stem/progenitor cells with similar properties arise from two neurogenic regions of adult human brain. Exp Neurol *156*, 333-344.

Legue, E., and Joyner, A.L. (2010). Genetic fate mapping using site-specific recombinases. Methods Enzymol *477*, 153-181.

Lemasson, M., Saghatelyan, A., Olivo-Marin, J.C., and Lledo, P.M. (2005). Neonatal and adult neurogenesis provide two distinct populations of newborn neurons to the mouse olfactory bulb. J Neurosci *25*, 6816-6825.

Leonard, B.W., Mastroeni, D., Grover, A., Liu, Q., Yang, K., Gao, M., Wu, J., Pootrakul, D., van den Berge, S.A., Hol, E.M.*, et al.* (2009). Subventricular zone neural progenitors from rapid brain autopsies of elderly subjects with and without neurodegenerative disease. J Comp Neurol *515*, 269-294.

Lepousez, G., Nissant, A., and Lledo, P.-M. (2015). Adult Neurogenesis and the Future of the Rejuvenating Brain Circuits. Neuron *86*, 387-401.

Lin, R., and Iacovitti, L. (2015). Classic and novel stem cell niches in brain homeostasis and repair. Brain Res.

Livet, J., Weissman, T.A., Kang, H., Draft, R.W., Lu, J., Bennis, R.A., Sanes, J.R., and Lichtman, J.W. (2007). Transgenic strategies for combinatorial expression of fluorescent proteins in the nervous system. Nature *450*, 56-62.

Lledo, P.M., Merkle, F.T., and Alvarez-Buylla, A. (2008). Origin and function of olfactory bulb interneuron diversity. Trends Neurosci *31*, 392-400.

Lledo, P.M., and Saghatelyan, A. (2005). Integrating new neurons into the adult olfactory bulb: joining the network, life-death decisions, and the effects of sensory experience. Trends Neurosci *28*, 248-254.

Lois, C., and Alvarez-Buylla, A. (1993). Proliferating subventricular zone cells in the adult mammalian forebrain can differentiate into neurons and glia. Proc Natl Acad Sci U S A *90*, 2074-2077.

Lois, C., and Alvarez-Buylla, A. (1994). Long-distance neuronal migration in the adult mammalian brain. Science *264*, 1145-1148.

Lois, C., Garcia-Verdugo, J.M., and Alvarez-Buylla, A. (1996). Chain migration of neuronal precursors. Science *271*, 978-981.

Luskin, M.B. (1993). Restricted proliferation and migration of postnatally generated neurons derived from the forebrain subventricular zone. Neuron *11*, 173-189.

Mao, X., Fujiwara, Y., Chapdelaine, A., Yang, H., and Orkin, S.H. (2001). Activation of EGFP expression by Cre-mediated excision in a new ROSA26 reporter mouse strain. Blood *97*, 324-326.

Merkle, F.T., Fuentealba, L.C., Sanders, T.A., Magno, L., Kessaris, N., and Alvarez-Buylla, A. (2014). Adult neural stem cells in distinct microdomains generate previously unknown interneuron types. Nat Neurosci *17*, 207-214.

Merkle, F.T., Mirzadeh, Z., and Alvarez-Buylla, A. (2007). Mosaic organization of neural stem cells in the adult brain. Science *317*, 381-384.

Merkle, F.T., Tramontin, A.D., Garcia-Verdugo, J.M., and Alvarez-Buylla, A. (2004). Radial glia give rise to adult neural stem cells in the subventricular zone. Proc Natl Acad Sci U S A *101*, 17528-17532.

Ming, G.L., and Song, H. (2005). Adult neurogenesis in the mammalian central nervous system. Annu Rev Neurosci *28*, 223-250.

Ming, G.L., and Song, H. (2011). Adult neurogenesis in the Mammalian brain: significant answers and significant questions. Neuron *70*, 687-702.

Mirzadeh, Z., Merkle, F.T., Soriano-Navarro, M., Garcia-Verdugo, J.M., and Alvarez-Buylla, A. (2008). Neural stem cells confer unique pinwheel architecture to the ventricular surface in neurogenic regions of the adult brain. Cell Stem Cell *3*, 265-278.

Mombaerts, P., Wang, F., Dulac, C., Chao, S.K., Nemes, A., Mendelsohn, M., Edmondson, J., and Axel, R. (1996). Visualizing an olfactory sensory map. Cell *87*, 675-686.

Mori, T., Buffo, A., and Gotz, M. (2005). The novel roles of glial cells revisited: the contribution of radial glia and astrocytes to neurogenesis. Curr Top Dev Biol *69*, 67-99.

Mori, T., Tanaka, K., Buffo, A., Wurst, W., Kuhn, R., and Gotz, M. (2006). Inducible gene deletion in astroglia and radial glia--a valuable tool for functional and lineage analysis. Glia *54*, 21-34.

Morrison, S.J., and Spradling, A.C. (2008). Stem cells and niches: mechanisms that promote stem cell maintenance throughout life. Cell *132*, 598-611.

Morshead, C.M., Reynolds, B.A., Craig, C.G., McBurney, M.W., Staines, W.A., Morassutti, D., Weiss, S., and van der Kooy, D. (1994). Neural stem cells in the adult mammalian forebrain: a relatively quiescent subpopulation of subependymal cells. Neuron *13*, 1071-1082.

Ninkovic, J., and Gotz, M. (2013). Fate specification in the adult brain--lessons for eliciting neurogenesis from glial cells. Bioessays *35*, 242-252.

Ninkovic, J., Mori, T., and Gotz, M. (2007). Distinct modes of neuron addition in adult mouse neurogenesis. J Neurosci *27*, 10906-10911.

Okano, H.J., Pfaff, D.W., and Gibbs, R.B. (1993). RB and Cdc2 expression in brain: correlations with 3H-thymidine incorporation and neurogenesis. J Neurosci *13*, 2930-2938.

Ortega, F., Gascon, S., Masserdotti, G., Deshpande, A., Simon, C., Fischer, J., Dimou, L., Chichung Lie, D., Schroeder, T., and Berninger, B. (2013). Oligodendrogliogenic and neurogenic adult subependymal zone neural stem cells constitute distinct lineages and exhibit differential responsiveness to Wnt signalling. Nat Cell Biol *15*, 602-613.

Palmer, T.D., Willhoite, A.R., and Gage, F.H. (2000). Vascular niche for adult hippocampal neurogenesis. J Comp Neurol *425*, 479-494.

Parras, C.M., Galli, R., Britz, O., Soares, S., Galichet, C., Battiste, J., Johnson, J.E., Nakafuku, M., Vescovi, A., and Guillemot, F. (2004). Mash1 specifies neurons and oligodendrocytes in the postnatal brain. EMBO J *23*, 4495-4505.

Peretto, P., Merighi, A., Fasolo, A., and Bonfanti, L. (1997). Glial tubes in the rostral migratory stream of the adult rat. Brain Res Bull *42*, 9-21.

Petreanu, L., and Alvarez-Buylla, A. (2002). Maturation and death of adult-born olfactory bulb granule neurons: role of olfaction. J Neurosci *22*, 6106-6113.

Pilz, G.A., Shitamukai, A., Reillo, I., Pacary, E., Schwausch, J., Stahl, R., Ninkovic, J., Snippert, H.J., Clevers, H., Godinho, L.*, et al.* (2013). Amplification of progenitors in the mammalian telencephalon includes a new radial glial cell type. Nature communications *4*, 2125.

Platel, J.C., Gordon, V., Heintz, T., and Bordey, A. (2009). GFAP-GFP neural progenitors are antigenically homogeneous and anchored in their enclosed mosaic niche. Glia *57*, 66-78.

Ponti, G., Obernier, K., and Alvarez-Buylla, A. (2013a). Lineage progression from stem cells to new neurons in the adult brain ventricular-subventricular zone. Cell Cycle *12*, 1649-1650.

Ponti, G., Obernier, K., Guinto, C., Jose, L., Bonfanti, L., and Alvarez-Buylla, A. (2013b). Cell cycle and lineage progression of neural progenitors in the ventricular-subventricular zones of adult mice. Proc Natl Acad Sci U S A *110*, E1045-1054.

Price, J.L., and Powell, T.P. (1970). The morphology of the granule cells of the olfactory bulb. J Cell Sci *7*, 91-123.

Reynolds, B.A., and Weiss, S. (1992). Generation of neurons and astrocytes from isolated cells of the adult mammalian central nervous system. Science *255*, 1707-1710.

Richards, L.J., Kilpatrick, T.J., and Bartlett, P.F. (1992). De novo generation of neuronal cells from the adult mouse brain. Proc Natl Acad Sci U S A *89*, 8591-8595.

Riquelme, P.A., Drapeau, E., and Doetsch, F. (2008). Brain micro-ecologies: neural stem cell niches in the adult mammalian brain. Philos Trans R Soc Lond B Biol Sci *363*, 123-137.

Ritsma, L., Ellenbroek, S.I., Zomer, A., Snippert, H.J., de Sauvage, F.J., Simons, B.D., Clevers, H., and van Rheenen, J. (2014). Intestinal crypt homeostasis revealed at single-stem-cell level by in vivo live imaging. Nature.

Rousselot, P., Lois, C., and Alvarez-Buylla, A. (1995). Embryonic (PSA) N-CAM reveals chains of migrating neuroblasts between the lateral ventricle and the olfactory bulb of adult mice. J Comp Neurol *351*, 51-61.

Sakamoto, M., Kageyama, R., and Imayoshi, I. (2014). The functional significance of newly born neurons integrated into olfactory bulb circuits. Front Neurosci *8*, 121.

Sanai, N., Tramontin, A.D., Quinones-Hinojosa, A., Barbaro, N.M., Gupta, N., Kunwar, S., Lawton, M.T., McDermott, M.W., Parsa, A.T., Manuel-Garcia Verdugo, J.*, et al.* (2004). Unique astrocyte ribbon in adult human brain contains neural stem cells but lacks chain migration. Nature *427*, 740-744.

Sauer, B. (1998). Inducible gene targeting in mice using the Cre/lox system. Methods *14*, 381-392.

Schindelin, J., Arganda-Carreras, I., Frise, E., Kaynig, V., Longair, M., Pietzsch, T., Preibisch, S., Rueden, C., Saalfeld, S., Schmid, B.*, et al.* (2012). Fiji: an open-source platform for biological-image analysis. Nat Meth *9*, 676-682.

Seidenfaden, R., Desoeuvre, A., Bosio, A., Virard, I., and Cremer, H. (2006). Glial conversion of SVZ-derived committed neuronal precursors after ectopic grafting into the adult brain. Mol Cell Neurosci *32*, 187-198.

Seri, B., Garcia-Verdugo, J.M., McEwen, B.S., and Alvarez-Buylla, A. (2001). Astrocytes give rise to new neurons in the adult mammalian hippocampus. J Neurosci *21*, 7153-7160.

Shen, Q., Wang, Y., Kokovay, E., Lin, G., Chuang, S.M., Goderie, S.K., Roysam, B., and Temple, S. (2008). Adult SVZ stem cells lie in a vascular niche: a quantitative analysis of niche cell-cell interactions. Cell Stem Cell *3*, 289-300.

Shepherd, G.M., Chen, W.R., Willhite, D., Migliore, M., and Greer, C.A. (2007). The olfactory granule cell: from classical enigma to central role in olfactory processing. Brain Res Rev *55*, 373-382.

Snippert, H.J., van der Flier, L.G., Sato, T., van Es, J.H., van den Born, M., Kroon-Veenboer, C., Barker, N., Klein, A.M., van Rheenen, J., Simons, B.D.*, et al.* (2010). Intestinal crypt homeostasis results from neutral competition between symmetrically dividing Lgr5 stem cells. Cell *143*, 134-144.

Spalding, K.L., Bergmann, O., Alkass, K., Bernard, S., Salehpour, M., Huttner, H.B., Bostrom, E., Westerlund, I., Vial, C., Buchholz, B.A.*, et al.* (2013). Dynamics of hippocampal neurogenesis in adult humans. Cell *153*, 1219-1227.

Spassky, N., Merkle, F.T., Flames, N., Tramontin, A.D., Garcia-Verdugo, J.M., and Alvarez-Buylla, A. (2005). Adult ependymal cells are postmitotic and are derived from radial glial cells during embryogenesis. J Neurosci *25*, 10-18.

Suh, H., Consiglio, A., Ray, J., Sawai, T., D'Amour, K.A., and Gage, F.H. (2007). In vivo fate analysis reveals the multipotent and self-renewal capacities of Sox2+ neural stem cells in the adult hippocampus. Cell Stem Cell *1*, 515-528.

Suhonen, J.O., Peterson, D.A., Ray, J., and Gage, F.H. (1996). Differentiation of adult hippocampus-derived progenitors into olfactory neurons in vivo. Nature *383*, 624-627.

Taverna, E., Gotz, M., and Huttner, W.B. (2014). The cell biology of neurogenesis: toward an understanding of the development and evolution of the neocortex. Annu Rev Cell Dev Biol *30*, 465-502.

Treloar, H.B., Feinstein, P., Mombaerts, P., and Greer, C.A. (2002). Specificity of glomerular targeting by olfactory sensory axons. J Neurosci *22*, 2469-2477.

Trepel, M. (2008). Neuroanatomie: Struktur und Funktion (Urban & Fischer).

Ventura, R.E., and Goldman, J.E. (2007). Dorsal radial glia generate olfactory bulb interneurons in the postnatal murine brain. J Neurosci *27*, 4297-4302.

Weinandy, F., Ninkovic, J., and Gotz, M. (2011). Restrictions in time and space - new insights into generation of specific neuronal subtypes in the adult mammalian brain. Eur J Neurosci *33*, 1045-1054.

Whitman, M.C., and Greer, C.A. (2009). Adult neurogenesis and the olfactory system. Prog Neurobiol *89*, 162-175.

Winner, B., and Winkler, J. (2015). Adult Neurogenesis in Neurodegenerative Diseases. Cold Spring Harbor perspectives in biology *7*.

World Health Organization (2006). Neurological Disorders: Public Health Challenges (World Health Organization).

Zhao, C., Teng, E.M., Summers, R.G., Jr., Ming, G.L., and Gage, F.H. (2006). Distinct morphological stages of dentate granule neuron maturation in the adult mouse hippocampus. J Neurosci *26*, 3-11.

Zhuo, L., Sun, B., Zhang, C.L., Fine, A., Chiu, S.Y., and Messing, A. (1997). Live astrocytes visualized by green fluorescent protein in transgenic mice. Dev Biol *187*, 36-42.

Zong, H., Espinosa, J.S., Su, H.H., Muzumdar, M.D., and Luo, L. (2005). Mosaic analysis with double markers in mice. Cell *121*, 479-492.

Acknowledgements

Without any doubt, this thesis would not have been possible if it were not for the support, help and encouragement of many people.

First of all, I would like to thank **Magdalena Götz** for giving me the opportunity to write my medical thesis in her lab and for strengthening my interest in science. I am very grateful for your help, patience and support over the last few years and to be able to have worked in your lab together with so many great scientists.

I would also like to thank **Jovica Ninkovic** for being a great supervisor. Thank you for introducing me to all the different techniques and the basics of adult neurogenesis but also for your input regarding presentations and posters.

I am also very thankful to my great colleague **Filippo Calzolari** who did an amazing job continuing the project. Without you the project would not have become what it is today. Thank you for sharing your knowledge, your helpful comments and the many great discussions. I am very grateful to have worked with you.

Thanks also to my office colleagues **Simona**, **Anna**, **Ana-Luisa** and **Tobias**. Thank you all for fruitful discussions, entertaining breaks and creating such a nice working atmosphere.

I would also like to thank **Ruth** and **Silvia** especially for making my start so much easier. Thank you for your support and sharing your knowledge with me.

I am really glad to have worked with so many talented colleagues **Melanie, Joana, Pia, Tessa, Gregor** and **Sophia**. Thank you for many fruitful discussions and for creating such a good atmosphere.

I especially want to thank **Stefania** who accompanied me until the end. Thank you for your support, your humour and the lovely coffee breaks, which we now have to continue outside of Neuherberg!

Thanks also to **Timu, Andrea, Angelika** and especially **Emily** for their superb technical support over the time.

Last but not least, I want to thank some very important people in my life.

Sabrina, thank you for your patience and for listening. I am very grateful to know that you are here.

My parents-in-law **Ingrid** and **Lutz**, who were always interested in the progress of the project and of whose support I could always count on.

I would also thank my **grandmas** as well as **grandparent-in-laws** for their support and continuous interest in my work.

My parents. Thank you for your endless support and trust in me, even though this thesis caused extra semesters ;). Thank you for believing in me and always encouraging me to do the things I love, even though it might seem like a detour at first.

The last person I would like to thank is my husband, **Philipp**. Without much ado, I guess this thesis would not have been the same or even written without him. I thanked a lot of people for their support, but his encouragement and persistence throughout the whole thesis, from the experimental to the writing part, exceled everything I could have hoped for.

Thank you for your humour, especially in the harder times. I cannot put into words how much it means to me to know that you are by my side. You are my point of reference.